An investigation of the molecular properties of 1,1,1-trichloro methyl silane using laser spectroscopy.

M B PELLE

Dissertation submitted in partial fulfilment of the requirements for the degree master of science at the Potchefstroom campus of North-West University

Supervisor: Prof C. A. Strydom

Co-supervisor: Dr A. du Plessis

November 2008

DECLARATION

I, Makungwane B Pelle, declare herewith that the dissertation entitled, an investigation of the molecular properties of 1,1,1-trichloro methyl silane using laser spectroscopy which I herewith submit to the North- West University as partial completion of the requirements set for the Master of Science degree, is my own work, has not already been submitted to any other university.

Signature of Student .....MBPelle.....

Date.....28/04/2009.....

ACKNOWLEDGEMENTS

I am grateful to the following people, institutions and companies, for their contribution in making this study a success.

- My supervisor, Prof Christien Strydom for an opportunity to be part of the femtochemistry group, and for supporting me through the toughest time of my life when I was busy with this research project. Thank you for your words of advice, and encouragement.
- My co-supervisor, Dr Anton Du Plessis for his guidance during this study and for his helpful comments.
- A big thank you to Henk Van Wyk for your generosity and patience, the time you took to teach me about lasers, you always found time to answer my questions.
- Dr Hennie for his help to run experiments, discussions over data, and above all, for giving me an understanding of mass spectrometry.
- North-West University and National Laser Center for their facilities
- Thanks to the competency area manager of the Femtochemistry Group, Dr Lourens Botha, for the support in the postgraduate studentship program
- To my parents for their love and support throughout this experience.
- Finally a special thank you to my kids Oarabile and Didintle, to my husband Meshack. Thanks for always being there when I needed them most, and for standing by me through all the ups and downs of this project.
- Above all, God for the strength and patience I received through him.

ABSTRACT

Silicon carbide (SiC) is formed from methyltrichlorosilane (CH_3SiCl_3) during a chemical vapour deposition process [Osterhold et al., 1994]. Silicon carbide is one of the important compounds for the Pebble Bed Modular Reactor (PBMR) process because it is used as a coating film in the kernel of the fuel cell. For the current chemical vapor deposition process at the PBMR to be improved, the process of the formation of silicon carbide layer from methyltrichlorosilane must be fully understood. Molecular mechanics, semi empirical, Hatree-Fock and Moller-Plesset modelling calculations were performed using the Spartan modelling program to obtain information about the molecular structure and properties of the CH_3SiCl_3 molecule. The electron densities, energy profiles for rotation as well as the infrared spectra were calculated using different (MMFF, DFT, 3-21G and STO-3G) basis sets. The results were confirmed by obtaining experimental UV/Vis absorption spectroscopy, FT-IR and Raman spectroscopy.

The nanosecond and femtosecond laser activation and ionization technique was used to ionize methyltrichlorosilane molecules at 795 nm and 397.5 nm of the femtosecond laser. Nanosecond lasers used include the Nd:YAG laser at 266 nm, as well as a tuneable dye laser at 212.5 nm. Product formation was analyzed using the time of flight mass spectrometry technique. The main difference between the nanosecond and femtosecond laser ionization is the detection of the parent ion $CH_3SiCl_3^+$ in the femtosecond mass spectra while in the nanosecond mass spectra it was not observed. The effect of experimental parameters (laser energy, laser focusing) in the time of flight spectrometer on ionization (peak signal) were investigated. The results obtained in this study demonstrate that by increasing laser energy the ion peak signal also increases. Also, the delay time between the laser pulse and the gas pulse had to be set appropriately to give the optimum signal which was found to be between 400 and 900 μs for the nanosecond laser and 0.6 to 2 ms for the femtosecond laser. The results showed that the best focusing position of the laser beam, using a lens to adjust the focus that gives optimum peak intensities, is between 0 and 1 mm for both the nanosecond and the femtosecond lasers.

OPSOMMING

Silikonkarbied (SiC) word deur 'n chemiese damp deponeringsproses uit metieltrichloorsilaan gevorm [Osterhold et al., 1994]. Silikonkarbied is een van die belangrike verbindings vir die korrelbed modulêre reaktor (PBMR) se proses, waar dit as 'n bedekkingslaag in die korrel van die brandstofsel gebruik word. Om die huidige chemiese damp deponeringsproses van PBMR te verbeter moet die proses waardeur die silikonkarbiedlaag gevorm word, beter verstaan word. Molekulêre meganika, semi-empiriese, Hatree-Fock en Moller-Plesset modellerings-berekeninge is deur die Spartan modeleringsprogram gedoen om inligting te bekom oor die molekulêre struktuur en eienskappe van die CH_3SiCl_3 molekule. Die elektrondigthede, energieprofiele vir rotasie asook die infrarooi spektra is bereken deur verskillende basisstelle te gebruik (MMFF, DFT, 3-21G en STO-3G). Die resultate is bevestig deur eksperimentele UV/Sigbare, FT-IR en Raman spektroskopie.

Die nanosekonde en femtosekonde laser aktivering en ionisasie tegnieke is gebruik om metieltrichloorsilaan molekules te ioniseer by 795 nm en 397.5 nm van die femtosekonde laser. Die nanosekondelasers wat gebruik is, sluit die Nd:YAG laser by 266 nm, sowel as die verstelbare kleurstoflaser by 212.5 nm in. Die belangrikste verskil tussen die nanosekonde en femtosekonde laser ionisasie is die waarneming van die ouerioon, $CH_3SiCl_3^+$ in die femtosekonde massa spektra, terwyl dit nie in die nanosekonde se massa spektra voorkom nie. Die uitwerking op ionisasie van eksperimentele parameters (laserenergie, laserfokus) in die vlugtydspektrometer is ondersoek. Die resultate van hierdie studie demonstreer dat deur die laserenergie te verhoog, die ioonpiek ook vergroot word. Die tyd tussen die laserpuls en die gaspuls moes ook so gestel word dat 'n optimale sein verkry is. Hierdie tydsverloop is vasgestel as tussen 400 en 900 μs vir die nanosekondelaser en as tussen 0.6 en 2 ms vir die femtosekondelaser. Die resulate het getoon dat die beste fokusposisie van die laserstraal, as 'n lens gebruik word om dit aan te pas vir optimum piek intensiteitwaardes, is tussen 0 en 1 mm vir beide die nanosekonde en femtosekonde lasers.

CONTENTS

CONTENTS

LIST OF ABBREVIATIONS

Ar	:	Argon
ArF	:	Argon fluoride
AM	:	Austin model
BBO	:	Beta barium borate
B3LYP	:	Becke-three-parameter Lee Yang and Parr
CPA	:	Chirped pulse amplifiers
3D	:	Three dimensional
DFT	:	Density Functional Theory
et al.	:	And others
FTIR	:	Fourier transform infrared
GC	:	Gradient corrected
GGA	:	Generalized gradient approximation
GTO	:	Gaussian type orbital
HCl	:	Hydrogen chloride
He	:	Helium
HOMO	:	Highest occupied molecular orbitals
IP	:	Ionization potential
IR	:	Infrared
KBr	:	Potassium bromide
KrF	:	Krypton fluoride
LDA	:	Local density approximation
LCAO	:	Linear combination of atomic orbitals
LiF	:	Lithium fluoride
LUMO	:	Lowest unoccupied molecular orbitals

MCP	:	Micro channel plate
MMFF	:	Molecular mechanics force field
MNDO	:	Modified neglect of differential overlap
MTS	:	Methyltrichlorosilane
MP	:	Moller Plesset
MPI	:	Multiphoton ionization
MPID	:	Multiphoton ionization dissociation
NaCl	:	Sodium chloride
Nd:YAG	:	Neodymium-doped yttrium aluminium garnet
Nd:YLF	:	Neodymium doped yttrium lithium fluoride
$Nd:YVO_4$	:	Neodymium doped yttrium ortho vanadate
NIR	:	Near infrared
PM3	:	Parameterized Model number 3
PMT	:	Photomultiplier tube
REMPI	:	Resonance enhanced multiphoton ionization
RHF	:	Restricted Hartree-Fock
SiC	:	Silicon carbide
STO	:	Slater type orbital
STO-NG	:	Slater type orbital number of Gaussian type orbitals
%T	:	Percentage transmittance
TOF-MS	:	Time of flight mass spectrometry
US OSHA Hazcom	:	United States Occupation, Safety and Health Administration hazard communication
UV	:	Ultraviolet
UV/VIS	:	Ultraviolet/Visible
Xe	:	Xenon

SYMBOLS FOR UNITS

Å	:	Angstrom
atm	:	Atmosphere
°C	:	Degrees Celsius
cm^{-1}	:	Per centimeter
eV	:	Electron volt
fs	:	Femtosecond
Hz	:	Hertz
J	:	Joule
J/mol	:	Joule per mol
K	:	Kelvin
Kcal/mol	:	kilocalorie per mol
kV	:	Kilo volt
MHz	:	Mega Hertz
mJ	:	Millijoule
mm	:	Millimeter
ms	:	Millisecond
mV	:	Millivolt
nm	:	Nanometer
%	:	Percentage
ps	:	Picoseconds
s^{-1}	:	Per second
μm	:	Micrometer
μs	:	Microsecond
W	:	Watt

Chapter 1

Introduction

1.1 Problem statement

The Pebble Bed Modular Reactor (PBMR) is a high pressure reactor which is currently being proposed for use in South Africa. The PBMR technology could provide South Africa with competitive power generation because it is considered as the leader of the next generation of nuclear energy systems [http://www.pbmr.co.za/]. The challenge in the nuclear industry is to regularly improve designs in order to provide safer, cleaner and more economical utilisation of nuclear power as an energy source. The PBMR (Pty) Ltd was formed by Eskom, South Africa's largest energy producer, with the cooperation of the South African Industrial Development Corporation, British Nuclear Fuels, and the Exelon Corporation [http://www.pbmr.co.za/].

Currently, South Africa has only one nuclear power plant which produces less than 10% of the country's electricity [http://www.pbmr.co.za/]. The rest of the power is produced by coal power plants located far away from the coast. This presents a problem, as most of the future growth of South Africa is expected to happen near the coast. Cape Town currently requires the majority of its power to be transmitted from power plants 1400 km away, which requires expensive and complicated transmission systems. To add to this, South Africa is expected to exceed its current electrical generation capacity dramatically starting from 2008 and the majority of the nation's coal power plants are scheduled to be shut down around 2025.

The PBMR could play a vital role to help meet the country's energy requirements from the next decade onwards. Its safe characteristics and positive attributes from an environmental point of view, add interest to the development of this technology. The country needs a way to generate power for the future, not from coal power plants, and that is how the development of the PBMR came about.

The study of the methyltrichlorosilane (MTS) molecule is of particular interest because it is the main precursor in the chemical vapour deposition process to form silicon carbide (SiC). Silicon carbide is one of the important compounds for the Pebble Bed Modular Reactor (PBMR) process, because it is used as a coating film in the kernel of their fuel cell.

For the current chemical vapor deposition process to be improved, the process of the formation of the silicon carbide layer from MTS must be fully understood. The first aim of the research project is to gain more information about the molecule and its structure, that involves the study of MTS molecule by laser ionization and to reveal ionization and dissociation processes of the molecule and, additionally, to interpret characteristic ionization and fragmentation of the molecule.

A lot of work has been done by different groups to study the MTS molecule. Mousavipour et al. [2004], studied the decomposition of methyltrichlorosilane in a flow system, whereby the products were measured by gas chromatography. Allendorf and Melius [1993] studied the thermochemistry of MTS. Osterhold and co-workers [1994] studied the dissociation reaction of MTS theoretically. Figure 1.1 shows the structure of methyltrichlorosilane molecule.

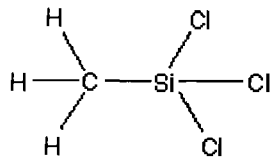

Figure 1.1 Chemical structure of the methyltrichlorosilane molecule

1.2 Physical and chemical properties of methyltrichlorosilane.

Methyltrichlorosilane also known as trichloromethylsilane, methylosilicochloroform and methylsilyl. Trichorosilane is derived from 1,1,1-trichloroethane by the replacement of a carbon with a silicon atom. The larger size of Si makes the CH_3SiCl_3 molecule less globular than 1,1,1-trichloroethane, so that the shape of the molecule is more tetrahedral [Prystupa et al., 1990]. Methyltrichlorosilane is a colourless liquid at room temperature with an acidic odour.

Methyltrichlorosilane is very harmful and hazardous as it produces carbon dioxide, carbon monoxide, oxides of sulphur and hydrogen chloride gas during decomposition. On contact with air methyltrichlorosilane emits corrosive fumes of hydrogen chloride [http://cameochemicals.noaa.gov/chemical/3974]. On contact with the skin or eyes it causes severe burns and it is a highly flammable liquid and vapour [http://cameochemicals.noaa.gov/chemical/3974]. It reacts violently with water, steam, moist air, alcohols, acetone and light metals with generation of heat and combustible hydrogen gas and corrosive hydrogen chloride gases. Methyltrichlorosilane reacts vigorously with water to generate gaseous hydrogen chloride as shown in the reaction [Armour, 2003]:

$$CH_3SiCl_3(l) + 3H_2O(l) \rightarrow CH_3\,Si(OH)_3 + 3HCl_3(g)$$

1.3 Uses of methyltrichlorosilane

Chlorinated organosilanes have several industrial applications. They serve as precursors to poly-dimethyl siloxanes, with applications ranging from dielectric media to hydraulic fluids and lubricants [Osterhold et al., 1994]. Methyltrichlorosilane is also commonly used in chemical vapour deposition processes used to produce SiC coatings, thin films, composites and powders [Osterhold et al., 1994]. It was discovered that the reactivity of chlorinated organosilicon compounds differs from simple organosilanes because Si-Cl (111-118 kcal mol^{-1}) bonds are stronger than either Si-H (90-95 kcal mol^{-1}) or Si-C (90-94 kcal mol^{-1}) bonds [Osterhold et al., 1994].

Methyltrichlorosilane is the most common reactant used in the process of producing silicon carbide, because it is non-pyrophoric and inexpensive. Pyrophoric chemicals are defined in the US OSHA Hazcom (United States Occupation Safety and Health Administration hazard communication) as chemicals which will ignite spontaneously in air at a temperature of 130 °F (54.4 °C) or below. Applications of silicon carbide include heat sinks and plates in power electronic systems for cars or in electrical engineering. In the pebble bed modular reactor (PBMR) silicon carbide layers are used, as it is deposited onto graphite in the small fuel kernels. For the PBMR fuel, small Uranium dioxide balls are run through a Chemical Vapour Deposition (CVD) furnace in an argon environment at a temperature of 1 000° C (1 832° F) Layers of specific chemicals are added to the kernel with extreme precision. The first layer deposited on the kernel is porous carbon. This is followed by a thin coating of pyrolitic carbon (a very dense form of carbon), a layer of silicon carbide and finally, another layer of pyrolitic carbon. Xu et al. [2001] measured the mechanical properties of silicon carbide under bending, shear and impact loading. Silicon carbide has the following special properties:

- High toughness: flexural strength of 860 MPa at room temperature and 1010 MPa at 1300 °C.
- Shear strength of 67.5 MPa
- Excellent impact resistance and extreme fracture toughness of 36.0 kJ m^{-2}.

Silicon carbide almost matches diamond in its hardness, and it is converted from coke and quartz at temperatures from 1600 to 2500 °C.

1.4 Previous studies of the decomposition reactions of methyltrichlorosilane

Papasouliotis et al. [1994] and Osterhold et al. [1994] studied the kinetics of thermal decomposition of MTS. It was reported that MTS decomposes under chemical vapour deposition conditions producing HCl, SiHCl, SiCl, and CH as well as other silanes and hydrocarbons as shown in the following proposed reactions [Osterhold et al., 1994]:

$$CH_3SiCl_3 \rightarrow CH_3\bullet + \bullet SiCl_3 \qquad (1)$$

$CH_3SiCl_3 \rightarrow CH_2SiCl_3\bullet + \bullet H$ (2)

$CH_3SiCl_3 \rightarrow CH_3SiCl_2\bullet + \bullet Cl$ (3)

$CH_3SiCl_3 \rightarrow H_2C\text{-}\ SiCl_2\bullet + \bullet HCl$ (4)

$CH_3SiCl_3 \rightarrow CH_3Cl\bullet + \bullet SiCl_2$ (5)

$CH_3SiCl_3 \rightarrow CH_3SiCl\bullet + \bullet Cl_2$ (6)

Josiek and Langlais [1996] studied the residence time dependent kinetics of chemical vapour deposition growth of silicon carbide in the MTS/H_2 system. They suggested the precursors $SiCl_3$ and CH_3 are formed by decomposition of MTS (reaction 1). They suggested $SiCl_2$, C_2H_2 or C_2H_4 are dominant reactive source species in the reaction. They concluded that $SiCl_3$ adsorbs more strongly on surface sites than $SiCl_2$, therefore at low residence times and temperatures the gas phase concentration of $SiCl_2$ should be lower than that of $SiCl_3$.

Allendorf and Melius [1993] reported reaction enthalpies for several possible decomposition pathways for methyltrichlorosilane and these are summarised in table 1.1. A favourable path is reaction 1, whereby the methyl radical and trichlorosilyl radical are formed.

Ge et al. [2007] discovered that reactions (1) to (3) are simple bond cleavage reactions with no transition states. The forward Gibbs free energies of activation for these three reactions were reported as 383, 423 and 454 kJ/mol at 0 K, respectively. At 1400 K the free energies are 159, 215 and 255 kJ/mol respectively. The decrease is due to the entropy increase when methyltrichlorosilane dissociates [Ge et al., 2007]. The Arrehnius factors are determined from the Arrehnius equation: $k = A \exp(-Ea/RT)$ where k is the rate coefficient, A is the pre-exponential factor constant, E_a is the activation energy, R is the universal gas constant, and T is the temperature (in degrees Kelvin). Reactions 1 to 3 have high A-factors of about 10^{16} s^{-1}. The least favourable pathway is reaction 3, which involves the breaking of strong Si-Cl bonds [Osterhold et al., 1994].

Methyltrichlorosilane can also undergo 1,2-elimination of HCl to produce CH_2SiCl_2 as shown in reaction (4). The HCl elimination reaction has the lowest energy of activation among all six reactions at 0 K which is 351 kJ/mol and 153 kJ/mol at 1400 K [Ge et al., 2007]. The fifth reaction of methyltrichlorosilane is a three centered Cl-shift reaction, in which a Cl atom shifts from Si to C along with Si-C cleavage to form CH_3Cl and $SiCl_2$. The free energy of activation for the reaction is 456 kJ/mol at 0 K and 422 kJ/mol at 1400 K [Ge et al., 2007].

Reaction 6 is also the least favourable pathway which involves the breaking of strong Si-Cl bonds [Osterhold et al., 1994]. Reaction 6 has lower A-factors of 10^{12} -10^{15} s^{-1} [Osterhold et al., 1994]. Reaction 6 is a two step reaction: CH_3SiCl_3 first undergoes an isomerism reaction to form CH_3SiCl_2Cl with a Si-Cl-Cl bridge, then CH_3SiCl_2Cl looses Cl_2 to form CH_3SiCl [Ge et al., 2007]. Bessmann et al. [1992] measured the deposition rate of silicon carbide on carbon coated fibres from methyltrichlorosilane in hydrogen as a function of temperature, pressure and total flow rate. In their study they reported the overall reaction as reaction 7. They did not take into account the mechanism of pyrolysis of MTS.

$$CH_3SiCl_3 \rightarrow SiC + 3HCl \qquad (7)$$

Mousavipour et al. [2004], studied the thermal decomposition of methyltrichlorosilane and measured the yields of products by gas chromatography. In their study they suggested mechanisms which showed a large amount of $SiCl_2$ produced during the initial steps of the decomposition of MTS. They proposed that further studies are necessary to investigate the role of $SiCl_2$ in the formation of the SiC film. They then concluded 'it is difficult to suggest a reliable mechanism for the formation of SiC film on the surfaces'.

Table 1.1 Enthalpies of reaction for pathways in the decomposition of CH_3SiCl_3 [Allendorf and Melius, 1993]

No.	Reaction	$\Delta H_r°$ (kJ/mol)
1.	$CH_3SiCl_3 \rightarrow CH_3\bullet + \bullet SiCl_3$	404
2.	$CH_3SiCl_3 \rightarrow CH_2SiCl_3\bullet + \bullet H$	428
3.	$CH_3SiCl_3 \rightarrow CH_3SiCl_2\bullet + \bullet Cl$	477
4.	$CH_3SiCl_3 \rightarrow H_2C\text{-}\ SiCl_2\bullet + \bullet HCl$	341
5.	$CH_3SiCl_3 \rightarrow CH_3Cl\bullet + \bullet SiCl_2$	341
6.	$CH_3SiCl_3 \rightarrow CH_3SiCl\bullet + \bullet Cl_2$	56

1.5 Symmetry of methyltrichlorosilane

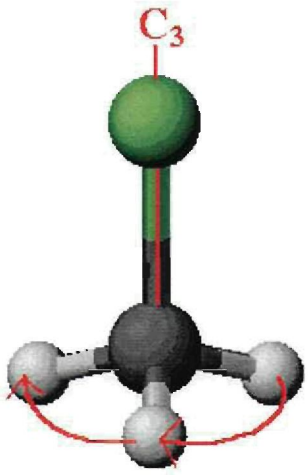

Figure 1.2 The Methylchloride molecule [Tafesse, 2007]

A molecule is said to possess a symmetry element if the corresponding symmetry operation transforms it into a shape which is indistinguishable from the original

[Tafesse, 2007]. The motion around a point or a plane that leaves a molecule the same is called a symmetry operation. An example of a symmetry operation on a tetrahedral molecule methylchloride (CH_3Cl) is shown in figure 1.2. The rotation by 120 ° around the C_3 axis of the CH_3Cl molecule leaves the molecule unchanged. C_3 is one of the symmetry elements of methyltrichlorosilane. The set of symmetry elements possessed by a particular molecule determines the point group to which the molecule belongs. It is convenient to classify molecules with the same set of symmetry elements by a label. This label summarizes the symmetry properties.

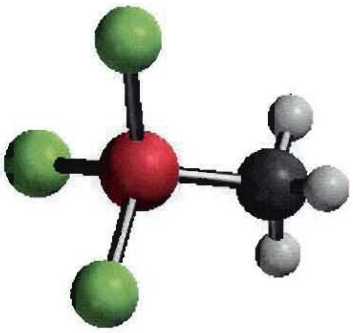

Figure 1.3 The ball and stick representation of a methyltrichlorosilane molecule

Molecules with the same label belong to the same point group, e.g. all tetrahedral molecules (such as methyltrichlorosilane and methylchloride) belong to the C_3 point group irrespective of their chemical formula. Associated with each point group is a character table. Methyltrichlorosilane belongs to the point group C_{3v} and has two possible conformations i.e. a staggered and an eclipsed form. The molecule possesses 8 atoms and has 18 normal modes of vibrations belonging to the following irreducible representations: $5A_1+1A_2+6E$ [Soliman et al., 1983]. The representation can be explained as 5 symmetric vibrations, three stretching and two deformation vibrations belonging to the A_1 representation; six doubly degenerate vibrations belonging to the E representation and a twisting vibration that belongs to the A_2 representation, which is the torsion mode about the Si-C axis. The $5A_1$ and 6E modes are all infrared and Raman active whereas the $1A_2$ is both infrared and Raman inactive. The distribution of normal modes of methyltrichlorosilane according to their symmetry are summarized in table 1.2

Table 1.2 The normal modes of methyltrichlorosilane placed according to symmetry species [Soliman et al., 1983].

Vibration	symmetry species	A_1	A_2	E
Stretching	CH	ν_1		ν_6
	SiC	ν_3		
	SiCl	ν_4		ν_9
Deformation	CH_3	ν_2		ν_7
	CH_3			ν_8
	$SiCl_3$	ν_5		ν_{10}
	$SiCl_3$			ν_{11}
Torsion	$SiCl_3$		ν_{12}	

1.6 Previous Raman and Infrared absorption studies

Methyltrichlorosilane was condensed with excess argon on the CsI backing of an optical helium cryostat at 15-20 K [Svyatkin et al., 1977]. The IR spectra were recorded using a Hitachyi-225 spectrometer with a resolution better than 0.5 cm^{-1} [Svyatkin et al., 1977]. Only the ν_{10} vibration which is the antisymmetric stretching vibration of Si-Cl at 580 cm^{-1} was assigned. The observed frequencies are summarized in table 1.3.

Table 1.3 Observed vibration frequencies of CH_3SiCl_3 molecule [Svyatkin et al., 1977]

Vibration frequencies cm^{-1}	Symmetry of vibrations
2992	E
2922	A_1
1416	E
1272	A_1
804	E
763	A_1
580	E
458	A_1
229	E
229	A_1
163	E

Burnelle and Duchesne, (1952) recorded spectra on a Perkin-Elmer spectrometer using NaCl and KBr prisms, and on a Beckman spectrometer equipped with LiF optics. Measurements were made on the substance in both gaseous and dissolved states. The observed wavenumbers of methyltrichlorosilane are summarized in table 1.4.

Table 1.4 Assignment of fundamentals of CH_3SiCl_3 [Burnelle and Duchesne, 1952]

Normal modes	Notation	IR ν in cm^{-1}	RAMAN ν in cm^{-1}
CH stretching	$\nu_1(a_1)$	2915	------
CH_3 deformation	$\nu_2(a_1)$	1271	------
SiC stretching	$\nu_3(a_1)$	764	761
Si-Cl stretching	$\nu_4(a_1)$	457	450
$SiCl_3$ deformation	$\nu_5(a_1)$	------	229
twisting	$\nu_6(a_2)$	------	------
CH stretching	$\nu_7(e)$	2987	------
CH_3 deformation	$\nu_8(e)$	1416	------
CH_3 rocking	$\nu_9(e)$	807	------
Si-Cl stretching	$\nu_{10}(e)$	578	576
$SiCl_3$ deformation	$\nu_{11}(e)$	------	164
$SiCl_3$ rocking	$\nu_{12}(e)$	------	229

Table 1.5 Observed IR and Raman wavenumbers (cm^{-1}) for methyltrichlorosilane- [Qtaitat and Mohamad, 1994]

IR				Raman				Assignment		
Gas	Rel int	solid	Rel int	Gas	Rel int	Liquid	Rel int & dopol.	solid	Rel int	ν_i Approximate description
2993	w			2987	w		vw,p	2974	vw	
2980	w	2975	vw	2973	w	2977	vw,p			
				2949	vw	2965	vw,p			Isotopic impurities
2933	m			2932	w	2938				
				2978	w					$\nu_1+\nu_{12}$
				2006	w	1994	vw,p	1994	w	$2\nu_2$
1215	w	1200	m			1204	vw,p	1205	vw	$2\nu_{10}$
1136	m									
1113	m	1110	m							
1027	m									
1008	sh									
760	m	752	w							$\nu_{10}+\nu_{12}$or isotopic impurity
		706	w							
694	m	693	m							$\nu_9+\nu_{12}$ iso imp
		682	w							
668	s	653	s							ν_3 Si-C stretch
644	s	645	s							$\nu_4+\nu_5$
548	s	545				546	vw,dp	546	w	ν_9 a-stretch
445R								444	s	
443Q	s	440	m	443	s	441	s,p	442	s	$2\nu_{11}$
440P		437	w							
		434	vw							
		425	vw					427	vs	
		422	w	425	vs	426	vs,p	423	vs	ν_4SiCl_3 sy-defor
		419	vw					420	m	
				292	vw					$2\nu_{12}$
				272	vvw					$2\nu_6$
				258	w	261	vw,p	265	vw	Impurity?
229R		230	m					231	w	
214Q	vs	220	s	221	s	221	s,dp	222	s	ν_5 sy-deform
221P				216	s					

Table 1.5 continues

IR				Raman						Assignment
Gas	Rel int	solid	Rel int	Gas	Rel int	Liquid	Rel int & dopol.	solid	Rel int	ν_i Approximate description
		207	m					207	w	ν_{11} $SiCl_3$ rock
				154	s			156	s	
149	vw	161	vw	146	s	150	s,dp	152	s	ν_{12} a-deform
				140	s					
136				136						
								118	vw	
								79	vw	
								68	vw	
								59	vw	Lattice modes
								51	vw	
								44	vw	

s, strong; m, moderate; w, weak; v, very; bd, broad; sh, shoulder; p, polarised; dp, depolarised; rel int, refer to relative intensity; *A, B* and *C* refer to IR band envelopes; P,Q and R refer to rotational- vibrational branches.

The vibrational frequencies of CH_3SiCl_3 in the vapour state was first reported by [Qtaitat and Mohamad, 1994], and are summarized in table 1.5.

Figure 1.4 shows the Raman spectra of the vapour (A), liquid (B) and solid (C) phases of CH_3SiCl_3. In the Raman spectrum of gaseous CH_3SiCl_3 there are two strong bands between 2900 and 3000 cm^{-1}. The CH_3 asymmetric and symmetric deformations occur at 1418 cm^{-1} and 1272 cm^{-1} The CH_3 rocking mode occurs at 802 cm^{-1}.

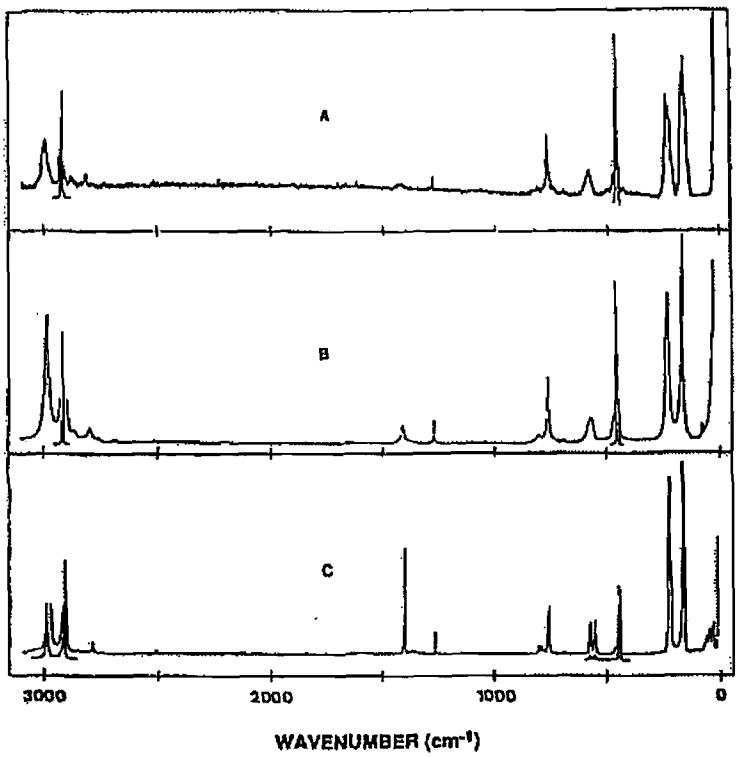

Figure 1.4 Raman Spectra of methyltrichlorosilane: (A) gas, (B) liquid, and (C) solid [Qtaitat and Mohamad, 1994]

The $SiCl_3$ symmetric and asymmetric stretches were observed occurring at 454 cm^{-1} and 580 cm^{-1} respectively. The SiCl rocking mode was observed at 221 cm^{-1} for CH_3SiCl_3. The torsional (internal rotation) vibration was not observed in either the Raman or the IR spectra of CH_3SiCl_3, as is expected for an A_2 mode which is the torsion mode about the Si-C axis and is forbidden to be observed in infrared and Raman spectra.

1.7 Aims of the study

Despite extensive research on the dissociation reactions and pyrolysis of the methyltrichlorosilane molecule, the photochemistry of MTS has remained relatively unexplored. The aims of this research project are twofold. Firstly, the aim was to study the molecule by performing modelling calculations using the Spartan program. Molecular modelling using Spartan program was employed to obtain a better

understanding of the molecular structure of MTS. Calculations of the FT-IR spectra, bond lengths and bond angles as well as the dipole moment are of importance.

The second focus of this work was to measure the infrared and Raman spectra and setup a laser multiphoton ionization experiment, using nanosecond and femtosecond laser systems. Molecular spectroscopy measurements including UV/Vis measurements, FTIR and Raman measurements were carried out in order to characterize the molecule further.

1.7.1 Methods and Approach

Nanosecond and femtosecond laser ionization of the MTS molecule was studied. The ionization process and product formation was analyzed using the time of flight mass spectrometry (TOF-MS) technique. The Nd:YAG laser at 266 nm wavelength, as well as a tuneable dye laser, which is frequency doubled into the deep UV region at 212.5 nm was used to study ionization. Femtosecond laser ionization or dissociation in the gas phase was also investigated using the 795 nm and the 397.5 nm wavelengths from a femtosecond laser system and ion products formed measured using the time of flight mass spectrometry technique.

The effect of different experimental variables using the time of flight mass spectrometry technique was studied. In particular the effect of laser energy on ionization (mainly peak signal) was investigated. Also the effect of varying delay time between the gas pulse and the laser pulse on peak signal was investigated. The experimental parameters were studied in order to optimise the system and to reveal the best working conditions of the system during ionization of MTS. The differences observed between the time of flight mass spectra obtained using the nanosecond and femtosecond laser was investigated.

1.7.2 Characterization

Various spectroscopic techniques will be used to characterize the MTS molecule and these include:

- UV/Vis spectroscopy
- FT-IR spectroscopy
- FT-Raman spectroscopy
- Time of flight mass spectrometry
- Nanosecond laser ionization
- Femtosecond laser ionization

Chapter 2

Molecular modelling

2.1 Introduction

Crystallography is the foundation for the development of molecular modelling. Using X-ray crystallography, chemists are able to determine the structures and bonding arrangements of molecules, including the structures of large complex molecules such as proteins and DNA. Chemists have many tools available to visualize the three-dimensional structure of molecules. The most popular are physical models such as Dreiding stick models, which are similar to the ball and stick models used in chemistry [Höltje et al., 2003]. Dreiding stick models became famous because they contained all the knowledge of the structure of molecules in chemistry in the 1960's. Prefabricated modular elements, such as different nitrogen atoms with correct number of bonds and angles corresponding to their hybridization states, made it possible to build up exact three dimensional (3D) models of the crystal structures. In the 1970's the 3D description of a molecule, colour coded and rotatable was possible on the computer screen. Virtual Dreiding models were created. Consequently mathematical modelling techniques were employed for the computation of physical states and their prediction.

Molecular modelling is a means to predict the structure of a molecule using a set of mathematical and chemical rules. The techniques are used in the fields of computational chemistry, computational biology and materials science for studying molecular systems ranging from small chemical systems to large biological molecules and material assemblies. The simplest calculations can be performed by hand, but computers are required to perform molecular modelling of any reasonably sized system. The common feature of molecular modelling techniques is the description of the molecular systems; the lowest level of information is individual atoms (or a small group of atoms). The benefit of molecular modelling is that it reduces the complexity

of the system, allowing many more particles (atoms) to be considered during simulations [http://en.wikipedia.org/wiki/Molecular_modelling].

Molecular modelling reduces the cost of research by limiting the number of physical experiments needed to be performed. By having a reasonable idea of the structure of a molecule, a researcher will know if a molecule will be useful for the goals of the research or if another molecule should be tested. A variety of modelling methods may be used in molecular modelling. They are Molecular Mechanics, Semi Empirical, Hartree-Fock and Density functional methods. The method to be used depends on the molecule that is being tested. Each of the molecular modelling methods has its strengths and weaknesses and is parameterized and optimized for different types of molecules. Some examples of the things to be considered when selecting a modelling method are; organic vs. inorganic molecules, metals and transition metals, periodic row of the atoms in the molecule and the ionic character of the molecule [http://www2.lv.psu.edu/jbe10/research/spartan/index.html].

The various molecular modelling methods use chemical theories and/or mathematical methods such as,
Huckel's rule, molecular orbital theory, quantum mechanics, Schrödinger's equation, and wave functions http://www2.lv.psu.edu/jbe10/research/spartan/index.html].
By performing calculations using all the molecular modelling methods the following can be calculated: bond angle, bond lengths, infrared spectrum, energy profile and dissociation energies for bonds in molecules. Theoretical measurements obtained can then be compared to experimental data and literature data available. Vibrational energies of the molecule in its ground state can be determined using modelling calculations, the representation of orbitals, electron densities and energy profiles for vibrations and rotations can be calculated as well as the transition states for reactions.

2.2 Basis sets

Basis sets are the sets of mathematical functions used to describe various atomic and molecular orbitals and their characteristics.

2.2.1 Minimal basis sets

Basis sets were first developed by J.C Slater, he invented the Slater Type Orbitals (STO's) that were used as basis functions due to their similarity to atomic orbitals of the hydrogen atom [http://www.shodor.org/chemviz/basis/index.html]. The term basis function was used instead of atomic orbital but it has the same meaning. The STO-NG (where N represents the number of GTOs (Gaussian Type Orbitals) combined to approximate the STO) are named "minimal" basis sets. The STO-3G minimal basis set is a gauss type basis set developed by combining 3 Gauss type functions(3G) to substitute a Slater type orbital (STO).

2.2.2 Extended basis sets

There are several types of extended basis sets, n- zeta (double zeta, triple zeta, quadruple zeta), polarized basis sets and diffuse basis sets [Spartan ´06, 2006]. Double zeta basis sets means two basis function for each atomic orbital that would be occupied in the ground state of a particular atom, therefore each atomic orbital is expressed as the sum of two STOs. Triple zeta and quadruple zeta basis sets work in the same way as the double zeta basis set, except that three or four basis function are used for each atomic orbital of an atom. The n-zeta calculation is done only for the valence orbital. Split valence basis sets may be introduced where there is a need to do calculations involving the inner shell electrons. Examples of Split-valence basis sets are 3-21G, 4-31G, and 6-31G. Looking at the 3-21G basis set, the 3 is used to describe gaussians for the inner shell orbital, the 2 describes gaussians for the first STO of the valence orbital and the 1 describes gaussian for the second STO.

Polarized basis sets can be explained as minimal or split valence basis sets that have polarization functions. In the minimal and n-zeta basis sets atomic orbitals were treated as existing only as individual orbitals for example 's', 'p', 'd' and 'f' . A better approximation is to account for the fact that sometimes orbitals share qualities [Spartan ´06, 2006]. As atoms are brought close together, their charge distribution causes a polarization effect (the positive charge is drawn to one side while the negative charge is drawn to the other) which distorts the shape of the atomic orbitals. In this case 's' orbitals begin to have a little of the 'p' characteristics and 'p' orbitals

begin to have a little of the 'd' characteristics. One asterisk (*) at the end of a basis set denotes that polarization has been taken into account in the 'p' orbitals, for example 6-31G* is a polarized split valence.

Diffuse basis sets are indicated by a '+' or 'aug' at the end of a basis set (6-31+G*) and are used where anions and intermolecular interactions should be taken into account.

2.3 Molecular modelling methods

A three dimensional model of a given molecule does not have an ideal geometry, thus after drawing a molecule in a modelling program, molecular structures should always be geometrically optimized using the minimum energy of the specific geometric state so that the molecule can be correctly represented in the three dimensional space. In the minimization procedure the molecular structure will be relaxed. This is normally done by applying a molecular mechanics method.

2.3.1 Molecular Mechanics method

Molecular mechanics is a computational method used to calculate molecular geometries and energies [Höltje et al., 2003]. Unlike quantum mechanical approaches the electrons and nuclei of the atoms are not included in the calculations. Molecular mechanics considers the atomic composition of a molecule to be a collection of masses interacting with each other via harmonic forces. The atoms in molecules are treated as rubber balls of different sizes joined together by springs of different lengths. Hooke's law is used to calculate the potential energy. In the calculation the total energy (E_{tot}) is minimized with respect to atomic coordinates where:

$$E_{tot} = E_{str} + E_{bend} + E_{tors} + E_{vdw} + E_{elec} + \ldots\ldots$$

where E_{str} is the bond stretching energy term, E_{bend} is the angle bending energy term, E_{tors} is the torsional energy term, E_{vdw} is the van der Waals energy term and E_{elec} is the electrostatic energy term [Höltje et al., 2003]. These equations together with the data required describing the behaviour of different kinds of atoms and bonds is called a force field.

Using molecular mechanics, calculations for large molecules can be done within a short time [http://www2.lv.psu.edu/jbe10/research/spartan/index.html]. The important

application of the molecular mechanics model is conformational searching for molecules with many degrees of freedom [Spartan '06, 2006]. It contains the simplest computational methods using SYBYL and MMFF force fields. The MMFF (molecular mechanics force field) is known to assign equilibrium conformation in a variety of molecules for which experimental data are available [Spartan '06, 2006]. It can be used for molecules containing more than 1000 atoms to perform fast conformational analysis. It also provides a reasonable account of conformational energy differences in larger organic molecules as obtained from high level quantum chemical calculations. Disadvantages of molecular mechanics force field calculations are that the models are not suitable for thermochemical
calculations and the parameters are not developed for inorganic systems. [http://www2.lv.psu.edu/jbe10/research/spartan/index.html]. SYBYL force fields work in the same way as MMFF but have an improved set of parameters for second row or greater elements.

2.3.2 Hartree-Fock method

The Hartree-Fock theory explains that each electron's motion can be described by a single-particle function (orbital) which does not depend on the motions of the other electrons. Hartree-Fock molecular orbital models are derived from the Schrödinger equation by requiring that electrons be treated as independent particles. This is known as the Hartree-Fock approximation [Spartan '06, 2006]. The motions of electrons in molecules (molecular orbitals) are approximated by a sum of motions of electrons in atoms [Spartan '06, 2006]. A second approximation is known as the LCAO or Linear Combinations of Atomic Orbitals approximation, and it distinguishes different Hartree-Fock models.

Hartree-Fock models can be applied for equilibrium and transition state structure determination and thermochemical comparisons (except for reactions involving bond breaking or bond making), and can thus provide information of whether the reaction is strongly or weakly exothermic or weakly or strongly endothermic. It is also able to order the stabilities of isomeric products and to identify the lowest energy tautomer

[Spartan '06, 2006]. Hartree-Fock models with larger basis sets (6-31G*.) provide a good account of the relative stabilities of different conformational arrangements.

2.3.3 Semi empirical methods (quantum based methods)

Methods that are used to try to find solutions for the Schrödinger equation by the Hartree-Fock methods are called *ab initio* methods. In *ab initio* methods the distribution of every electron is calculated. Thus the repulsion between the electrons is ignored, or physically it is assumed that one electron is not affected by the presence of the other electron. The calculations are restricted to the valence shell electrons of the atoms by an approximation of the Hartree-Fock model. This type of molecular model is called a semi-empirical model.

Semi-empirical molecular orbital calculation models have the simplest methods based on quantum mechanics, usable for calculations of geometries of transition states as well as to obtain reaction energies (thermodynamics) and activation energies (kinetics) [http://www2.lv.psu.edu/jbe10/research/spartan/index.html]. Calculations for molecules containing up to 200 atoms can be done with semi empirical methods.

For very large molecules the number of possible overlap integrals of outer orbitals becomes too large. Semi empirical parameters named the MNDO (Modified Neglect of Differential Overlap) were developed to handle or reduce the number of overlap integrals in the Schrödinger equation. MNDO can also handle s and p orbitals but not d orbitals or heavy elements. That is when it became necessary to expand the basis sets to include more interactions and as was done in the Austin model 1(AM1) [Spartan '06, 2006]. The MDNO model was improved to the MDNO number 3, (PM3) with an improved set of parameters to include transition metals.

The semi empirical calculations using the AM1 and PM3 models provide the best molecular geometries. This makes them suitable for evaluation of properties such as polarities in molecules that depend on geometry. The disadvantages of the models are that neither of them can do calculations for molecules containing thousands of atoms, such as proteins. They also cannot calculate relative energies, that may help to conclude whether the molecule is weakly or strongly exothermic, thermo neutral or

weakly or strongly endothermic, or whether one isomeric product of a reaction is likely to be more or less stable than another. Also, neither AM1 nor the PM3 method accounts for conformational energy differences, as would be required to establish if a certain conformer has a good chance at actually being present.

2.3.4 Density functional and Moller-Plesset models

Density Functional Theory (DFT) is an *ab initio* method in which the total energy of a molecule is determined by electron density. Density functional models provide a way to characterize a many electron system in terms of electron density and make it possible to view the electron cloud in three dimensional space [Ghosh et al., 1984]. The density functional methods include the local density approximation method (LDA), which assumes that the energy and density in the given system can be treated as the same as that of a uniform electron gas. The Gradient corrected method (GC) or the generalized gradient approximation (GGA) uses the electron density as well as its gradients or points in the system where density is varying. Hybrid methods are a combination of Hartree-Fock exchange energy, local density approximation and gradient-corrected exchange energies and are used in order to improve performance of a particular molecule. Examples of the hybrid methods are the BLYP and B3LYP. Density functional models are more costly in terms of computation time than Hartree-Fock models. The models make use of the same basis sets as Hartree-Fock models; except that 3-21G and smaller basis sets (minimal basis sets) do not yield satisfactory results [Spartan '06, 2006].

The Moller-Plesset method is an *ab initio* method that improves on the Hartree Fock method by adding an electron correlation effect. For the Hartree-Fock models it was assumed that each electron moves independently from the others. Suppose there are two electrons in space in the Hartree-Fock model, it is assumed that the top electron stays in its position without moving while the bottom electron moves in the circle. In the Moller-Plesset model the top electrons will move away from the bottom electron to avoid excessive repulsion. This lowers the repulsion energy. The Moller-Plesset calculations begin with a Hartree-Fock calculation and subsequently correct for electron-electron repulsion also known as the electronic correlation. When the

correction uses up to second order mathematical functions as corrections, the model is named the MP2 while the use of third and fourth orders are MP3 and MP4 respectively.

The use of these models is to obtain thermochemical data of reactions, especially where bonds are formed or broken, and also to approximate the activation energies.

2.4 Conformational analysis

The changes in molecular conformations can be taken as movements on a multi-dimensional surface that describes the relationship between the potential energy and the geometry of the molecule. Each point on the potential energy surface represents the potential energy of a single conformation. Local minima of this energy surface correspond to stable conformations of a molecule. Well known examples of different conformations are the staggered and eclipsed forms of ethane, the anti-trans and gauche forms of *n*-butane or the boat and chair forms of cyclohexane [Höltje et al., 2003]. The rotation around the C_{sp3}-C_{sp3} bond in the ethane molecule is described as the sine like curve potential function (figure 2.1). The energy minima at 60°, 180° and 300° correspond to the staggered form, while the maxima at 120°, 240° and 360° correspond to the eclipsed form of ethane.

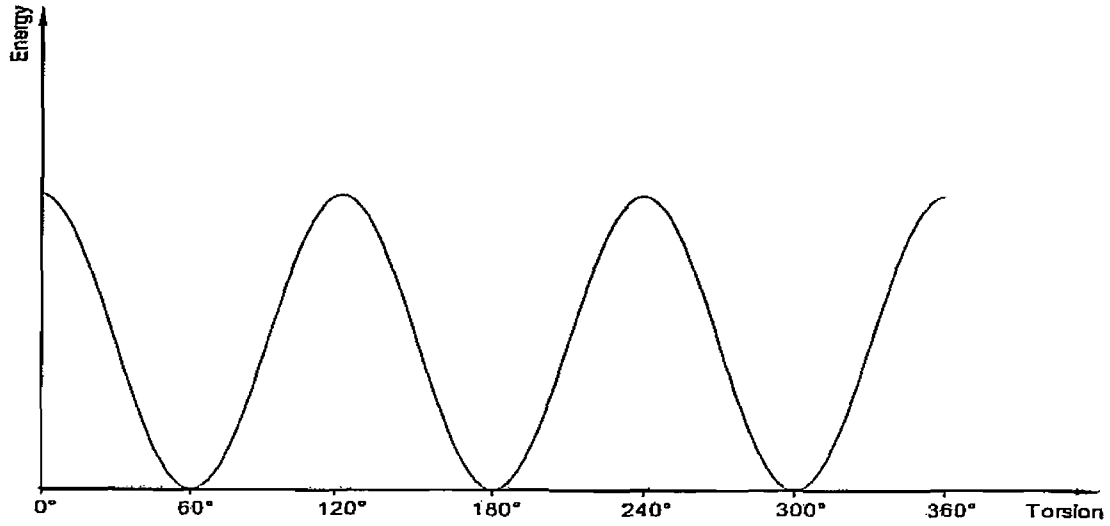

Figure 2.1 Potential energy curve of ethane shown as a function of the dihedral angle [Höltje et al., 2003].

2.5 Spartan modelling program

Spartan, created by Professor Warren Hehre, is a molecular modelling or computational chemistry program, which does high performance computing and art visualization. Spartan provides chemists with theoretical techniques (molecular mechanics, semi empirical method, Hartree-Fock, and DFT quantum mechanics based calculations) for the description of molecular structure, energies and investigation of reaction mechanisms. Spartan displays structural models, orbitals, electron densities and electrostatic potentials as iso-surfaces or slices [http://www2.lv.psu.edu/jbe10/research/spartan/index.html].

Graphical display of highest occupied molecular orbitals (HOMO) and lowest unoccupied molecular orbitals (LUMO) can be done using Spartan. The orbitals describe electron motion in molecules and also provide information about the chemical reactivity of molecules.

2.5.1 Electron density

Electron density is the number of electrons found at a particular point in space [Spartan '06, 2006]. It is usually measured in an X-ray diffraction experiment that is then used to locate atomic positions, with the assumption that most electrons are closely associated with atoms. A space filling model or a Van der Waals surface is generated to represent the positions of most electrons. This is known as electron density and it reveals the overall molecular size and shape of the molecule. Bond density is also important, but it contains fewer electrons in total and it involves atomic connectivity [Spartan '06, 2006].

2.5.2 The electrostatic potential

The electrostatic potential can be described as the interaction of energy of a positive charge with a molecule. It indicates a balance between repulsive interactions involving the positively charged nuclei and attractive interactions involving the negatively charged electrons. Regions where the balance is toward attraction are said

to be electron rich and are subject to attack by electrophiles, while regions where the balance is toward repulsion are said to be electron poor and subject to attack by nucleophiles [Spartan '06, 2006].

The charge distribution in a molecule provides information regarding its physical and chemical properties [Henre et al., 1998]. For example, organic molecules that are charged or polar, tend to soluble in water. Chemical reactions are associated with charged sites, and the most highly charged site in a molecule is often the most reactive site. The type of charge is important, positively charged sites in a molecule are attacked by bases and nucleophiles, while negatively charged sites are subject to attack by acids and electrophiles. Molecular charge distributions can be described by electrostatic potential. The electrostatic potential is defined as the energy of interaction of a point positive charge with nuclei and electrons of a molecule, and the value depends on the location of the point positive charge [Henre et al., 1998]. If the point charge is placed in a positive charge region (an electron poor region), the point charge molecule interaction becomes repulsive and the electrostatic potential is positive. If the point charge is placed in a negative charge region (an electron rich region), the interaction then is attractive and the electrostatic potential is negative [Henre et al., 1998]. This means that by moving the point charge around the molecule a map of molecular charge distribution can be created. The electrostatic potential map paints the value of the potential onto the electron density surface [Spartan '06, 2006].

2.5.3 Previous studies of molecular structure of Methyltrichlorosilane

Hartree-Fock calculations were performed to obtain the optimized structure of MTS, using the program GAUSSIAN 90 with the RHF/3-21G*, RHF/6-31G*, MP2/6-31G* basis sets [Qtaitat and Mohamad, 1994]. The structural optimization was carried out with the parameters taken using the microwave spectroscopic results as input values [Takeo and Matsumura, 1977]. The optimized structural parameters calculated by the utilization of the mentioned basis sets are listed in table 2.1, and are compared with those reported by Takeo and Matsumura, [1977]. As indicated, methyltrichlorosilane has a C_{3v} symmetry with two possible conformations, the staggered and eclipsed forms. It has been found from the *ab initio* calculations that the staggered form is more stable than the eclipsed form by 584 (6.987 kJ/mol), 633 (7.573 kJ/mol), and

712 cm^{-1} (8.535 kJ/mol) using RHF/3-21G*, RHF/6-31G*, MP2/6-31G* basis sets, respectively [Qtaitat and Mohamad, 1994].

The calculated structural parameters with the RHF/3-21G* and RHF/6-31G* basis sets agree within 0.022 Å and 0.3° for the C-H distances and bond angles from the microwave spectroscopic data.

Table 2.1 Comparison of structural parameters, [a] rotational constants (MHz), and dipole moments (Debye) for methyltrichlorosilane as determined using molecular modelling and microwave spectroscopic results [Qtaitat and Mohamad, 1994].

Parameter	Microwave[b]	*Ab Initio*		
	r_s	RHF/321G*	RHF/6-31G*	MP2/6-31G*
r(Si-C)	1.848	1.849	1.858	1.849
r(Si-Cl)	2.026	2.035	2.047	2.042
r(C-H)		1.087	1.085	1.093
<(CSiCl)	110.3	110.4	110.5	110.4
<(SiCH)		110.7	110.5	110.3
<(ClSiCl)	108.6	108.5	108.4	108.5
<(HCH)		108.2	108.5	108.6
A		1758.9	1739.7	1749.8
B	1772.01	1758.9	1739.7	1749.8
C		1314.0	1300.1	1304.1
μ_1	1.91±0.01	2.422	2.469	2.426
-(E+1699)(Hartree)		0.286161	8.150165	8.792494

a) r is bond lengths in Å, < is bond angles in degrees.

b) Values taken from [Takeo and Matsumura., 1977]

2.5.4 Local ionization potential

The local ionization potential shows the ease or difficulty of electron removal (ionization). Like the negative regions of the electrostatic potential, regions of low local ionization potential are likely to be subject to attack by electrophiles.

2.6. Results and discussion

2.6.1 The electrostatic potential map

The electrostatic potential map for methyltrichlorosilane was obtained with the semi empirical calculation and AM1 basis sets. The molecule is represented in figure 2.2a as the ball and sick representation of MTS where the green atoms represent chlorine, the red atom is silicon, the black atom is carbon and the white atoms are hydrogen atoms. Colours towards red represent more negative potentials identifying electron rich regions, while colours towards blue represent positive potentials, identifying electron poor regions. Colours in between (orange, yellow and green) represent intermediate values of the potential. An electrostatic potential map for the trichloromethylsilane molecule show 3 chlorines to be red(indicating electron rich regions) silicon blue and 3 hydrogens between blue and green (indicating electron poor regions).

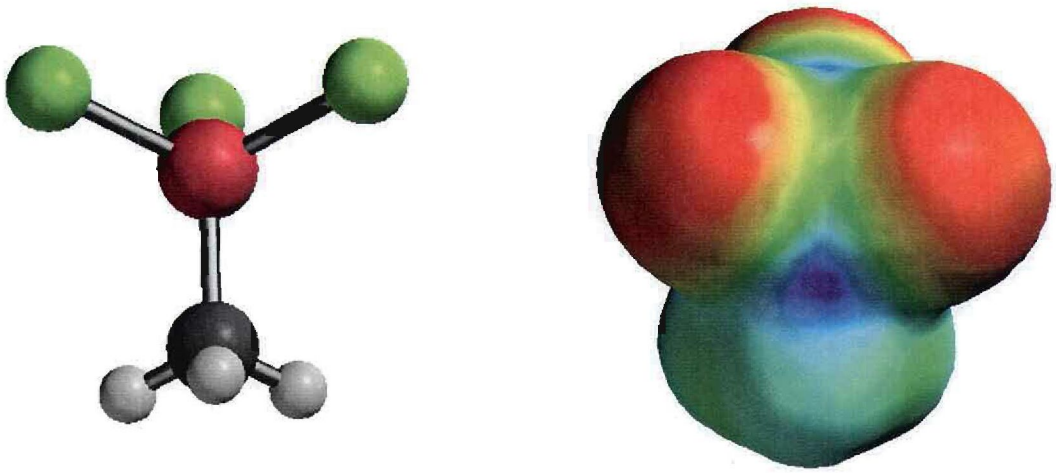

a b

Figure 2.2 (a) Ball and stick model of MTS, (b) Electrostatic potential map of MTS

2.6.2 The local ionization potential map

As explained, the local ionization potential map paints the amount of the local ionization potential onto an electron density surface. The colours toward red show low ionization potential, while colours toward blue show the high ionization potential. An example of the local ionization potential map of MTS calculated with the semi empirical calculation method and AM1 basis sets is reported in figure 2.3. The map shows that chlorine positions have lower ionization potential (they are red) than the hydrogen positions in blue [Spartan '06, 2006].

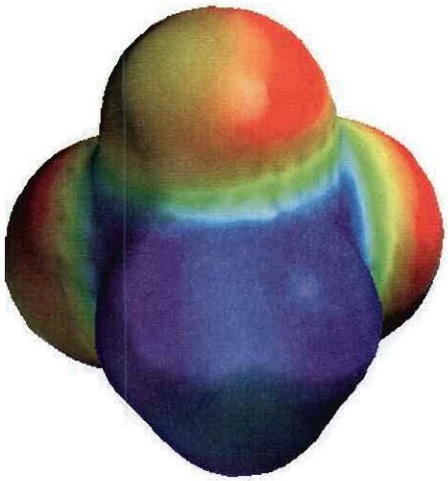

Figure 2.3 Ionization potential map of MTS

2.6.3 The LUMO and HOMO map

LUMO and HOMO maps for methyltrichlorosilane calculated with the semi empirical calculation method and AM1 basis sets are shown figure 2.4. The HOMO is indicated by two orbital surfaces. One surface extends into carbon's non-bonding regions opposite the three hydrogens. The other surface covers the three CH bonding regions. The unoccupied orbitals have higher (more positive) energies (the carbon surface in the HOMO) than the occupied orbitals (hydrogen surface in the HOMO).

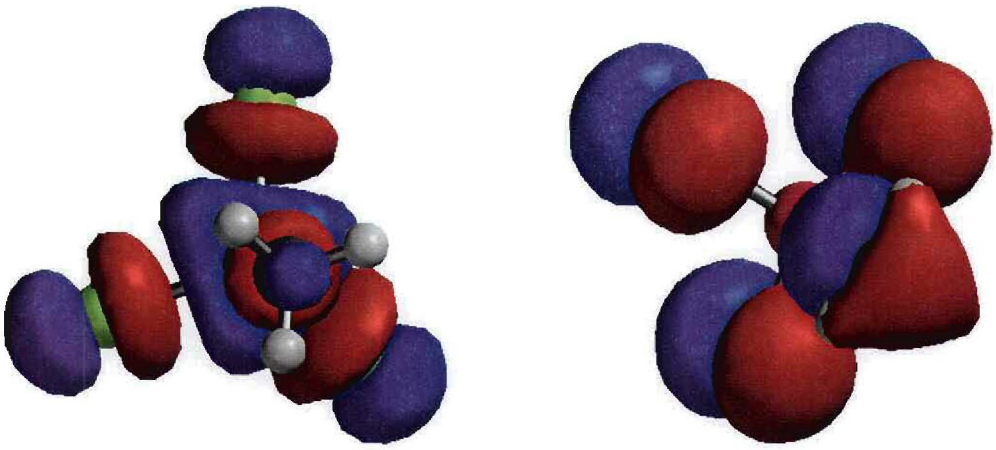

a b

Figure 2.4 (a) The LUMO map for MTS and (b) the HOMO map of MTS.

2.7 Dipole moment

The dipole moment is the measure of polarity of a polar covalent bond. It is defined as the product magnitude of charge on the atoms and the distance between the two bonded atoms. Its common unit is debye and SI unit is coulomb meter. Even if the total charge on a molecule is zero, chemical bonds behave in such a way that the positive and negative charges do not completely overlap in molecules. Such molecules are said to be polar because they possess a permanent dipole moment [http://hyperphysics.phy-astr.gsu.edu/hbase/electric/dipole.html#c1].

For the molecular model shown in figure 2.5 (left), the ball and wire representation of the methyltrichlorosilane molecule was used. The green atoms represent chlorine, the red atom is silicon, the black atom is carbon and the white atoms represent hydrogen atoms. The dipole moment was calculated using the Hartree-Fock method with the STO-3G basis set. MTS has three polar covalent Si-Cl bonds. For the surface on the right (figure 2.6b) the representation indicates where electrons are on the molecule, the red colour represents partial negative charge, while the blue colour represents partial positive charge. As shown the entire molecule has a molecular dipole moment resulting from the vector sum of the three Si-Cl bond dipole moments. The dipole moment was calculated as 3.3 debye.

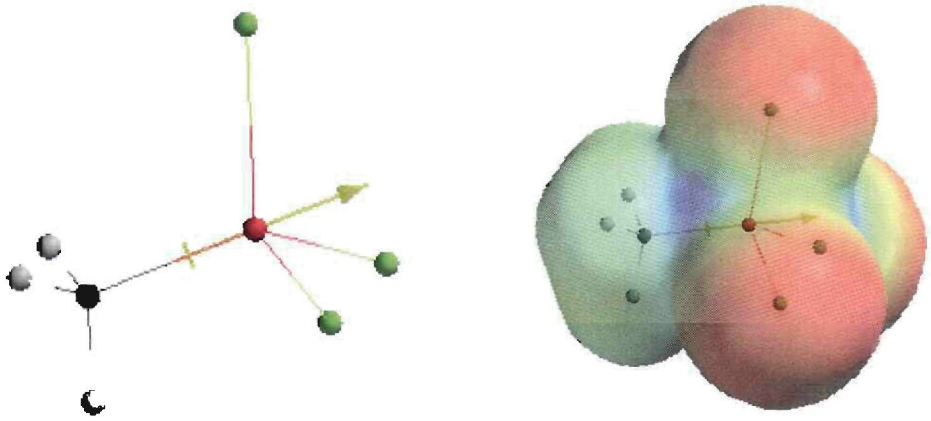

a b

Figure 2.5 (a) The ball and wire representation of methyltrichlorosilane showing the dipole moment and (b) the electrostatic potential combined with a.

2.8 Bond lengths and bond angles

The calculations were done using the Hartree-Fock and Moller-Plesset models. The restricted Hartree-Fock (RHF) calculations were performed using the Spartan program with RHF/3-21G* and RHF/6-31G* basis sets as well as the Moller Plesset method with the MP2/6-31G* basis set. These basis sets were used in order to compare the calculations with previously reported values. The optimized structural parameters calculated are summarized in table 2.2 and compared with those previously reported [Qtaitat and Mohamad, 1994]. The calculations agree well with the results when using similar basis sets which are RHF/3-21G* and RHF/6-31G*. Due to Spartan not having the MP2/6-31G* basis set under Hartree-Fock, the Moller Plesset method with the MP2/6-31G* was utilized.

Table 2.2 Structural parameters for methyltrichlorosilane calculated using Spartan (bond length in Å and bond angles in degrees).

Spartan Calculations			Literature [Qtaitat and Mohamad, 1994]		
	RHF/3-21G*	RHF/6-31G*	MP2/6-31G*	RHF/3-21G*	RHF/6-31G*	MP2/6-31G*
r(Si-C)	1.849	1.858	1.853	1.849	1.858	1.849
r(Si-Cl)	2.035	2.047	2.044	2.035	2.047	2.042
r(C-H)	1.087	1.085	1.093	1.087	1.085	1.093
<(CSiCl)	110.45	110.54	110.39	110.4	110.5	110.4
<(SiCH)	110.68	110.46	110.33	110.7	110.5	110.3
<(ClSiCl)	108.47	108.39	108.54	108.5	108.4	108.5
<(HCH)	108.24	108.47	108.60	108.2	108.5	108.6

2.9 Infrared calculations

The infrared spectrum of trichloromethylsilane was calculated by performing calculations with the Hartree-Fock method and the 3-21G basis set. The calculated spectrum (figure 2.6) that compared best to literature and experimental data was obtained using the equilibrium geometry option in the Hartree-Fock model with the 3-21G basis set. FT-IR measurements for the CH_3SiCl_3 molecule were done using a Vertex 70 FT-IR spectrometer coupled to a Raman II (FT-Raman). All measurements were done at room temperature. The spectrum obtained is shown in figure 2.7. Table 2.2 summarizes the calculated wavenumbers, literature data and experimental data. Data presented in table 2.2 is discussed in section 3.7.1.

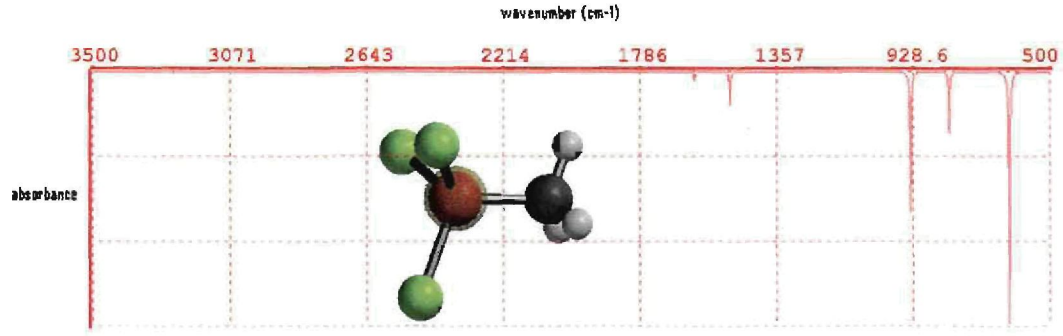

Figure 2.6 Infrared spectrum of the CH_3SiCl_3 molecule calculated with the Hartree-Fock method and the 3-21G basis set.

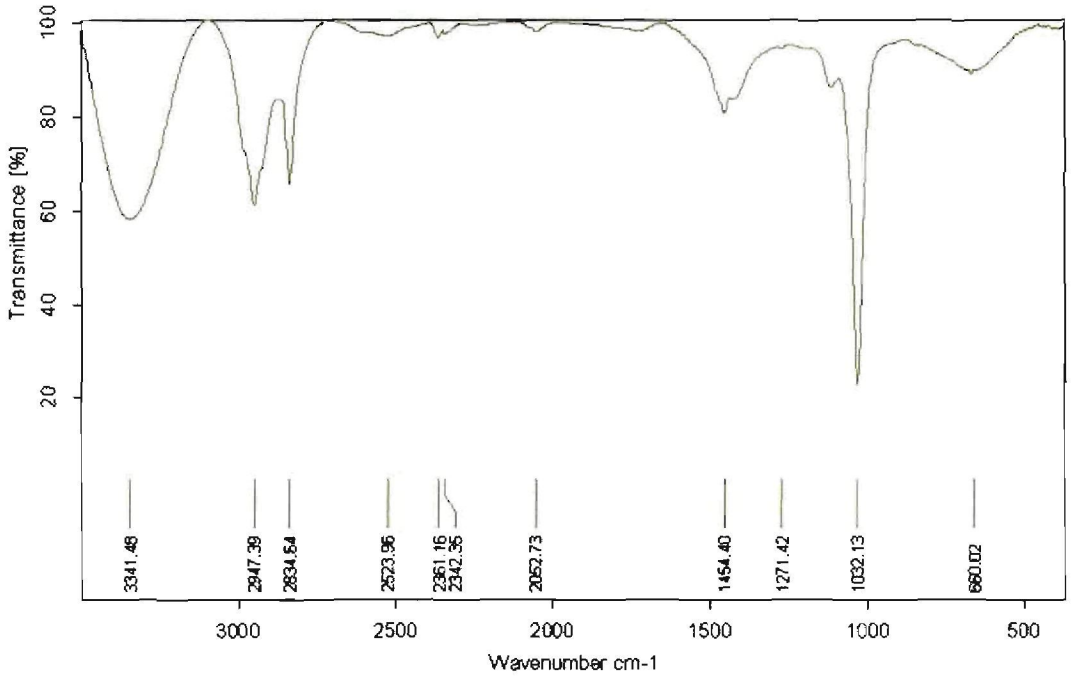

Figure 2.7 The infrared spectrum of methyltrichlorosilane as obtained with the Vertex 70 FT-IR spectrometer coupled to a Raman II (FT-Raman) attachment.

Table 2.2 FT-IR measurements, Spartan calculated values and literature values of the CH_3SiCl_3 molecule

	Soliman et al. [1983]	Spartan	Experimental	
Normal modes	Vibrations wavelengths (cm^{-1})			Notation
	1	**2**	**3**	
CH stretching	2917	3063	2835	$\nu_1(a_1)$
CH_3 deformation	1270	1342	1271	$\nu_2(a_1)$
SiC stretching	762	749	---	$\nu_3(a_1)$
Si-Cl stretching	452	440	---	$\nu_4(a_1)$
$SiCl_3$ deformation	228	230	---	$\nu_5(a_1)$
CH stretching	2991	3148	2947	$\nu_7(e)$
CH_3 deformation	1411	1484	1454	$\nu_8(e)$
CH_3 rocking	805	849	---	$\nu_9(e)$
Si-Cl stretching	572	577	---	$\nu_{10}(e)$
$SiCl_3$ deformation	164	154	---	$\nu_{11}(e)$
$SiCl_3$ rocking	228	219	---	$\nu_{12}(e)$

2.10 Conformational analysis calculations of methyltrichlorosilane

The most general methods for conformational analysis are those that are able to give all minima on the potential energy surface [Höltje et al., 2003]. The number of minima increases with the number of rotatable bonds. Conformational energies can be calculated either by quantum mechanical or molecular mechanics methods. Molecular mechanics method (MMFF) was used for calculation of energy of methyltrichlorosilane and it is reported on figure 2.8.

The calculation is performed by varying systematically each of the torsion angles of a molecule in order to get all possible conformations. The step size used in this systematic search is 9°. That means during a full rotation of 180 anticlockwise, 20 conformations are generated. Decreasing the step size does not affect the results; only more conformers are generated. The energy minima in figure 2.9b at -180°, -66°, 66°

and 161° correspond to the staggered form of MTS, while the maxima at -123°, -9.5°, 9.5° and 123° correspond to the eclipsed form of MTS. The calculation results confirm literature and theoretical statements that the molecule belongs to the point group C_{3v}, has two possible conformations i.e. a staggered and an eclipsed form, the representations of both conformations are shown in figure 2.9. The staggered form are thus also indicated to be the more stable form, this corresponds to what others doing similar work observed [Takeo and Matsumura, 1977].

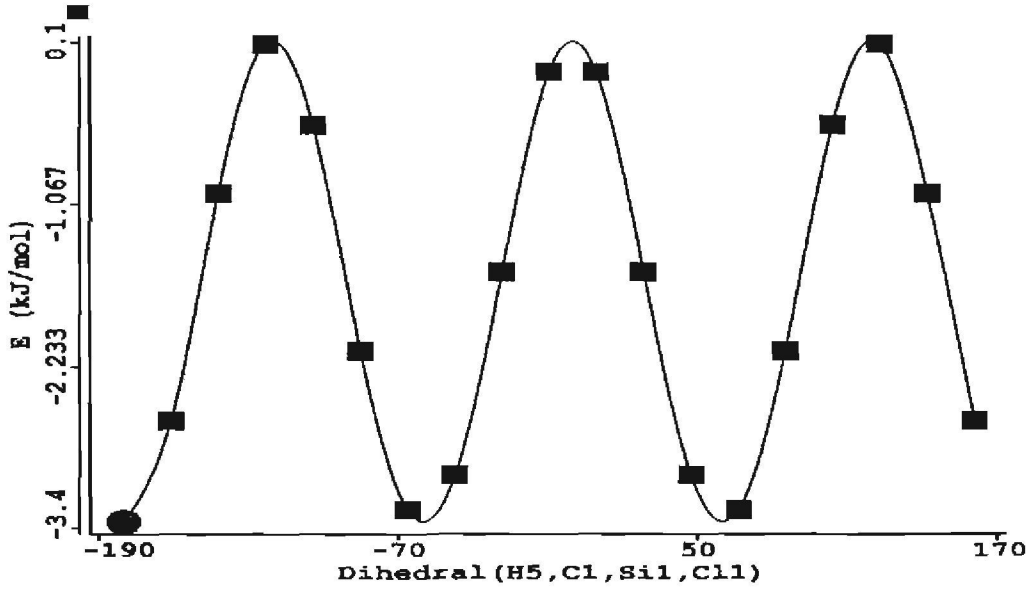

Figure 2.8 Potential energy curve as a function of dihedral angle for MTS calculated with molecular mechanics (MMFF)

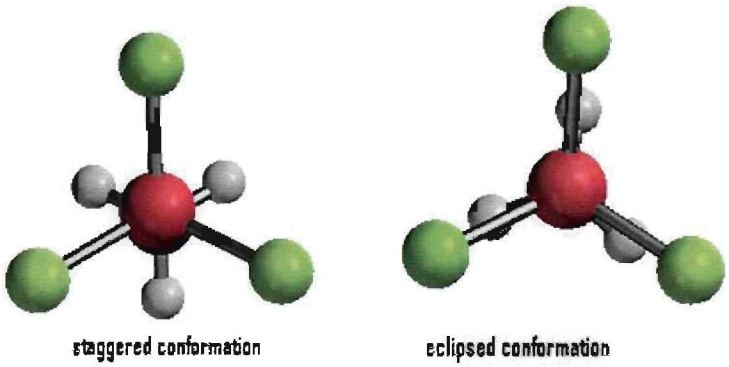

Figure 2.9 Two possible conformations of the methyltrichlorosilane molecule i.e. a staggered and an eclipsed form.

Chapter 3

Molecular absorption spectroscopy

3.1 Molecular absorption spectroscopy

Molecular absorption spectroscopy is the study of interaction between radiation and matter to perform an analysis that gives a plot of response or intensity as a function of wavelength or frequency in a spectrum. A spectrum can be used to obtain information about atomic and molecular energy levels, molecular geometries, chemical bonds, and interactions of molecules, Spectra are used to identify the components of a sample (qualitative analysis). Spectra may also be used to measure the amount of material in a sample (quantitative analysis).

Molecular absorption spectroscopy in the ultraviolet (UV) and visible (VIS) regions of the electromagnetic waves is concerned with the measured absorption of radiation during its passage through a gas, a liquid or a solid. The wavelength region generally used is from 190 to about 1000 nm.

The infrared absorption spectrum of a substance is sometimes called its molecular fingerprint. Although frequently used to identify materials, infrared spectroscopy also may be used to quantify the number of absorbing molecules.

Absorption spectroscopy, fluorescence spectroscopy, Raman spectroscopy, and surface-enhanced Raman spectroscopy commonly use laser light as an energy source.

3.2 Infrared spectroscopy

Infrared (IR) spectroscopy is one of the most common techniques used by chemists. It is the absorption measurement of different IR frequencies by a sample positioned in the path of an IR beam. The main goal of IR spectroscopic analysis is to determine the chemical functional groups in the sample. Different functional groups absorb characteristic frequencies of IR radiation. Using different sample holders or compartments, IR spectrometers can accept a wide range of sample types such as

gases, liquids, and solids. IR spectroscopy is an important and popular instrument for structural interpretation and compound identification.

Infrared spectroscopy is a type of spectroscopy that deals with the infrared region of the electromagnetic spectrum [http://www.wag.caltech.edu/home/jang/genchem /infrared.htm]. The light our eyes see is a small part of a broad spectrum of electromagnetic radiation. On the immediate high energy side of the visible spectrum is the ultraviolet, and on the low energy side is the infrared radiation regions. The portion of the infrared region most useful for analysis of organic compounds is not immediately next to the visible spectrum, but is that having a wavelength range from 2 500 to 16 000 nm [Skoog et al., 1998].

The electromagnetic spectrum is shown schematically in figure 3.1, along with the names associated with various regions of the electromagnetic spectrum. Our eyes can detect only a very limited range of wavelengths, the visible spectrum between about 400 and 700 nm. Absorption of microwave radiation is generally due to excitation of molecular rotational motion. Infrared absorption is associated with vibrational motions of molecules. Absorption of visible and ultraviolet (UV) radiation is associated with excitation of electrons, in both atoms and molecules, to higher energy states. Most molecules will undergo electronic excitation following absorption of light.

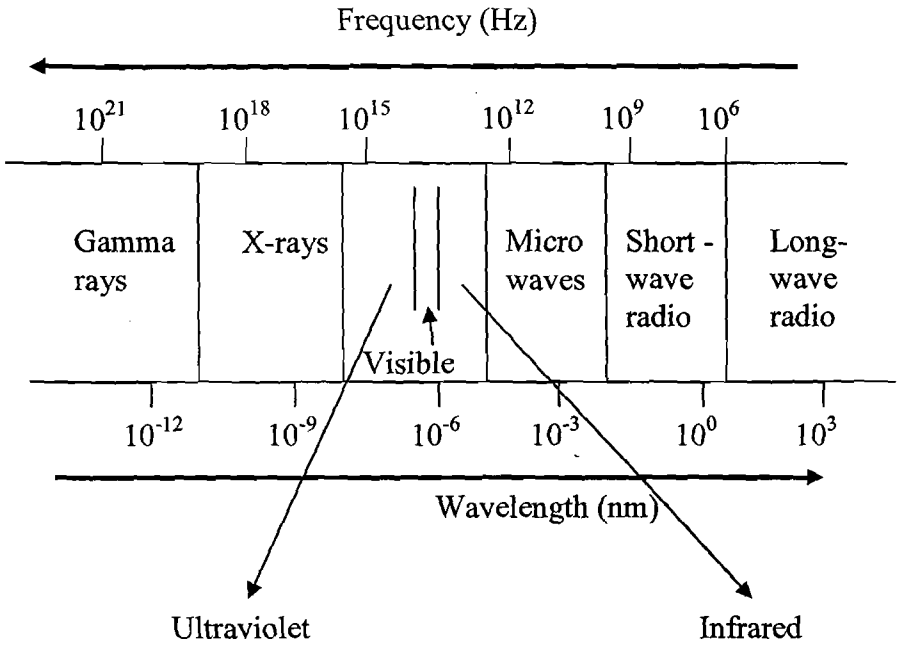

Figure 3.1 The electromagnetic spectrum

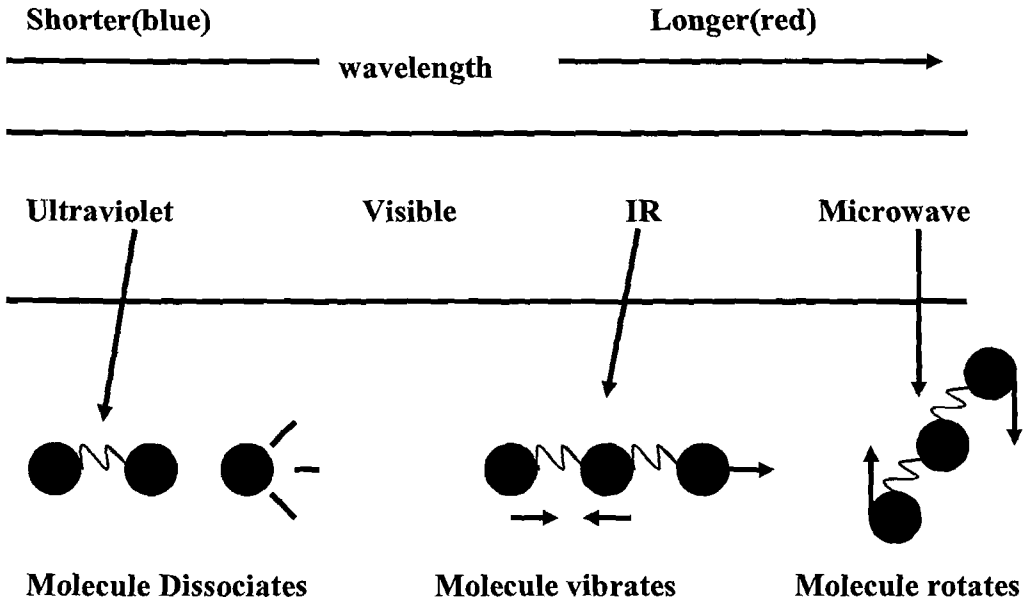

Figure 3.2 Molecular responses to radiation

[http://www.wag.caltech.edu/home/jang/genchem/infrared.htm]

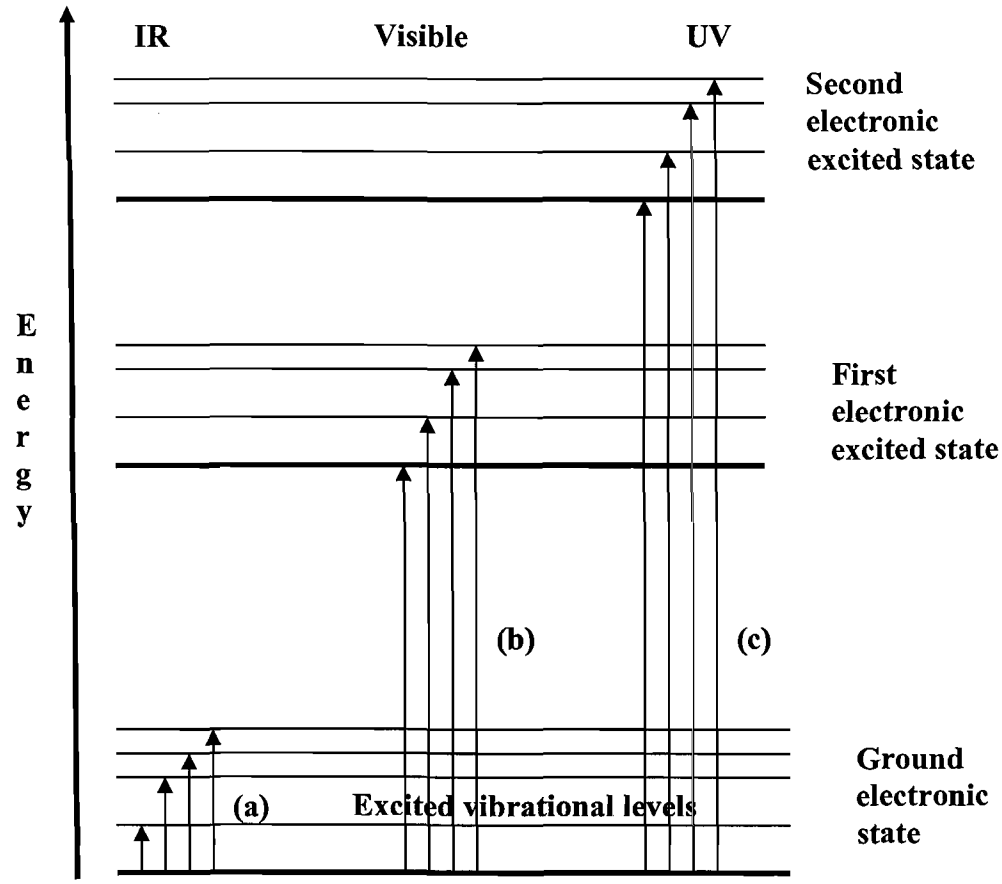

Figure 3.3 Energy levels of molecules and possible absorption of radiation in the IR, UV and visible. [http://www.wag.caltech.edu/home/jang/genchem/infrared.htm]

The responses of molecules to radiation are illustrated in figure 3.2, and figure 3.3 gives a representation of different energy levels in a molecule that may be excited when a molecule is exposed to radiation. The three groups of lines (figure 3.3) correspond to different electronic configurations. The lowest energy, most stable electron configuration is the ground state electron configuration. Photons in the infrared region of the spectrum have much less energy than photons in the visible or UV regions of the electromagnetic spectrum. They can excite vibrations in molecules [Skoog et al., 1998] as indicated in (a). Certain energies in the visible and UV regions of the spectrum can cause electrons to be excited into higher energy orbitals ((b) and (c)) of which some of the possible absorption transitions are indicated by the vertical arrows. Very energetic photons (UV to X-ray region of the spectrum) may cause an

electron to be ejected from the molecule which results in ionization [http://www.wag.caltech.edu/home/jang/genchem/infrared.htm].

There are many possible vibrational levels within each electronic state [http://www.wag.caltech.edu/home/jang/genchem/infrared.htm]. Transitions between the vibrational levels are indicated by the vertical arrows on the left side of the diagram. Microwave radiation is less energetic than infrared radiation. It cannot excite electrons in molecules, nor can it excite vibrations; it can only cause molecules to rotate.

Considering infrared spectroscopy of a molecule, only the vibrational energy levels are interpreted in this wavelength region and can be assigned to corresponding functional groups within the molecule.

The infrared portion of the electromagnetic spectrum is divided into three regions; the near-, mid- and far- infrared, named for their relation to the visible spectrum [http://en.wikipedia.org/wiki/Infrared_spectroscopy].

The far-infrared region, approximately 400-10 cm^{-1} (1000–30 μm), lying next to the microwave region, has low energy and may be used for rotational spectroscopy. The mid-infrared region, approximately 4000-400 cm^{-1} (30–1.4 μm), may be used to study the fundamental vibrations and associated rotational - vibrational structure. The higher energy near-IR region, approximately 14000-4000 cm^{-1} (1.4–0.8 μm), can excite vibrational levels as well as overtone or harmonic vibrations [Skoog et al., 1998].

The mid-infrared region (4000 cm^{-1} to 400 cm^{-1}) is of most interest for chemical analysis as it corresponds to changes in vibrational energies within molecules.

3.2.1 Uses and applications

IR spectroscopy is useful for identifying certain functional groups in a molecule. An IR spectrum of a certain compound is unique and can serve as a fingerprint (reference) for this compound. IR spectroscopy can also be used for determination of the molecular composition of surfaces, identification of chromatographic effluents, quantitative determination of compounds in mixtures, determination of molecular conformation (structural isomers) and stereochemistry (geometrical isomers).

IR spectroscopy is useful for identification of compounds by matching the spectrum of an unknown compound with that of references. IR spectroscopy can also be used for identification of functional groups in unknown substances.

3.2.2 Theory of Infrared radiation absorption

At temperatures above absolute zero, all the atoms in molecules are in continuous vibration with respect to each other. When the frequency of a specific vibration is equal to the frequency of the IR radiation directed at the molecule, the molecule can absorb the radiation. Each atom has three degrees of freedom, corresponding to motions along any of the three Cartesian coordinate axes (x, y, z). A polyatomic molecule of N atoms has $3N$ total degrees of freedom [Skoog et al., 1998]. However, 3 degrees of freedom are required to describe translation, i.e. the motion of the entire molecule through space. Additionally, 3 degrees of freedom correspond to rotation of the entire molecule.

Therefore, the remaining $3N - 6$ degrees of freedom are true, fundamental vibrations for nonlinear molecules. Linear molecules possess $3N - 5$ fundamental vibrational modes because only 2 degrees of freedom are sufficient to describe rotation. Among the $3N - 6$ or $3N - 5$ fundamental vibrations (also known as normal modes of vibration), those that produce a net change in the dipole moment may result in an IR activity and those that give polarizability changes may give rise to Raman activity. However, some vibrations can be both IR- and Raman-active.

The total number of observed absorption bands is generally different from the total number of fundamental vibrations. It is reduced because some modes are not IR active and a single frequency can cause more than one mode of motion to occur. Sometimes, additional bands are generated by the appearance of overtones (integral multiples of the fundamental absorption frequencies), combinations of fundamental frequencies, differences of fundamental frequencies, coupling interactions of two fundamental absorption frequencies and coupling interactions between fundamental vibrations and overtones or combination bands (Fermi resonance). The intensities of overtones, combinations, and difference bands are less than those of the fundamental bands. The

combination of all these factors then creates a unique IR spectrum for each compound.

3.2.3 Types of molecular vibrations

The major types of molecular vibrations are stretching and bending [Skoog et al., 1998]. A stretching vibration involves a change in the inter-atomic distance along the axis of the bond between two atoms. Bending vibrations occur as a result of a change in angle between the two bonds and the four types of bending vibrations include rocking, scissoring, wagging and twisting. Infrared radiation is absorbed and the associated energy is converted into one or more of these types of motion. The absorption involves discrete, quantized energy levels. However, an individual vibrational motion is usually accompanied by other rotational motions. These combinations lead to the absorption bands, not the discrete lines that are observed in the mid IR region. For simple diatomic or triatomic molecules, the nature of vibrations can be easily defined. The analysis is more challenging for large molecules made up of many atoms.

IR spectra are obtained by observing changes in transmittance (or absorption) intensity as a function of frequency (or wavenumber). Most dispersive instruments separate and measure IR radiation using commercial spectrometers or Fourier transform spectrometers.

3.2.4 Fourier Transform Infrared Spectrometers

There are three basic spectrometer components in a Fourier Transform Infrared Spectrometer (FT-IR): radiation source, interferometer, and detector. A FT-IR instrument uses a system called an interferometer to collect a spectrum [http://www.thermo.com/nicolet/]. The interferometer consists of a beamsplitter and two mirrors. The IR beam goes from the source to the beamsplitter which splits the beam into two parts. One part is transmitted to a moving mirror; one part is reflected to a fixed mirror, then the two parts recombines at the beamsplitter in order to produce repetitive interference signals measured as a function of optical path difference by a detector. When the beams are combined an interference pattern is created, since some

of the wavelengths recombine constructively and some destructively. This interference pattern is called an interferogram. This interferogram then goes from the beamsplitter to the sample, where some energy is absorbed and some is transmitted. The transmitted portion reaches the detector. The detector reads information about every wavelength in the infrared range simultaneously. To obtain the infrared spectrum, the detector signal is sent to the computer, and an algorithm called a Fourier transform is performed on the interferogram to convert it into a single beam spectrum. A reference or "background" single beam spectrum is also collected without a sample. The sample single beam spectrum is collected and subtracted from the background single beam spectrum to produce a transmittance or "%T" spectrum. This transmittance spectrum can be converted to absorbance by taking the negative log of the data points. The x-axis of the FT-IR spectrum is typically displayed in wavenumbers (cm^{-1}). This unit is the reciprocal of the actual wavelength of light measured in centimetres at a point in the infrared spectrum. As its name implies, the interferometer produces interference signals, which contain infrared spectral information generated after passing through a sample.

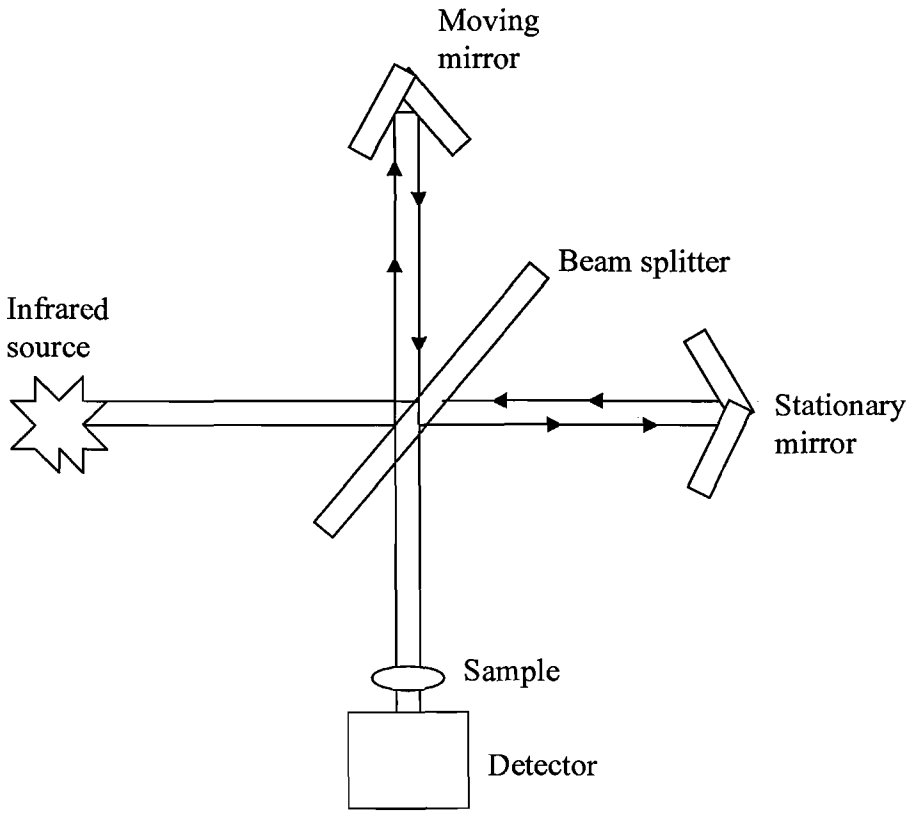

Figure 3.4 The interferometer of the FT-IR [http://www.thermo.com/nicolet/]

3.2.5 Dispersive instruments

Dispersive infrared instruments are usually double beam recording instruments [Skoog et al., 1998]. The light source is sent through both a sample and a reference path, through a chopper, and directed to a diffraction grating. This grating is similar to a prism. It separates the wavelengths of light in the spectral range and directs each wavelength individually through a slit to the detector. Each wavelength is measured one at a time, with the slit width determining the spectral bandwidth and the grating moving to select the wavelength being measured. The x-axis of a dispersive infrared spectrum is typically in nanometres which can be converted to wavenumbers by dividing by 10^7 and taking the reciprocal.

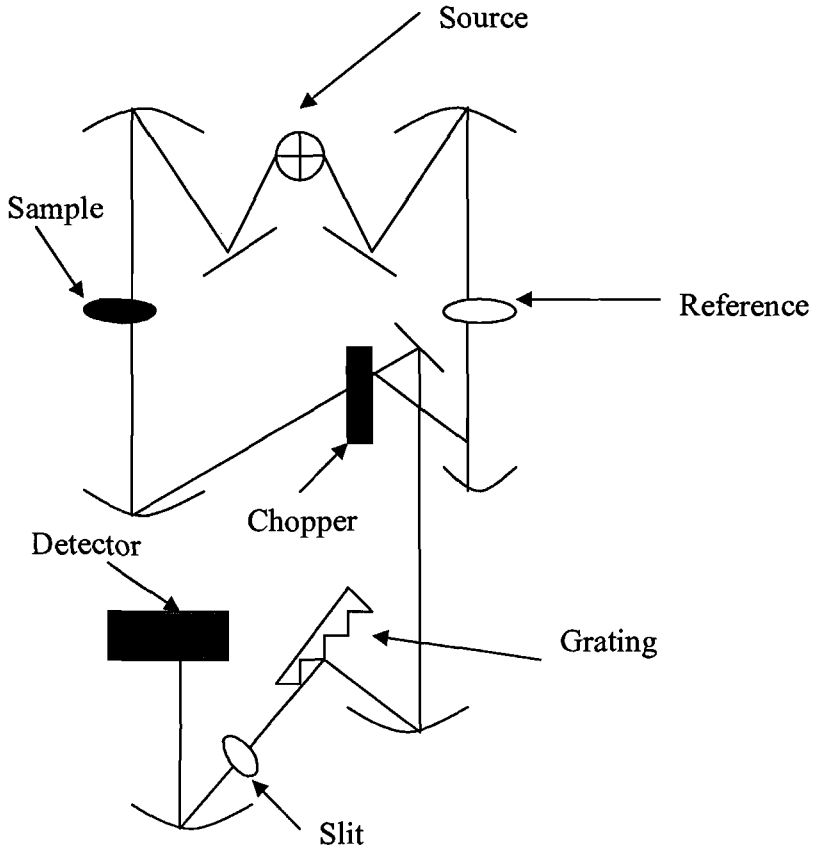

Figure3.5 Schematic of a dispersive IR instrument [http://www.thermo.com/nicolet/].

3.3 Raman spectroscopy

When radiation passes through a transparent medium, the sample scatters a fraction of the radiation in all directions. C. V. Raman discovered that the visible wavelength of a small fraction of the radiation scattered by certain molecules differs from the incident beam and that the shifts in the wavelengths depend on the chemical structure of the molecules responsible for the scattering [Skoog et al., 1998]. Raman spectroscopy is the measurement of the wavelength and intensity (by spectrometer) of scattered light from a sample, as a result of the sample being irradiated by a laser source of visible or near infrared monochromatic radiation. Scattering may occur either elastically, or inelastically. The elastic process is termed Rayleigh scattering, whilst the inelastic process is termed Raman scattering. The Raman scattered light occurs at wavelengths that are shifted from the incident light by an amount equal to the energies of molecular vibrations.

But, a small fraction of light (approximately 1 in 10^7 photons) is scattered at optical frequencies different from, and in most cases lower than, the frequency of the incident photons[http://carbon.cudenver.edu/public/chemistry/classes/chem4538/raman.htm#Introduction]. The process leading to this inelastic scatter is termed the Raman effect. Raman scattering can occur with a change in vibrational, rotational or electronic energy of a molecule. The difference in energy between the incident photon and the Raman scattered photon is equal to the energy of a vibration of the scattering molecule [http://www.kosi.com/raman/index.html].

3.3.1 Raman scattering

In quantum mechanics the scattering is described as an excitation to a virtual state with nearly coincident de-excitation and a change in vibrational energy. The scattering event occurs in 10^{-14} seconds or less [http://www.kosi.com/raman/index.html]. The virtual state description of scattering is shown in figure 3.6. Most photons are elastically scattered, a process which is called Rayleigh scattering. In Rayleigh scattering, the emitted photon has the same wavelength as the absorbing photon.

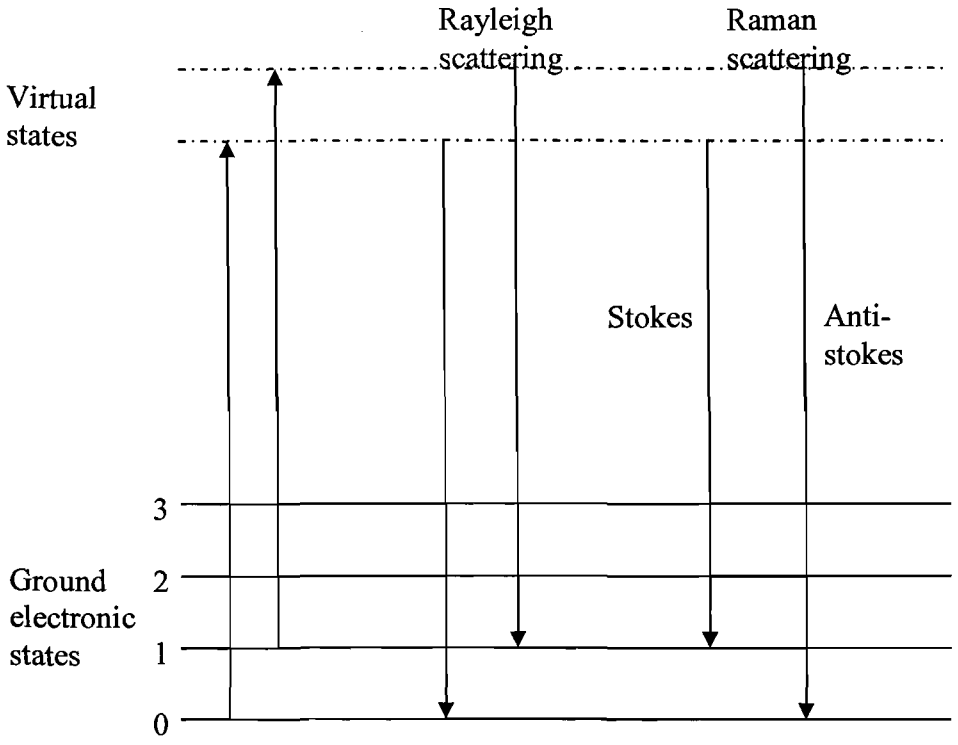

Figure 3.6 Representation of Raman scattering and Rayleigh scattering [Skoog et al., 1998]

At room temperature the thermal population of vibrational excited states is low, but not zero. Therefore, the initial state is the ground state, and the scattered photon will have lower energy (longer wavelength) than the exciting photon. This Stokes shifted scatter is what is usually observed in Raman spectroscopy. Figure 3.6 gives a representation of Raman Stokes scattering.

A small fraction of the molecules are in vibrationally excited states. Raman scattering from vibrationally excited molecules leaves the molecule in the ground state. The scattered photon appears at higher energy, as shown in figure 3.6. This anti-Stokes-shifted Raman spectrum is always weaker than the Stokes-shifted spectrum, but at room temperature it is strong enough to be useful for vibrational frequencies less than about 1500 cm^{-1}. The Stokes and anti-Stokes spectra contain the same frequency information. The anti-Stokes spectrum is also used when the Stokes spectrum is not directly observable, for example because of poor detector response.

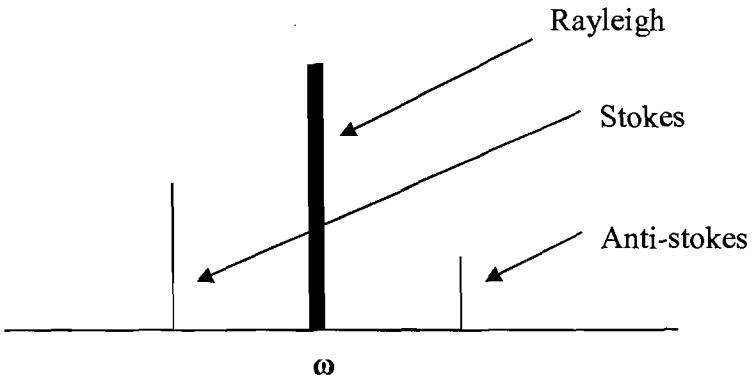

Figure 3.7 An example of a schematic Raman spectrum [http://carbon.cudenver.edu/public/chemistry/classes/chem4538/raman.htm#Introduction]

Stokes lines will be at smaller wavenumbers (or longer wavelengths) than the incident radiation. In the example spectrum (figure 3.7), the Stokes and anti-Stokes lines are equally displaced from the Rayleigh line. This occurs because in either case one vibrational quantum of energy is gained or lost.

Since Raman scattering is not very efficient, a high power excitation source such as a laser is needed. Lasers are used as a photon source due to their high intensity. This is necessary as the Raman effect is weak, typically the Stokes lines are $\sim 10^5$ times weaker than the Rayleigh scattered component Also, since the interest is in the energy (wavenumber) difference between the excitation and the Stokes lines, the excitation source should be monochromatic.

3.3.2 Uses and applications

Infrared (IR) and Raman spectroscopy both measure the vibrational energies of molecules but these methods rely on different selection rules. The spectroscopic selection rule for infrared spectroscopy is that only transitions that cause a change in dipole moment can be observed. In fact for centrosymmetric (centre of symmetry) molecules the Raman active modes are IR inactive, and vice versa. This is called the rule of mutual exclusion.

For a vibrational motion to be IR active, the dipole moment of the molecule must change. For example, the symmetric stretch in carbon dioxide is not IR active because there is no change in the dipole moment. The asymmetric stretch is IR active due to a change in dipole moment.

Raman spectroscopy is used in pharmaceutical production processes, range from monitoring to controlling manufacturing processes of the products. In the field of forensic sciences, Raman spectroscopy is used for the identification of unknown substances.

3.4 Ultraviolet-Visible (UV-VIS) absorption spectroscopy

Molecular absorption spectroscopy is based on the measurement of the transmittance or absorption by the chromospheres contained in transparent cells having a path length of b cm [Skoog et al., 1998]. Absorbance is directly proportional to the path length, b, and the concentration, c, of the absorbing species. The amount of light, I, transmitted through a solution of an absorbing chemical in a transparent solvent can be related to its concentration by Beer's Law:[Skoog et al., 1998]

$$A = -\log T = \log P/Po. = ebc,$$

where P_0 is the power of incident light intensity, P is the power of light after passing through the sample, A is the absorbance, b is the cell path length in cm, c is the solution concentration in moles/litre, and e is the molar absorptivity [Skoog et al., 1998]. Ultraviolet-visible spectroscopy (UV/ VIS) is the spectroscopy of photons in the UV-visible region. Molecules are exposed to light in the visible and in the ultraviolet (UV) and near infrared (NIR) ranges. Most molecules absorb ultraviolet or visible light radiation. Figure 3.8 shows electronic states within a molecule when an atom or molecule absorbs energy in the ultraviolet or visible wavelength range. Electrons are typically promoted from their ground state (E_0) to an excited state (E*). In a molecule, the atoms can rotate and vibrate with respect to each other. These vibrations and rotations also have discrete energy levels, which can be considered as being packed on top of each electronic level. An absorption spectrum show a number of absorption bands corresponding to structural groups within the molecule.

Wavelengths between 190 and 400 nm is for ultraviolet light and from 400 nm to 800 nm is for visible light absorption.

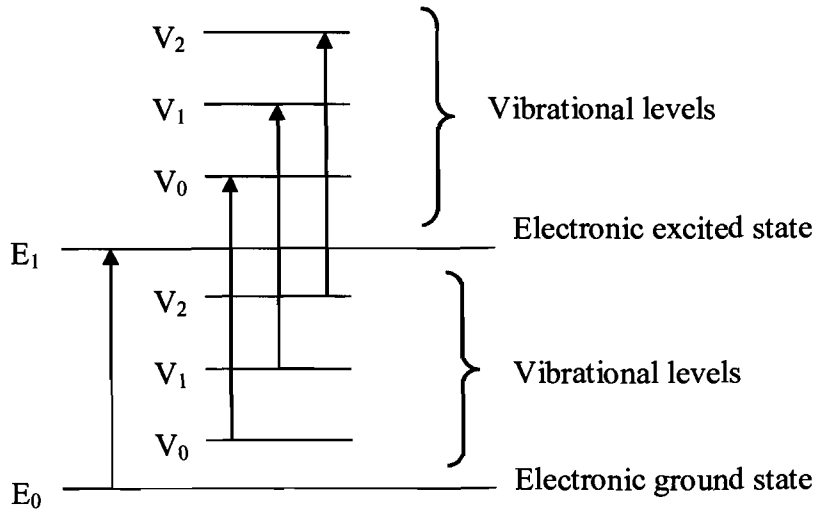

Figure 3.8 Electronic states within a molecule
[http://www.chemistry.ccsu.edu/glagovich/teaching/316/uvvis/uvvis.html]

3.4.1 Types of absorbing electrons in organic molecules

The electrons that contribute to absorption by an organic molecule are those that participate in bond formation between atoms and are therefore associated with more than one atom [Skoog et al., 1998]. Also non-bonding, or unshared outer electrons that are largely localized for example in atoms such as oxygen and halogens, absorbs UV light. The molecular orbitals associated with single bonds in organic molecules are named sigma (σ) orbitals and the corresponding electrons are sigma (σ) electrons. The double bond in organic molecules has two types of molecular orbitals, a sigma (σ) molecular orbital corresponding to one pair of bonding electrons and a pi (π) molecular orbital corresponding to the other pair. Many organic compounds contain non-bonding electrons that are specified by symbol *n*.

3.4.2 Types of electronic transitions

There are three types of electronic transition which can be considered: I -transitions involving pi, sigma, and *n* electrons, II: transitions involving charge-transfer electrons, III: transitions involving *d* and *f* electrons.

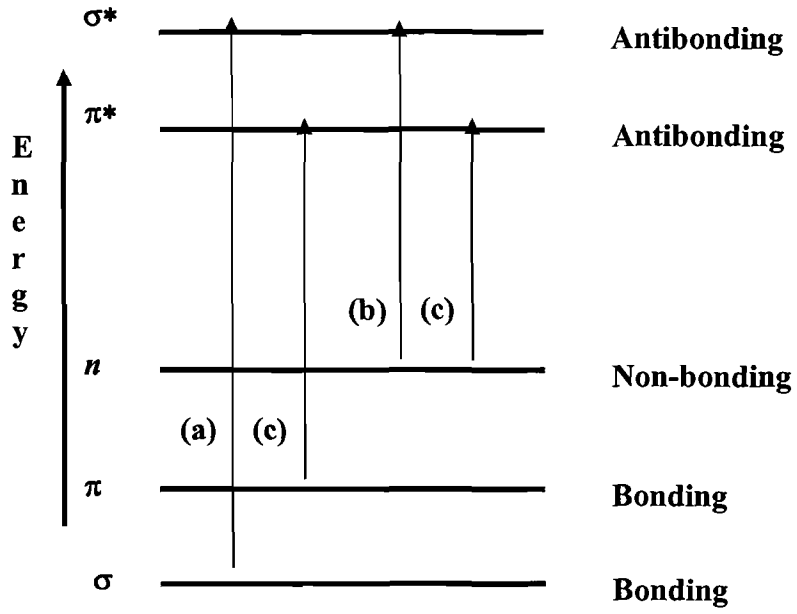

Figure 3.9 Electronic molecular energy levels [Skoog et al., 1998]

Figure 3.9 gives a schematic presentation of possible electronic transitions that can occur in a molecule and the transitions are as follows:

(I) Transitions involving pi, sigma, and *n* electrons

(a) $\sigma \rightarrow \sigma$ Transitions

An electron in a bonding σ orbital is excited to the corresponding anti-bonding orbital. The energy required is large. For example, methane (which has only C-H bonds, and can only undergo $\sigma \rightarrow \sigma^*$ transitions) shows an absorbance maximum at 125 nm. Absorption maxima due to $\sigma \rightarrow \sigma^*$ transitions are not seen in typical UV-Vis. spectra)

(b) $n \rightarrow \sigma$ Transitions

Saturated compounds containing atoms with lone pairs (non-bonding electrons) are capable of $n \rightarrow \sigma^*$ transitions. These transitions usually need less energy than $\sigma \rightarrow \sigma^*$ transitions. They can be initiated by light whose wavelength is in the range 150 - 250 nm. The number of organic functional groups with $n \rightarrow \sigma^*$ peaks in the UV region is small.

(c) $n \rightarrow \pi$ and $\pi \rightarrow \pi$ Transitions

Most absorption spectroscopy of organic compounds is based on transitions of n or π electrons to the π^* excited state. This is because the absorption peaks for these transitions fall in an experimentally convenient region of the spectrum (200 - 700 nm). These transitions need an unsaturated group (compounds containing double bonds or triple bonds) in the molecule to provide the pi electrons.

(II) Charge - Transfer Absorption

Many inorganic species show charge-transfer absorption and are called charge-transfer complexes. For a molecule to have charge-transfer behaviour one of its components must have electron donating properties and another component must be able to accept electrons. Absorption of radiation then involves the transfer of an electron from the donor to an orbital associated with the acceptor.

(III) Transitions involving *d* and *f* electrons.

Transition metals are characterized by having five partially occupied *d* orbitals (3*d* in first series and 4*d* in the second series) capable of occupying two electrons each [Skoog et al., 1998]. The spectral characteristics or absorption process of transition metals are as a result of electronic transitions between various energy levels of the *d* orbitals

3.4.3 Type of instruments

The UV-Vis spectral range is approximately 200 to 900 nm, as defined by the working range of typical commercial UV-Vis spectrophotometers [http://www.chem.vt.edu/chem-ed/spec/uv-vis/uv-vis.html]. The short-wavelength limit for simple UV-Vis spectrometers is the absorption of ultraviolet wavelengths less than 200 nm by atmospheric gases. Working at wavelengths below 175 nm requires a vacuum spectrometer and a suitable vacuum UV light source. The long-wavelength limit is usually determined by the wavelength response of the detector in the spectrometer.

The light source is usually a deuterium discharge lamp for UV measurements and a tungsten-halogen lamp for visible and near infrared (NIR) measurements. The instruments automatically change lamps when scanning between the UV and visible regions. The detector in single-detector instruments is a photodiode, phototube, or photomultiplier tube (PMT). UV-Vis-NIR spectrometers utilize a combination of a PMT and a Peltier-cooled lead sulphide IR detector. The light beam is redirected automatically to the detector when scanning between the visible and NIR regions.

3.4.3.1 Single beam instruments

Single-Beam spectrophotometers are often sufficient for making quantitative absorption measurements in the UV-Vis spectral region. The concentration of an analyte in solution can be determined by measuring the absorbance at a single wavelength and applying Beer's law. Single-beam spectrophotometers can utilize a fixed wavelength light source or a broadband source. The simplest instruments use a single-wavelength light source, such as a light-emitting diode, a sample container, and a photodiode detector. Instruments with a broadband source have a dispersing element and aperture or slit to select a single wavelength before the light passes through the sample cell.

3.4.3.2 Double beam instruments

Double beam spectrophotometers split the light beam into two paths. One path passes through the sample, and the other path passes through a blank. A spectrophotometric blank is basically everything that is in the sample except the component being measured. With the double beam approach P and P_0 are measured at the same time (or nearly so), which corrects for a variation in lamp intensity or drift in instrument electronics.

3.4.4 Uses and applications

UV/Vis spectroscopy is used in the quantitative determination of transition metal ions and conjugated organic compounds in solution.

Most organic compounds, especially those with a high degree of conjugation, also absorb light in the UV or visible regions of the electromagnetic spectrum. The solvents for these determinations are often water for water soluble compounds, or ethanol for organic-soluble compounds. (Organic solvents may have significant UV absorption; not all solvents are suitable for use in UV spectroscopy. Ethanol absorbs very weakly at most wavelengths.)

3.5 Instrumentation

3.5.1 Infrared and Raman instrumentation

The Vertex 70 FT-IR spectrometer coupled to a Raman II also known as FT-Raman is shown if figure 3.10. The system can easily be switched between the infrared and Raman measurement regions and the switching is controlled by software.

The Vertex FT-Raman system was used to measure Infrared and Raman spectra of methyltrichlorosilane. The Vertex FT-IR 70 system can be optionally equipped with optical components to cover the spectral range from 15 cm^{-1} in the far IR, through the mid and near IR up to the visible/UV spectral range at 28000 cm^{-1}. With its pre-

aligned optical components and permanently aligned interferometer, range change is easy.

The Vertex FT-IR spectrometer can measure samples in a pure liquid form, diluted liquids, solids in solution or as a solid (suspension, pellet). It contains different compartments that can accommodate samples in different phases.

The Raman II configuration provides a spectral range of 3600–50 cm^{-1} (Stokes shift). The diode-pumped, air-cooled Nd:YAG laser source (1064 nm) is controlled by the software. The system is equipped with a Germanium diode detector. Liquid nitrogen is used to cool the Germanium detector. [http://www.brukeroptics.com/]

Figure 3.10 The Vertex 70 FT-IR spectrometer coupled to a Raman II (FT-Raman)

3.5.2 Ultraviolet-Visible (UV-VIS) absorption instrumentation

The instrument used to measure UV/Vis absorption of the methyltrichlorosilane in this study was the Ocean Optics USB4000 spectrometer. The instrument consists of a radiation source (Deuterium-Tungsten light source), an optical system including a spectral apparatus, a sample compartment, a radiation detector which is a 3648 element linear silicon detector and allows wavelength range measurements of 200 nm to 1100 nm.

The instrument connects to a computer that operates in Windows, Macintosh or Linux systems though a USB port. An Ocean Optics HG-1 Mercury-Argon lamp is used for calibrating the spectrometer. The SpectraSuite is placed into scope mode and the spectrum of the light source is measured. The integration time is adjusted to accommodate several peaks that are not off scale on the screen. The user stores reference spectra.

The sample in a cuvette is placed into the sample holder for measurements. The light from the light source transmits through an optical fibre to the sample. The light interacts with the sample. Another optical fibre collects and transmits the result of the interaction to the spectrometer. The spectrometer measures the amount of light and transforms the data collected by the spectrometer into digital information. The spectrometer passes the sample information to SpectraSuite. SpectraSuite compares the sample to the reference data and displays processed spectral information.

3.6 Experimental

3.6.1 Samples

The sample used in this study was pure (99.9%) methyltrichlorosilane in liquid, obtained from Merck, South Africa. All measurements were done at room temperature. For the infrared measurements the 1 M, 0.1 M and 0.01 M concentrations of MTS solution in methanol was prepared in a fume cardboard. A few drops of the solution were placed inside the liquid compartment and allowed to spread before the measurements were taken. The reported results of the infrared measurements are of 1 M solution of MTS as the spectrum compared better with values reported in literature than other concentrations. The pure sample of MTS was used for the Raman measurements as a complementary method to identify all functional groups of the MTS molecule that were not observed in the infrared measurements. UV/Vis measurements were made to obtain absorption range of the molecule.

3.7 Results and discussion

3.7.1 IR and Raman results

Results obtained are summarized below and are compared to literature and calculated values in table 3.1 and 3.2.

Table 3.1 Assignment of peaks from the Infrared spectrum of methyltrichlorosilane.

	Soliman et al. [1983]	Spartan	Experimental	
Normal modes	Vibrations frequencies cm^{-1}			Notation
CH stretching	2917	3063	2835	$v_1(a_1)$
CH_3 deformation	1270	1342	1271	$v_2(a_1)$
SiC stretching	762	749	---	$v_3(a_1)$
Si-Cl stretching	452	440	---	$v_4(a_1)$
$SiCl_3$ deformation	228	230	---	$v_5(a_1)$
CH stretching	2991	3148	2947	$v_7(e)$
CH_3 deformation	1411	1484	1454	$v_8(e)$
CH_3 rocking	805	849	---	$v_9(e)$
Si-Cl stretching	572	577	---	$v_{10}(e)$
$SiCl_3$ deformation	164	154	---	$v_{11}(e)$
$SiCl_3$ rocking	228	219	---	$v_{12}(e)$

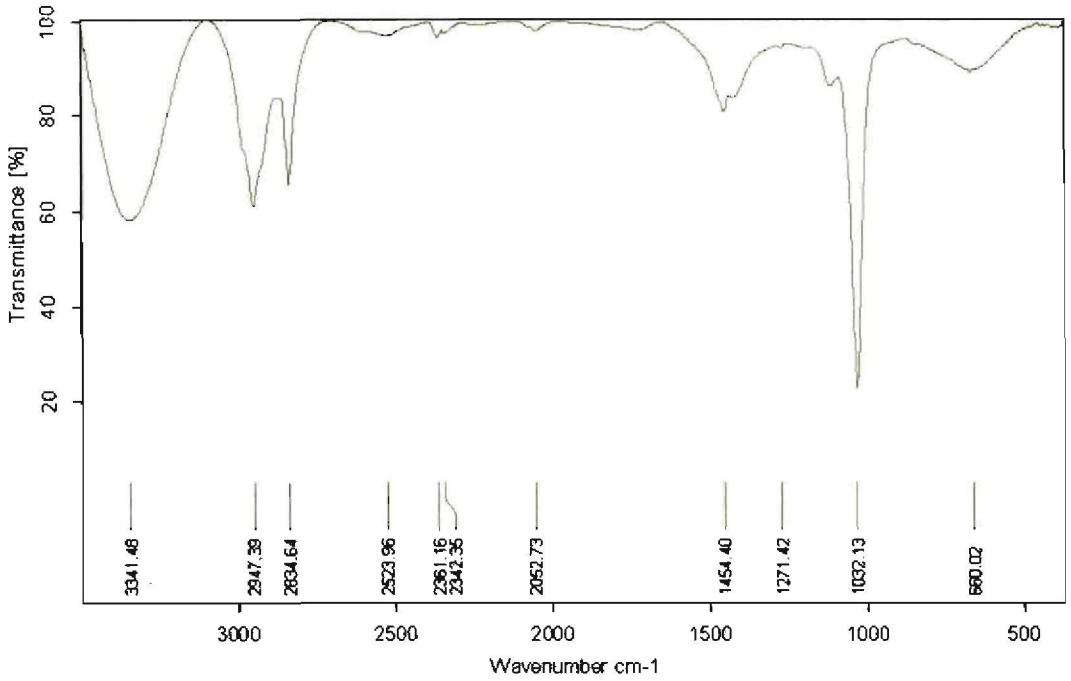

Figure 3.11 Infrared spectrum of methyltrichlorosilane as obtained with the Vertex 70 FT-IR spectrometer coupled to a Raman II (FT-Raman)

Table 3.2 Assignment of peaks from the Raman spectrum of methyltrichlorosilane

	Burnelle and Duchesne, 1952	Experimental	
Normal modes	Vibrations frequencies cm^{-1}		Notation
CH stretching	---	2914	$\nu_1(a_1)$
CH_3 deformation	---	---	$\nu_2(a_1)$
SiC stretching	761	761	$\nu_3(a_1)$
Si-Cl stretching	450	450	$\nu_4(a_1)$
$SiCl_3$ deformation	229	231	$\nu_5(a_1)$
CH stretching	---	2987	$\nu_7(e)$
CH_3 deformation	---	1406	$\nu_8(e)$
CH_3 rocking	---	---	$\nu_9(e)$
Si-Cl stretching	576	568	$\nu_{10}(e)$
$SiCl_3$ deformation	164	162	$\nu_{11}(e)$
$SiCl_3$ rocking	229	231	$\nu_{12}(e)$

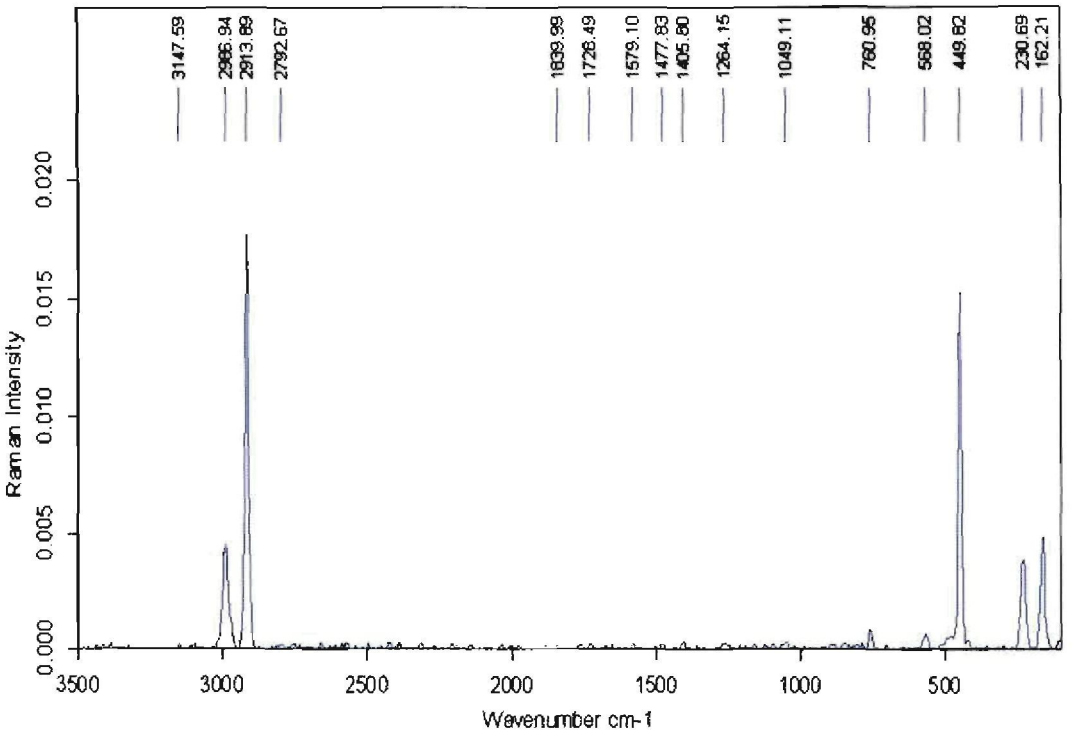

Figure 3.12 Raman spectrum of methyltrichlorosilane as obtained with the Vertex 70 FT-IR spectrometer coupled to a Raman II (FT-Raman)

IR and Raman spectra of MTS produced strong bands of CH in the region 3000 to 2800 cm^{-1} for the symmetric and asymmetric stretches. SiCl showed a strong band at 450 cm^{-1} in the Raman spectrum that is not observed in the IR spectrum, the peak is very useful to identify the chlorosilane species in the MTS molecule. The peaks observed at 2361, 2342 and 660 cm^{-1} from the infrared spectrum are due to impurities. The broad band observed at 3342 cm^{-1} in the IR spectrum is caused by the presence of the OH group in a molecule, which is from the methanol used as a solvent. A strong peak at 1032 cm^{-1} is assigned to the CO absorption band due to the methanol used to dilute the MTS sample. From the Raman spectrum, the $SiCl_3$ symmetric and asymmetric stretches were observed occurring at 450 and 468 cm^{-1} respectively. The Si-C stretch is assigned to the weak band at 761 cm^{1}. The $SiCl_3$ symmetric and asymmetric deformations were observed occurring at 231 and 162 cm^{-1} respectively. The torsional (internal rotation) mode was not observed in either the Raman or IR Spectra, as it is expected for an A_2 mode. The recorded Raman measurements correspond to what was previously reported, thus Raman measurements are the

appropriate method over infrared for characterization of methyltrichlorosilane molecule.

3.7.2 Ultraviolet-Visible (UV-VIS) results

After background subtraction, two strong absorption bands (λ_{max}) at 201 and 232 nm were observed for methyltrichlorosilane (figure 3.13). The absorption bands are assigned to the $n \rightarrow \sigma$ transition which is due to the chlorine atom because it has lone pairs or non bonding electrons.

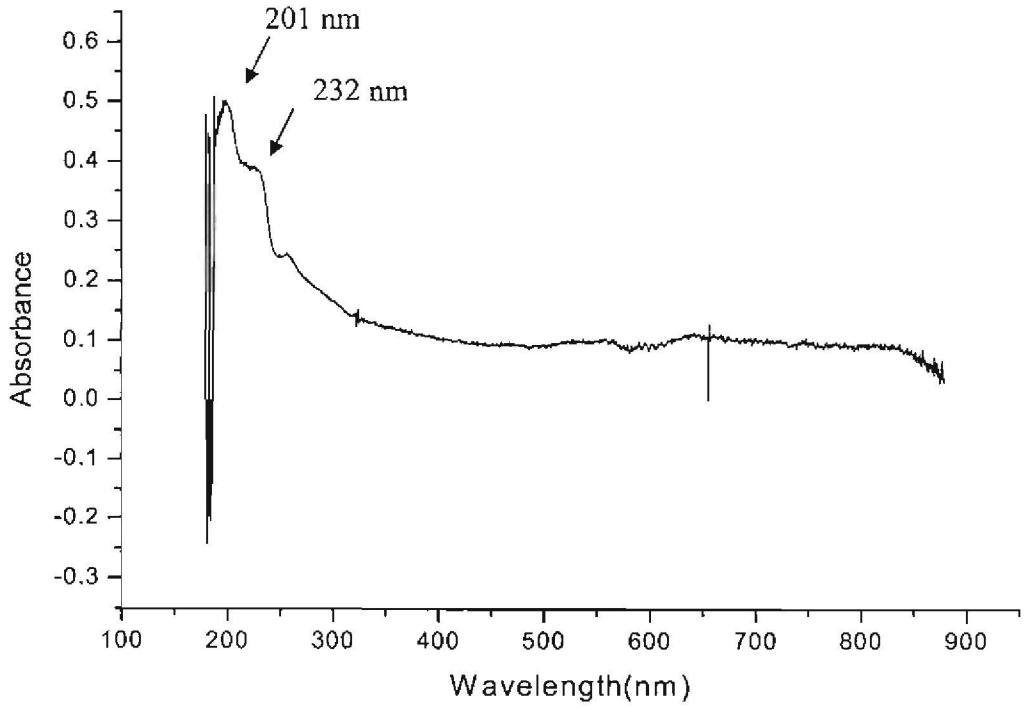

Figure 3.13 UV/Visible spectrum of methyltrichlorosilane as obtained with the Ocean Optics USB4000 spectrometer.

Chapter 4

Theoretical background of laser multiphoton ionization time of flight mass spectrometry

4.1 Introduction

Time of fight mass spectrometry (TOF-MS) can be described as a method of separating ions and measuring the travelling times of the ions over a known distance to reach the detector. The mass to charge ratio (m/z) of the ions determine the time of flight of the ions and thus it is used to identify the different ions[Copley and Udovic, 1993]. In TOF-MS, ions originating in the ion source are accelerated with an electric field to a known kinetic energy and released into a flight tube chamber of length L. Ions are released into the flight tube in short, well defined packets. The same energy is given to all the ions in the ion source. Since the ions have different masses, they travel at different velocities. The lighter ions arrive first at the detector followed by the heavier ions at the back. The ions become separated into individual packets related to their mass number. The detector generates a fast electric signal for each ion or packet of ions and amplifies this signal sequentially and each packet can then be measured as a mass peak.

There are different ways that ions can be generated. Ions can be generated by colliding the sample atoms or molecules with electrons using an electron gun, which is the most popular and simplest technique. Another technique is by exposing the sample atoms or molecules to high intensity laser light, during which the laser energy will cause the atom or molecule to be excited and in some instances give off an electron and therefore ionize. Another way to create ions is to charge two surfaces in the ion source to a high voltage difference (positive and negative), this will cause the sample gas between them to break down into an ion cloud or plasma.

Analysis of the ions follows the creation once they leave the ion source at the same time. Using electrons to create ions is complicated because the ionizing process cannot be started and stopped quickly in order to release all the ions at the same time.

To do this, the start time must be controlled with an electrical pulse. The electrical pulse is achieved as the two plates in the ion source are pulsed with high voltage which can be switched on at the right time to allow all the ions to start moving at the same time. Since a small group of ions close together at the detector is required, a fast pulse is required. This is very simple with a pulsed laser and typical laser sources produce ions during a pulse of only a few nanoseconds.

The advantages of using TOF mass spectrometer are its ease of construction and operation and ability to obtain a full mass spectrum in a few seconds [Opsal et al., 1985]. One disadvantage of the TOF mass spectrometer is the requirement for low-pressure conditions (10^{-6} torr). At low pressures the ions will have fewer collisions along the path to the detector. The method is also not practical for liquid-phase experiments since the entire setup is designed for the gas phase. The method requires ionization, and is therefore not suitable for detecting a neutral atom or molecule without ionization. The method also does not provide direct information on how the fragment ions were formed.

4.2 Basic principle of TOF-MS

Figure 4.1 gives a schematic representation of a TOF mass spectrometer. Ions are created in the ion source and extracted through an extraction grid. The ion source region contains a number of charged grids used to accelerate the ions into the flight tube (field free region). All the ions formed in the source region are accelerated in the presence of an electric field (E = V/d). Once the ions enter the field free region they travel and enter the reflector (reflectron) and then turn around and drift at their final velocities until they reach the detector which is a micro channel plate. The final velocities of the ions differ in proportion to their different mass to charge ratios (m/z). The flight time of each ion is directly proportional to the square root of its mass to charge ratio:

$$t \; a \; (m/z)^{1/2} \qquad (1)$$

where t is the flight time of the ion,
m is the atomic mass of the ion and
z is the charge of the ion (in our case usually z=1).

Hence, ions with smaller m/z ratios arrive at the detector earlier than those with larger m/z values. Data averaged over many pulses can be converted to a plot of signal intensity recorded as a function of flight time providing a complete TOF mass spectrum on the oscilloscope. Averaging can be done and data acquisition transferred onto a computer. An oscilloscope was used in this study.

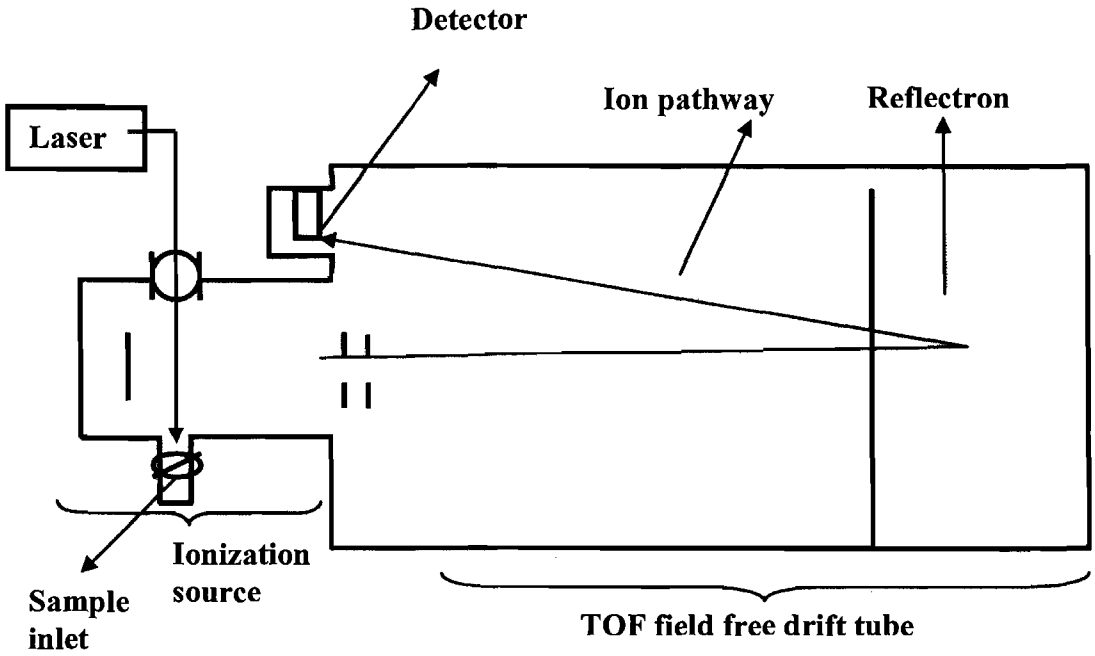

Figure 4.1 Schematic representation of the TOF mass spectrometer.

4.3 Resonant two photon ionization

Ionization is the process of converting an atom or molecule into an ion by adding or removing electrons. In the TOF-MS positive ions are detected, due to the fact that the extraction grids are charged with a positive electric field, thus resulting in acceleration and detection of positive ions only. A positively charged ion is produced when an electron bonded to an atom or a molecule absorbs enough energy to be released. The amount of energy required is called the ionization potential (IP). Photo-ionization can occur if the photon absorbed by the molecule has greater energy than the molecule's ionization potential and therefore high photon energy ultraviolet radiation is typically used for photo-ionization [Lubman, 1987].

Resonance enhanced multiphoton ionization (REMPI) utilizes laser radiation to ionize a molecule from the ground state in a two or more step process via absorption of two or more photons. REMPI is achieved when the laser frequency is tuned to the energy value between real intermediate electronic states of an atom or molecule whereby there is resonant absorption of a single or multiple photons by an atom or molecule to an electronically excited intermediate state, followed by another photon which ionizes the atom or molecule [Mcnab and Shiell, 1994]. If the laser is not tuned to the energy difference between electronic states, the probability of multiphoton ionization (MPI) to occur is smaller.

The multiphoton ionization method applied mostly in chemistry is called resonant two photon ionization (R2PI). In the R2PI process one photon excites the molecule to an excited electronic state and the second photon ionizes the molecule. The two photons can have the same or different frequencies, but the sum of their energies must exceed the ionization potential of the molecule.

For multiphoton ionization to occur the energy required is typically between 0.1 and 10 eV [Mcnab and Shiell, 1994]. Most organic compounds have ionization potentials between 7 and 13 eV. An ionization potential of 7 eV requires two photons of 354 nm wavelength for ionization and 13 eV requires two 191 nm photons. Near ultraviolet (UV) pulsed lasers sources such as Nd:YAG and excimer pumped dye lasers are used to achieve R2PI of molecules with the ionization potential between 7 and 13 eV [Lubman, 1987]. The ionization potential of methyltrichlorosilane is 11.36 eV [http://www.enviroequip.com/pdf/TN-106_Correction_Factors.pdf], and is equivalent to one photon of 109.4 nm, thus two photons of wavelength of 218.8 nm are required for ionization of MTS. The available laser to use is the Nd: YAG and tuneable dye lasers which can be frequency doubled into the deep ultraviolet region, to ionize the methyltrichlorosilane molecule. The reason for using short-pulse lasers to excite the molecule is that if the molecule has a shorter lifetime than the pulse duration of the nanosecond laser, the molecule may relax after excitation and not be ionised thus avoiding detection. Because the pulsed laser has a short pulse duration (for example 6 ns for the Nd:YAG laser), the relaxation does not take place and therefore cannot affect the ionization process.

4.4 Mechanisms in laser multiphoton ionization dissociation

There are two mechanisms that are used to explain laser multiphoton ionization dissociation (MPID), the first mechanism is known as the ladder switching mechanism [Andrews and Demidov, 2002]. In the ladder switching mechanism, multiphoton ionization occurs by absorption of photons by the molecule followed by fragmentation. The extent of fragmentation in ladder switching is controlled by the absorption wavelength of the molecule. This leads to the ability to control fragmentation which allows the possibility to selectively ionize components in a mixture or molecule. For longer laser pulse lengths (nanoseconds) there is enough time for one or more intermediate states to be reached in the excitation ladder to dissociate and produce neutral fragments. These fragments then absorb further photons and either reaches the ionization limit or fragment further [Andrews and Demidov, 2002].

A second mechanism used to explain laser multiphoton ionization dissociation (MPID) is called the ladder climbing mechanism. In the ladder climbing mechanism, only the parent species absorb photons and all fragment ions originate directly from excited states of the parent ion [Andrews and Demidov, 2002]. The molecule absorbs photons fast enough such that the excitation energy of the molecule increases and the molecule ionizes before it even has a chance to undergo fragmentation. The ladder switching mechanism allows neutral fragments to absorb photons and produce smaller fragment ions, whereas all of the ladders climbing fragment ions originate directly from the parent species. If dissociation of a molecule occurs on a time scale longer than the pulse length of the laser used at the time, ladder switching cannot occur. Thus, the ladder climbing mechanism is the dominant MPID process at very short (femtosecond and picosecond) pulse lengths and ionization is efficient. The competition between the two mechanisms depends on the structure of the molecule and the ionization timescale involved.

4.5 Laser

A laser is a device that emits beams of light which are coherent, monochromatic and collimated. The term laser is an acronym for Light Amplification by the Stimulated Emission of Radiation. A typical laser emits light in a narrow, low- divergence beam, with a narrow wavelength spectrum ("monochromatic" light). All the photons that make up a laser beam have a fixed phase relationship with one another.

Absorption of ultraviolet (UV) light by a molecule can cause the excitation of an electron from the ground electronic state to an excited electronic state [http://teaching.shu.ac.uk/hwb/chemistry/tutorials/molspec/uvvisab1.htm]. Photons associated with the ultraviolet region have high energy, enough to cause a molecule to lose an electron. The two types of lasers that were used in this study are the Nd:YAG laser and the dye laser. The use of ultraviolet pulsed lasers such as frequency-quadrupled Nd:YAG (266 nm) and excimer-pumped and frequency doubled dye lasers (in this case at 212.5 nm) are relevant because they provide high enough photon energies to cause ionization of the methyltrichlorosilane molecule. Laser operation depends on the net production of stimulated emission. Net emission is the difference between stimulated emission and absorption and it can be achieved if there are more species in the upper state than in the lower state which is known as population inversion [Wayne, 2005].

4.5.1 Principle of laser system

A typical laser system is represented in figure 4.2. The laser system has a lasing medium within a cylindrical tube with a mirror at each end. One mirror is totally reflecting which is usually named a back reflector, the other is partially transmitting and it is known as the output coupler. The species in the lasing medium is pumped to excite species from the lower state to the upper state (population inversion). In the excited system some of the excited species will lose their energy by spontaneous emission. The photons produced can interact with further excited species to stimulate the emission of more photons thus amplifying radiation. Spontaneous emission causes stimulated emission. Light amplification continues until population inversion is

destroyed. Light is then produced in pulses because population inversion is created and destroyed (pulsed lasers). Lasers in which population inversion is maintained, by adding new supplies of excited species are called continuous wave lasers. [Wayne, 2005]

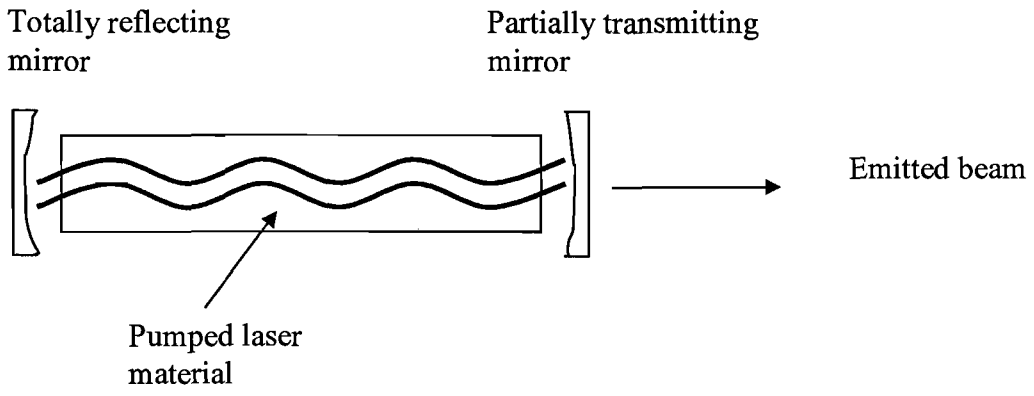

Figure 4.2 Schematic of a laser system

4.5.2 The Nd:YAG laser

Nd:YAG (neodymium-doped yttrium aluminium garnet; Nd:$Y_3Al_5O_{12}$) is a crystal that is used as a lasing medium for solid state lasers. The laser operation of Nd:YAG was demonstrated for the first time by Geusic et al. in 1964 [http://en.wikipedia.org/wiki/Nd:YAG].

Nd:YAG lasers are optically pumped. Laser pumping is the act of energy transfer from an external source using flash lamps or laser diodes into the gain medium of a laser. The energy is absorbed in the medium, producing excited states in its atoms. When the number of electrons in one excited state exceeds the number of electrons in the ground or a less-excited state, population inversion is achieved. The Neodymium: Yttrium Aluminum Garnet laser consists of a four-level system given in figure 4.3.

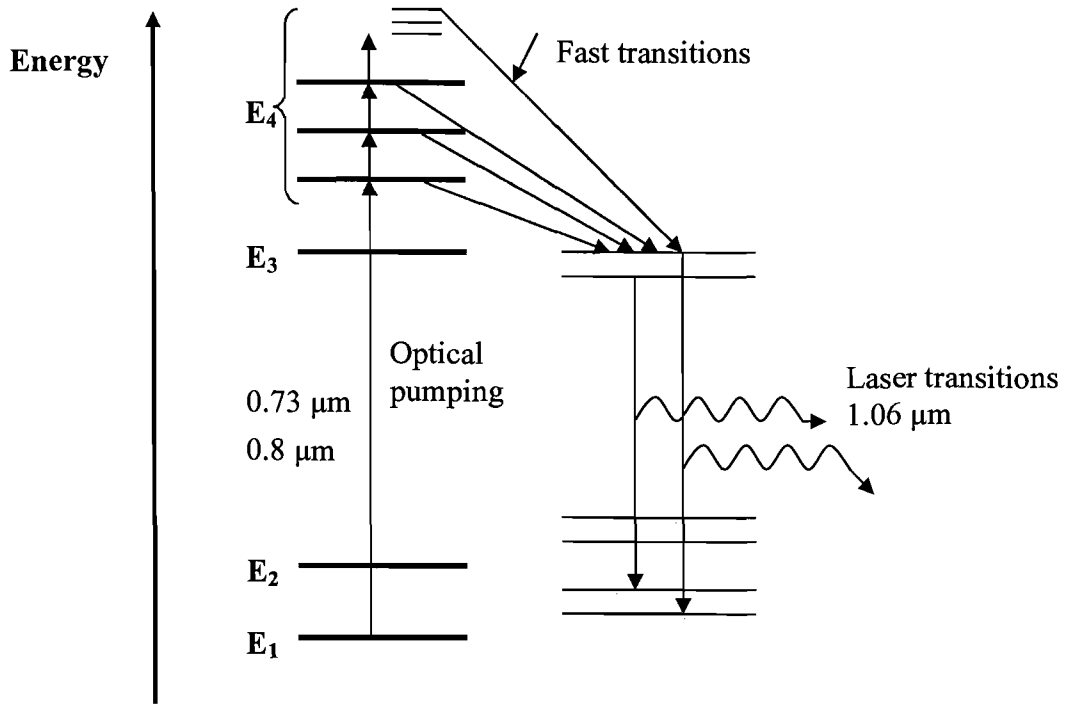

Figure 4.3 Energy level diagram of the Nd:YAG laser

The upper energy levels of Nd^{3+} ions are populated by pumping the ground-state atoms with light near 0.72 μm (720 nm) and 0.83 μm (830 nm) using flash lamps or tungsten lamps. The pumping creates a population inversion. The Nd^{3+} ions vibrationally relax from the upper energy levels to the upper laser level. From this level, the main lasing transition radiates light at 1.06 μm (1060 nm). The ions return to the ground state from the lower laser level through vibrational relaxation. [http://en.wikipedia.org/wiki/Nd:YAG].

A schematic representation of the Nd:YAG laser is shown in figure 4.4. Nd:YAG lasers typically emit light in the infrared region of the spectrum with a wavelength of 1064 nm. The 1064 nm beam is focused on a doubling crystal to produce both the 1064 nm and the 532 nm beams. The Nd:YAG lasers are commonly frequency doubled, tripled or quadrupled to produce 532 nm (green, visible), 355 nm (UV) and 266 nm (UV) light when those wavelengths are needed. Nd:YAG lasers can operate in both pulsed and continuous mode.

Nd:YAG lasers are used for many different applications. Namely, for cutting, welding and marking of metals and other materials, and also in research applications such as Raman spectroscopy, remote sensing and mass spectroscopy as well as for pumping dye lasers.

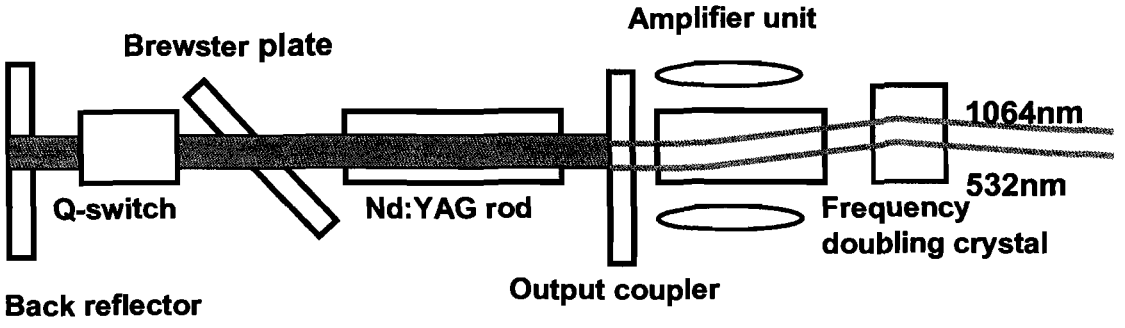

Figure 4.4 Schematic of a Nd:YAG laser

4.5.3 The excimer laser

Excimer laser is a form of ultraviolet laser, which uses a mixture of chemically inert gases such as argon(Ar), krypton(Kr) or xenon(Xe) and a reactive gas, usually a halide diatomic molecule such as fluorine(F_2) or chlorine(Cl_2) as lasing medium [Telle et al., 2007]. The word excimer is a combination of excited dimer, used to explain the fact that excimer lasers are based on molecular compounds formed from two species with at least one of the species in its excited electronic state. The compounds, such as argon fluoride (ArF), krypton fluoride (KrF) and xenon chloride (XeCl), formed in excimer lasers do not bond or react if both (Xe and Cl) reactants are in the ground state.

The lifetime of excimer gas molecules are very short (nanoseconds) and the molecule only exists as long as it is in its excited state. In this case the excited states are charge transfer states [http://en.wikipedia.org/wiki/Excimer]. When the molecule decays under emission of a photon to the ground state, the molecule forms separate atoms again [Telle et al., 2007].

The wavelengths produced by excimer lasers are in the ultraviolet region, most common excimer lasers emit at 193 nm (ArF), 248 nm (KrF), 308 nm (XeCl) and 353 nm (XeF). The excimer laser used in this study is the XeCl laser at 308 nm and it is used to pump a dye laser.

The schematic for the excimer laser as used in this study is represented in figure 4.5. A mixture of 5% HCl in He, Ar and Xe is used. The lasing medium has a laser tube with gas mixture that is refilled regularly with fresh gas because the gas degrades during use. There is a high reflector for the 308 nm wavelength and an output coupler. The beam produced has a pulse length of 30 ns and pulse energy of 250 mJ [Telle et al., 2007].

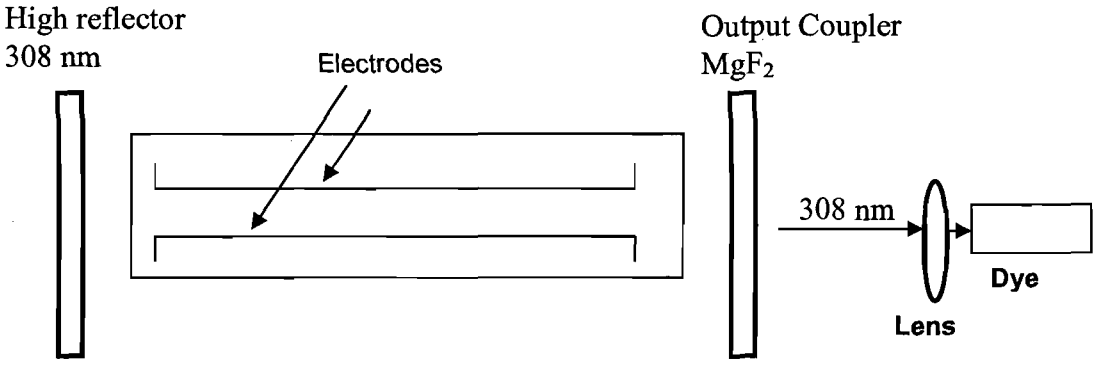

Figure 4.5 Schematic of the XeCl excimer laser

4.5.4 The dye laser

Dye lasers use a dye solution as an active medium; the organic dye absorbs the energy of a source and then reradiates the energy as laser radiation. When comparing dye lasers to solid-state lasing media, a dye can be used to produce a much wider range of wavelengths, i.e. from 360 nm to 950 nm depending on the type of dye used [http://www.lasalle.edu/academ/chem/laser_web/dye_laser.htm]. The wide bandwidth makes them suitable to be used as tuneable lasers.

The dye laser is used in research facilities requiring several laser wavelengths, due to its ability to produce light of several wavelengths. Dye lasers are used in spectroscopy, in biomedical applications as well as to treat scars on the body.

The dye solution can be replaced by another type in order to generate different wavelengths using the same laser. Examples of different dyes used for dye lasers are rhodamine 6G, fluorescein, coumarin, stilbene, umbelliferone, tetracene, malachite green [http://www.lasalle.edu/academ/chem/laser_web/dye_laser.htm]. The dye laser used in this study consists of a cuvette filled with solutions of Stilbene dye. The wavelength range for the Stilbene dye laser is 412 to 443 nm. The dye laser is pumped by an excimer laser at a wavelength of 308 nm. This beam is focused onto the dye solution. The dye solution is pumped continuously to create a population inversion. A dye laser can be considered to be a four-level system as given in figure 4.6. The electron is pumped (excited) into an upper level, E_3, by absorption of high-energy radiation. Following the excitation, vibrational energy is lost causing the dye molecules to go to the lowest vibrational state of the excited electronic state, E_2. Emission occurs to the vibrational levels of the ground electronic state of the dye ($E_2 - E_1$). Dye molecules in this lower level (E_1) can either absorb some of the laser radiation again and be raised back to the higher level, or they can lose their remaining energy and decay back to the E_0 level. Emission will occur between the E_2 and E_1 energy states, from this level, the main photons radiate lasing light at 425 nm.

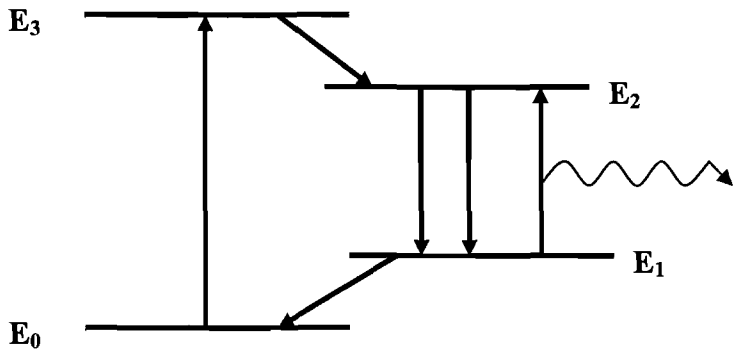

Figure 4.6 Energy level diagram of a dye laser

Figure 4.7 gives the schematic representation of the dye laser (Lambda Physik 3400 Göttingen W. German) as used in this study. When the pump beam is focused in the dye cell the stimulated emission is emitted perpendicular to the pump beam. The 425 nm dye laser beam is furthermore doubled using the BBO (beta barium borate) doubling crystal, to obtain a 212.5 nm beam in addition to the 425 nm beam. The 425 nm beam is dumped and the 212.5 nm beam is focused into the TOF system.

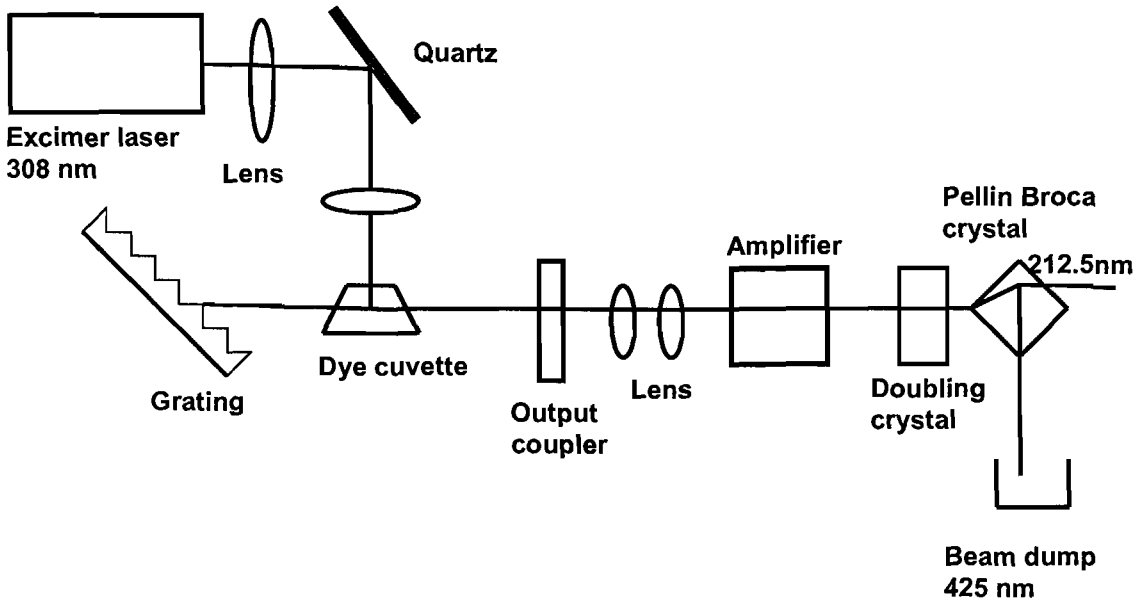

Figure 4.7 Schematic of dye laser as used in this study.

4.5.5 Femtosecond laser

A femtosecond laser is a laser that emits optical pulses with a duration below 1 ps, in the domain of femtoseconds (1 fs=10^{-15} s). Femtosecond lasers usually are Ti:sapphire lasers because they use titanium sapphire as the lasing medium [http://en.wikipedia.org/wiki/Ti-sapphire_laser].

Ti:sapphire lasers (Ti:Al_2O_3 lasers, titanium-sapphire lasers) are tuneable lasers which emit red and near infrared light in the range from 650 to 1100 nm. These lasers are mainly used in scientific research because of their tuneability and their ability to generate ultra short pulses.

Ti:sapphire (Ti:Al_2O_3) is a solid state crystal with Ti^{3+} ions embedded in the sapphire (Al_2O_3) material. It is a leading material in the field of femtosecond lasers. A

Ti:sapphire laser is usually pumped with another laser with a wavelength of 514 to 532 nm [http://www-atom.fysik.lth.se/Kurser/FLaserfysik/KHz%20Lab.doc]. Lasers that are usually used to pump Ti:sapphire are argon ion lasers (514.5 nm), Nd:YAG (neodymium-doped yttrium aluminium garnet), Nd:YLF (neodymium doped yttrium lithium fluoride) and Nd:YVO (neodymium doped yttrium ortho vanadate) lasers (527-532 nm). Ti:sapphire lasers operate best at wavelengths near 800 nm.

Titanium sapphire has a four level energy diagram, which is typical for solid laser materials. The unique property of this material is its broad absorption band, with the peak absorption around 500 nm.

4.5.5.1 Types of Ti:sapphire lasers

4.5.5.1.1 Mode locked oscillators

Mode locking is a method or a group of methods used to obtain ultra short pulses from lasers which are then called mode locked lasers [http://www.rp-photonics.com/mode_locked_lasers.html]. In mode locked lasers the laser resonator contains an active element which causes the formation of a short pulse circulating in the laser resonator.

Mode locked oscillators generate ultra short pulses with a typical duration between 10 femtoseconds and a few picoseconds [http://en.wikipedia.org/wiki/Ti-sapphire_laser]. The pulse repetition rate is in most cases around 70 to 90 MHz. Ti:sapphire oscillators are normally pumped with a continuous-wave laser beam from an argon or frequency-doubled Nd:YVO_4 laser. Typically, such an oscillator has an average output power of 0.5 to 1.5 watt.

4.5.5.1.2 Chirped-pulse amplifiers

Amplification of a short laser pulse can be difficult and damaging to optical components, a short laser pulse must be stretched in time before it is amplified and then recompressed. This process is known as Chirped Pulse Amplification (CPA) [http://www.rp-photonics.com/chirped_pulse_amplification.html]. A stretched pulse will not damage optics, because the energy is spread out over time, which means it

has a low intensity. Amplification of the pulse increases the amount of energy, but the intensity is not raised to a level that would damage laser optics.

Chirped-pulse amplifiers generate ultra short high intensity pulses with a duration of 20 to 100 femtoseconds. A typical one stage amplifier can produce pulses of up to 5 millijoules in energy at a repetition frequency of 1000 Hz, while an improved device can produce pulses up to several joules with a repetition rate of up to 10 Hz [http://en.wikipedia.org/wiki/Ti-sapphire_laser]. Usually, amplifier crystals are pumped with a pulsed frequency-doubled Nd:YLF laser at 527 nm and operate at 800 nm. Two different designs exist for the amplifier: regenerative amplifier and multi-pass amplifier.

Regenerative amplifiers operate by amplifying single pulses from an oscillator. The term chirped-pulse refers to a construction that is necessary to prevent the pulse from damaging the components in the laser.

A multi-pass amplifier is based on a setup in which the incoming laser pulse makes a fixed number of passes through the gain medium. It is often called a 2- pass or 4-pass amplifier. In a multi-pass amplifier, mirror arrays are used to direct the pulse a number of times through the gain medium with different directions. Multi-pass amplifiers are usually used as power amplifiers to boost the energy of pre-amplified pulses. The pulse diameter is increased, as well as the beam quality.

4.5.5.2 Applications of titanium-sapphire lasers

Titanium-sapphire is suitable for pulsed lasers since it can be applied over a wide spectrum of frequencies. However, with an appropriate design, titanium-sapphire can also be used in continuous wave lasers with very narrow line widths tuneable over a wide range.

These lasers are used to study very fast chemical reactions, including the breaking of bonds between atoms in molecules. They have important applications in medicine, micromachining and spectroscopy.

Chapter 5

Experimental techniques

5.1 Introduction

The present chapter provides a description of all the experimental apparatus used for laser ionization time of flight mass spectrometry in this study. All experimental preparations with MTS were done in a fume cupboard. The block diagram in figure 5.1 shows the major components of the experimental apparatus used for the present study. At the centre of the block diagram is a custom built TOF mass spectrometer. The sample is inserted through a pulsed valve that is driven by the pulse driver. The ionization source region is fitted with a quartz lens with windows for transmission of the UV and IR laser beams. Two oil rotary pumps, each connected to a turbo pump, separately pump down the ion source and flight tube regions respectively, to an operating vacuum of 10^{-6} torr.

Pulsed UV radiation is produced by a Continuum Surelite Model SLI/10 Nd:YAG laser with a 6 ns pulse length. The 1064 nm Nd:YAG wavelength is frequency quadrupled to obtain 266 nm radiation. Beam paths of the mentioned laser are discussed in the next sections. The beam is focused through a 170 mm focal length quartz lens into the source region. Positive ions formed by the ionization process are accelerated into the flight tube of 70 cm length, then move at constant velocity up to the reflectron where they turn around and eventually continue at constant velocity until colliding on the microchannel plate (MCP) detector (Hamamatsu Model F1552-01). The pulse generator (model Stanford Research Systems Inc., DG 535) was used to trigger the laser and the oscilloscope. At t = 195 μs (after releasing the gas at t = 0 μs), the Nd:YAG laser was allowed to fire. The triggering is mainly used to provide enough time for the gas molecules to travel from the nozzle to the interaction or ionization region, and is also used to trigger the data collection electronics. This allows the zero time on the TOF spectra to correspond to the arrival time of the UV laser beam at the source region when ionization takes place.

In a typical experiment, data is collected and signals averaged over 32 to 64 laser pulses using a 200 MHz digitizing oscilloscope (Tektronix,TDS Model 360). Raw

data is collected as signal intensity versus flight time. The collected data is converted and stored as intensity versus flight time squared because mass-to-charge ratio is directly proportional to the square of flight time (see section 4.2).

A TOF-MS system is used for analysis of the decomposition of the methyltrichlorosilane (CH_3SiCl_3) molecule. The wavelengths used were 266 nm for Nd:YAG laser, 212.5 nm for the dye laser, 795 nm and 397.5 nm of the femtosecond laser. The wavelengths chosen were used in order to observe the difference in ionization and/or dissociation of the methyltrichlorosilane molecule. The use of different wavelengths and different parameters that may affect ionization due to the nanosecond and femtosecond lasers were also studied. This is done with the aim to find ways of controlling the dissociation of the molecule, which can theoretically be done using femtosecond coherent control. Figure 5.2 shows a picture of the TOF-MS system used in this study.

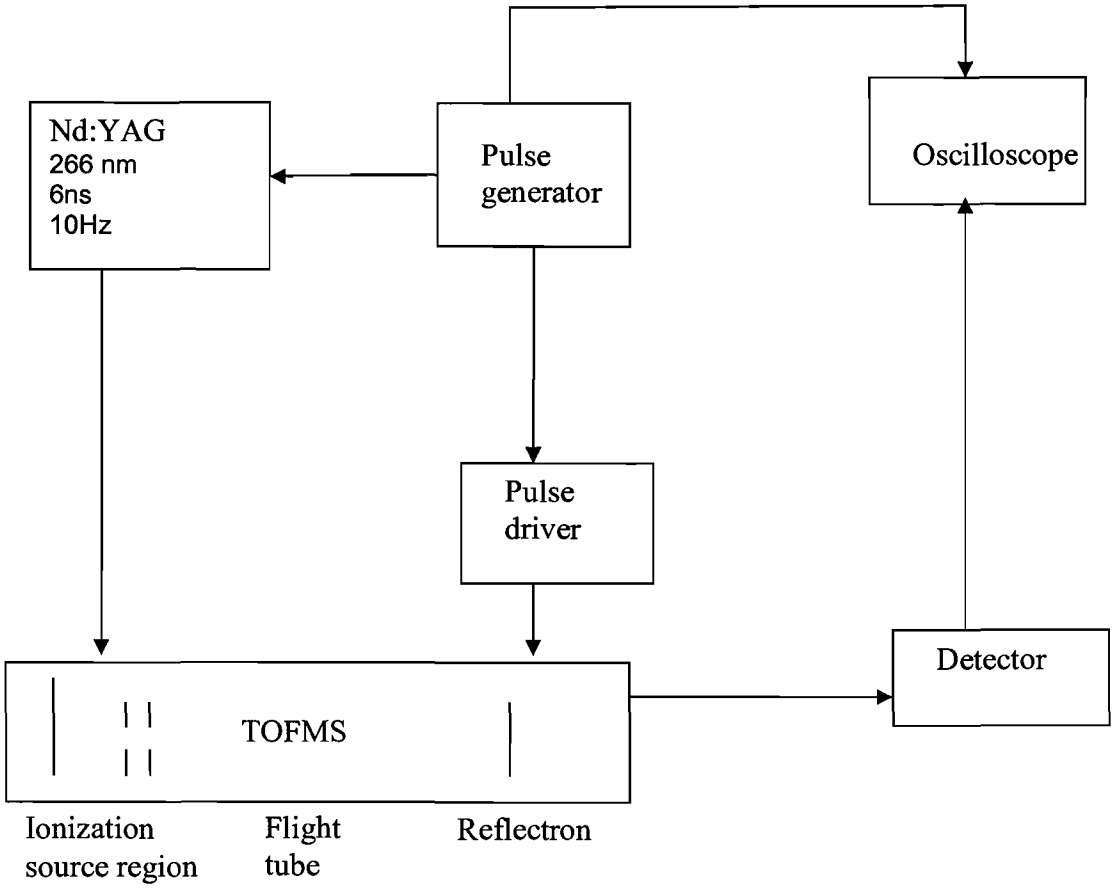

Figure 5.1 Block diagram showing components of the nanosecond laser ionization system and the time of flight mass spectrometer used in this study.

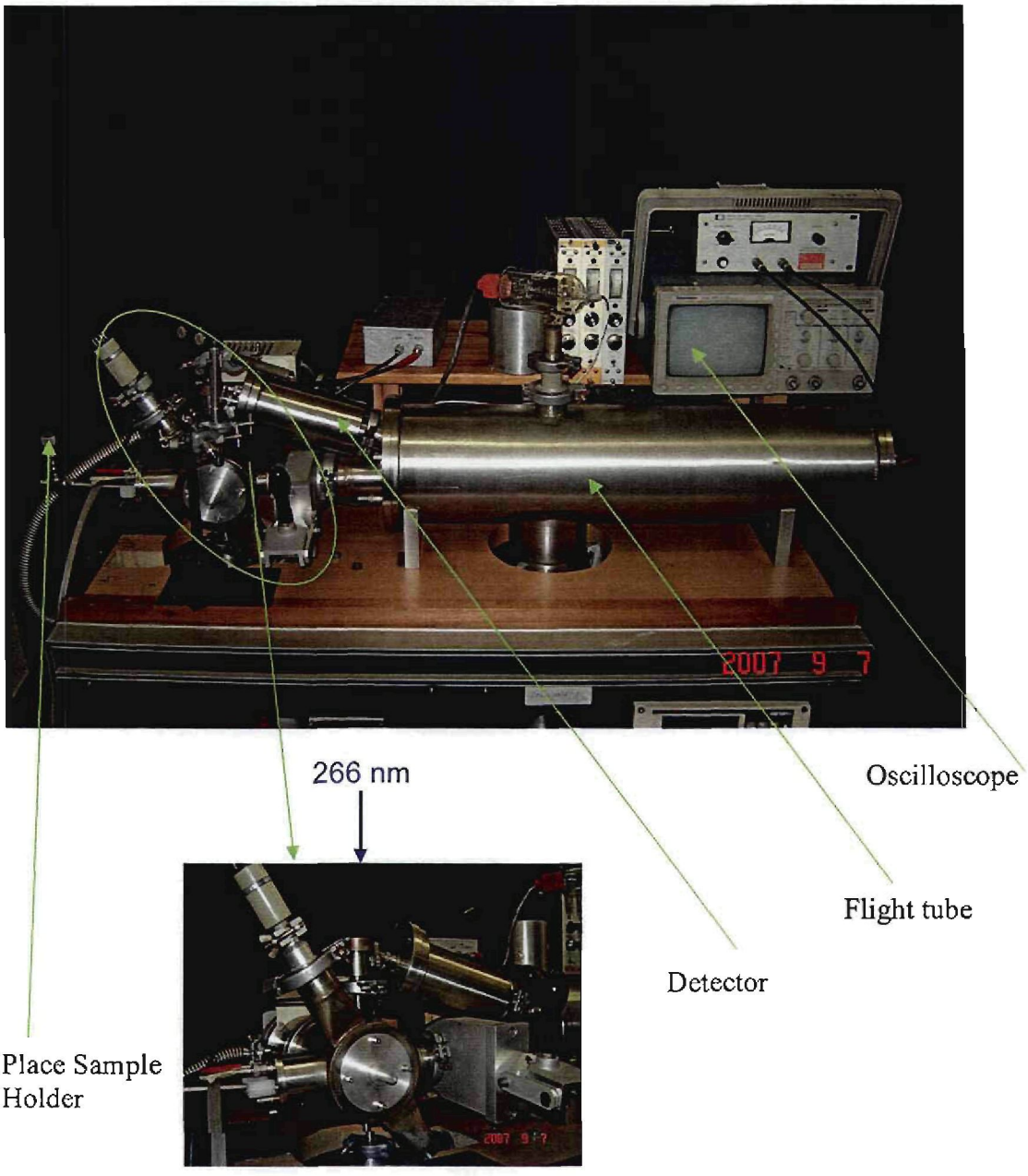

Figure 5.2 The TOF mass spectrometer.

5.2 Experimental setup for measuring the ionization and dissociation of the methyltrichlorosilane molecule using the Nd:YAG laser

A Continuum Surelite Model SLI/10 Nd:YAG laser (figure 5.3) that produces the 532 nm wavelength doubled emission of 266 nm was used to provide the photons for ionization. The 532 nm (green) and the 1064 nm emission from the laser is split using a dichroic crystal (a material that causes a beam of light of two wavelengths to be split up into two separate beams of the different wavelengths). The crystal splits the two wavelengths (532 and 1064 nm) and the 1064 nm is dumped, the 532 nm radiation is doubled by a frequency doubling crystal to produce the 266 nm radiation. This radiation is split again with a Pellin Brocca beam splitting crystal into 532 nm radiation, which is dumped, and the 266 nm radiation is then focused into the ionization chamber of the TOF mass spectrometer. The 532 nm wavelengths were focused into the ionization chamber before producing the 266 nm, to see if ionization occurs using these high energy pulses. No signal was observed for both wavelengths, corresponding to the model of resonant enhanced multiphoton ionization relevant to nanosecond ionization (resonant enhancement occurs only where the difference between energy levels correspond to the energy of the specific wavelengths, which is not the case with 532 nm, but is the case with 266 nm).

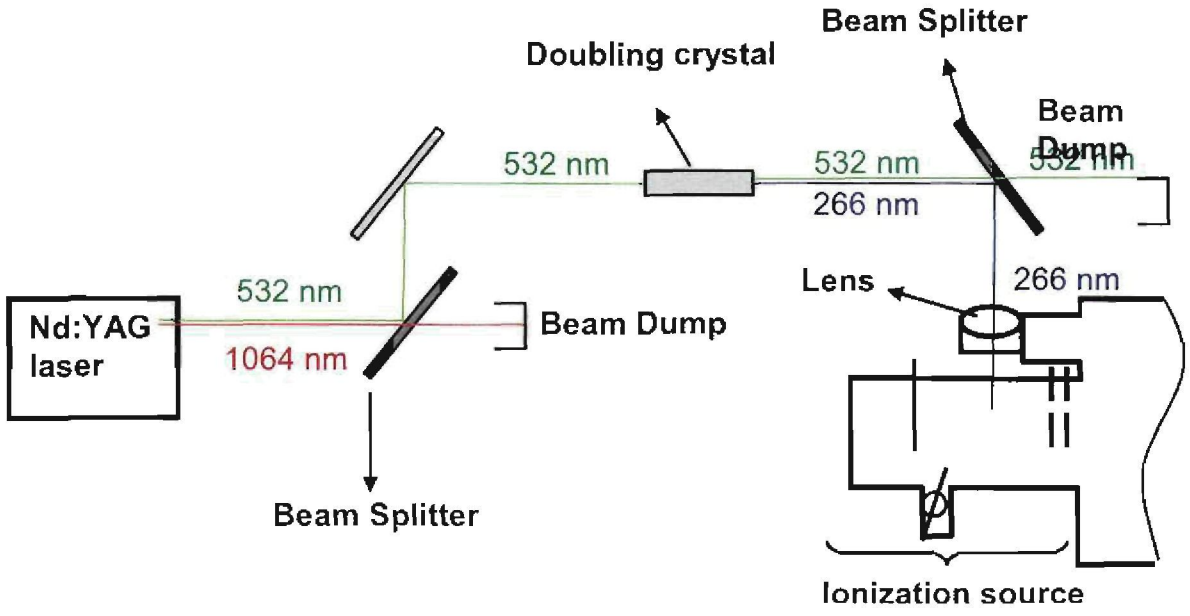

Figure 5.3 Scheme of how the 266 nm beam is produced from the Nd:YAG laser.

The gas sample was introduced by a pulsed valve into the source region where it was excited by the laser beam from the Nd:YAG laser of 266 nm. The ions travel from the ion source through the time of flight tube to the detector (shown in figure 5.2). Argon gas was used as a carrier gas. The vacuum pressure of the instrument was between 10^{-6} and 10^{-5} torr as measured by a pressure gauge. Data, averaged over 32 to 34 pulses, is converted to a plot of signal intensity recorded as a function of flight time providing a complete TOF mass spectrum on the oscilloscope. The Nd:YAG pulsed laser at 266 nm with laser energy of 2.9 mJ, a pulse length of 6.3 ns and a repetition rate of 10 Hz was used.

5.3 Experimental setup for measuring the ionization and dissociation of the methyltrichlorosilane molecule using the dye laser

Figure 5.4 gives the schematic representation of the dye laser (Lambda Physik 3400 Göttingen W. Germany) as used in this study. When the pump beam is focused in the dye cell the stimulated emission is emitted perpendicular to the pump beam. The 425 nm dye laser beam is furthermore doubled using the BBO (beta barium borate) doubling crystal, to obtain a 212.5 nm beam in addition to the 425 nm beam. The 425 nm beam is dumped and the 212.5 nm of laser energy 0.15 mJ beam and pulse length of 25 ns is focused into the TOF system.

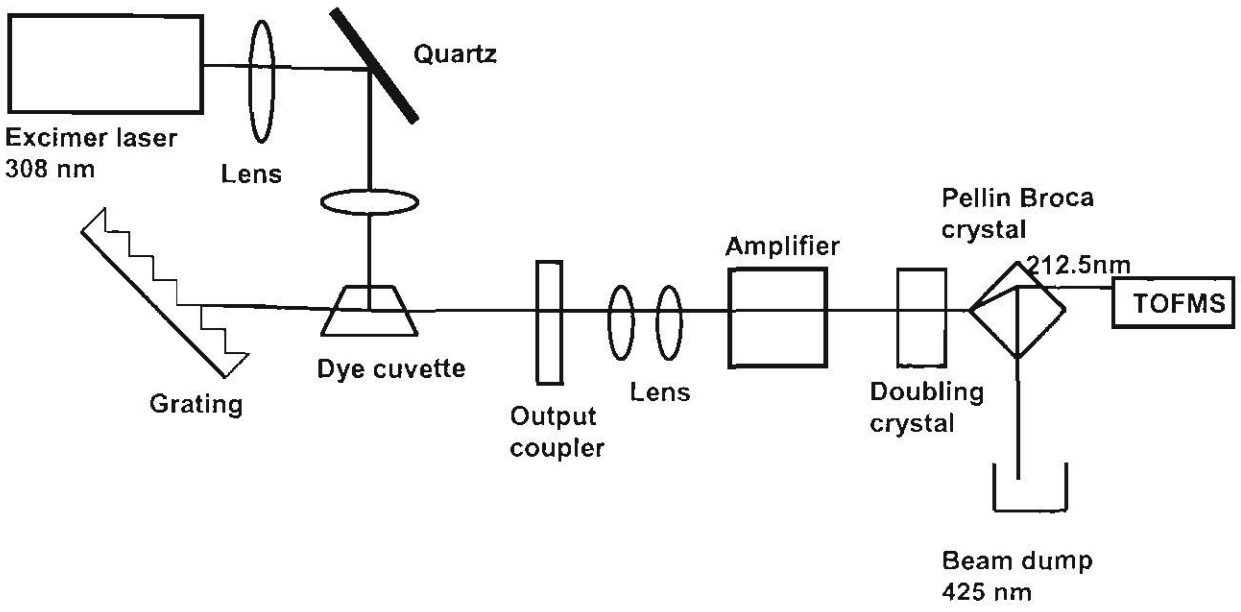

Figure 5.4 Schematic representation of dye laser as used in this study.

5.4 Experimental optimization procedures for nanosecond laser ionization studies

The goal of this part of the study is to ionize the methyltrichlorosilane molecule using the Nd:YAG laser at 266 nm. Parameters that affect ionization in the TOF-MS were investigated. The parameters are optimized for the TOF system and conditions investigated for the ionization of methyltrichlorosilane molecule. The laser voltage (1.05 kV to1.2 kV) and therefore the corresponding pulse energy was varied (from 0.2 to 1.76 mJ) to observe how it affects ionization. Lens focusing and defocusing in the ionization region was also varied (-5 mm to 5 mm) while observing the effect it has on ionization. Different spectra were recorded when changing the lens focus. The delay time of opening the pulse valve for gas molecules to interact with the laser and be ionised was varied from 140 μs to 1000 μs in steps of 20 μs to investigate which time gives high signals in ionization of the methyltrichlorosilane molecule. The peak intensities of the Si^+, $Si^{35}Cl^+$ and $^{35}Cl^+$ ion peaks on the spectrum were observed to analyse how the above mentioned parameters affect the ionization of MTS. A large signal change or absorption of the mentioned peaks (Si^+ ion peak, $Si^{35}Cl^+$ and $^{35}Cl^+$) was observed as a result of varying different parameters compared to other peaks.

5.5 Experimental setup for measuring the ionization and dissociation of the methyltrichlorosilane molecule using the femtosecond laser

A schematic representation of the femtosecond laser facility is shown in figure 5.5. A femtosecond mode-locked beam at 795 nm wavelength is emitted from a Ti:Sapphire oscillator. This oscillator is pumped by a continuous wave diode-pumped solid state laser (Nd:YVO_4 laser) to produce pulses from the oscillator of a pulse duration of 120 fs at a repetition rate of 76 MHz. This pulse train is sent through a regenerative amplifier which contains a pulse stretcher. The pulses are stretched from 120 fs to 200 ps through the stretcher, which is followed by a regenerative amplifier stage, and is pumped by a pulsed diode-pumped solid state laser (Nd:YLF laser). The beam is then passed through a compressor resulting in ultra-short pulses with a duration of approximately 120 fs at 795 nm wavelength and 1 mJ pulse energy with a repetition rate of 1 kHz.

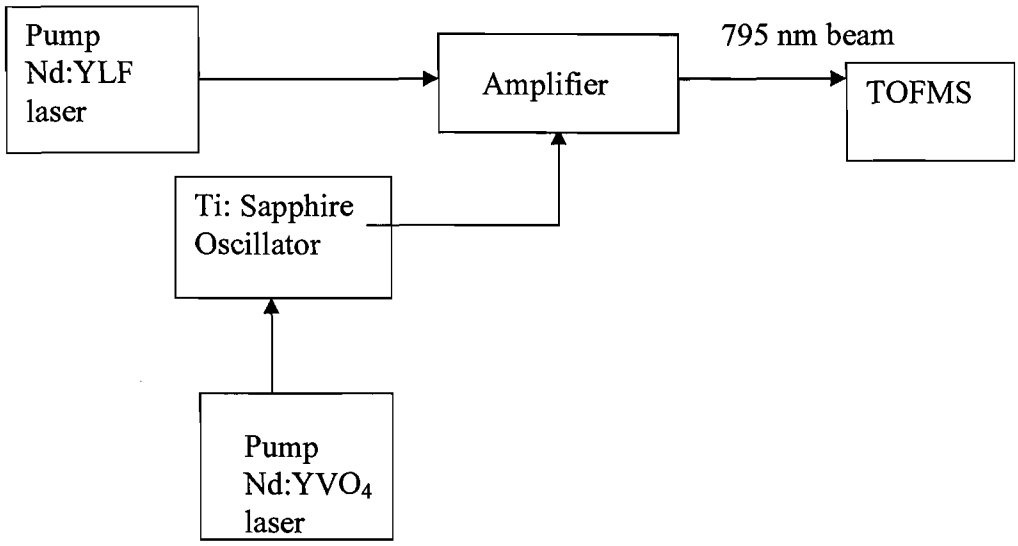

Figure 5.5 Schematic representation of the femtosecond laser as used in this study

5.6 Experimental procedures of femtosecond laser time of flight mass spectrometry

A Schematic of the experimental setup for the femtosecond laser ionization is shown in figure 5.6. The sample gas was inserted by a pulsed valve into the source region of the time of flight instrument. The pressure in the vacuum chamber was typically 10^{-6} to 10^{-5} torr. A lens (f = 170 mm) was employed to focus the laser pulses in the gas sample. The repetition rate of the laser was set at 1 kHz. A photodiode placed in front of the ionization chamber of the TOF-MS was used to trigger the 200 MHz digitizing oscilloscope (Tektronix, TDS Model 360). The ions drift through a 70 cm long field-free vacuum tube. A microchannel plate detector measured the ion TOF spectra, which were used to determine the ion masses. Both 795 nm and 397.5 nm were used in this study. The femtosecond laser fundamental output at 795 nm was frequency doubled by using a frequency doubling crystal to give the 795 nm and the 397.5 nm which were split by using a beam splitter. The 795 nm was dumped and the 397.5 nm beam was focused through a 170 mm focal length quartz lens into the source region. Optimized settings from nanosecond studies were used and ionization and dissociation was observed as a function of laser energy and wavelength, and the femtosecond ionization compared to nanosecond ionization.

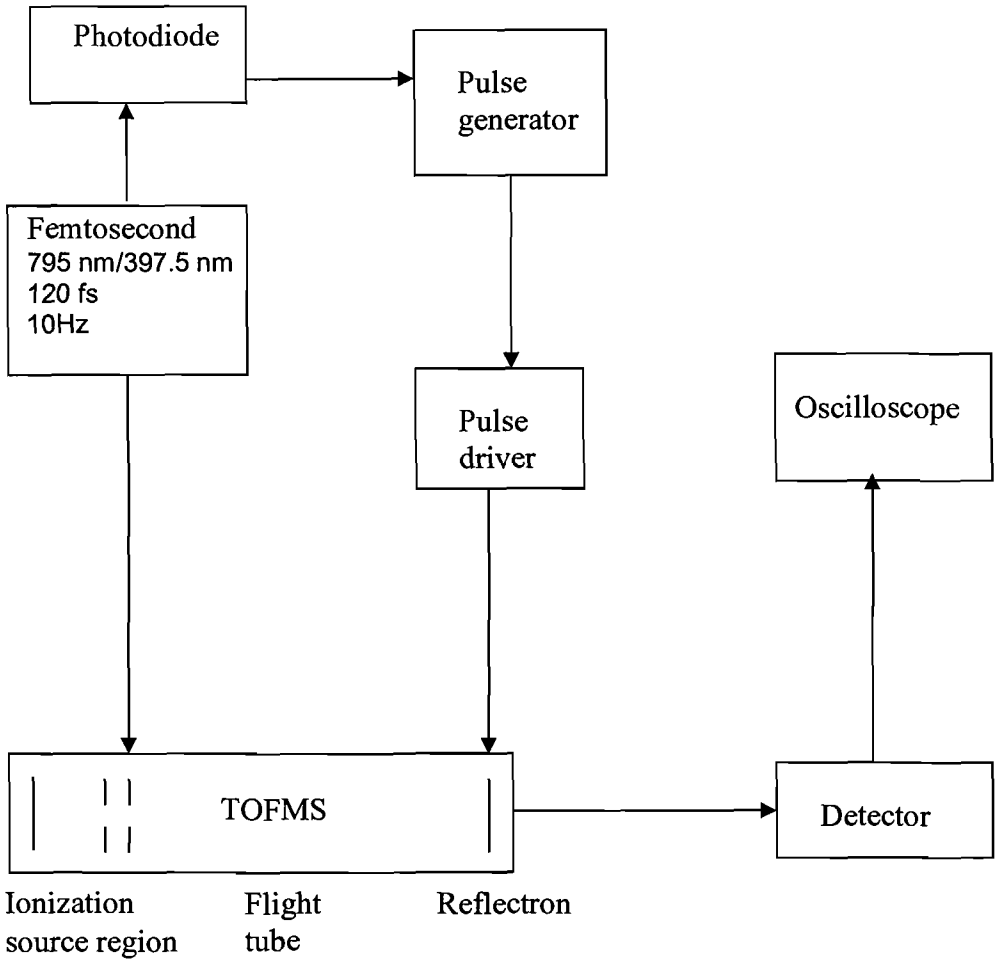

Figure 5.6 Block diagram showing components of the femtosecond laser ionization system and the time of flight mass spectrometer used in this study.

Chapter 6

Results and discussion of laser multiphoton ionization time of flight mass spectrometry of methyltrichlorosilane

6.1 Calibration of the TOF-MS

N_2O was used to calibrate the TOF-MS. The N_2O gas pipe was connected to the sample holder and N_2O was pumped into the TOF-MS system. The TOF mass spectrum is plotted as signal in millivolts versus time in microseconds. The mass of the ions is obtained by using the formula in equation (1):

$$t = k(m)^{1/2} \qquad (1)$$

where t is the flight time of the ions, m is the mass of the ions and k is a constant depending on the instrument parameters. Figure 6.1 gives the mass spectrum of the N_2O gas. The hydrogen ion has a peak at 4.75 μs which is used as the k value to calculate the masses of the other ions. Hydrogen and carbon ions are present from the background gas in the system. The ions observed are C^+ at 16.2 μs, NO^+ at 25.6 μs, N_2^+ at 24.7 μs and N_2O^+ at 31.05 μs. From equation 1 the calibration was worked out for hydrogen peak.

$$t = k(m)^{1/2}$$

$$4.75 = 4.75\ (m)^{1/2}$$

$$m = 1$$

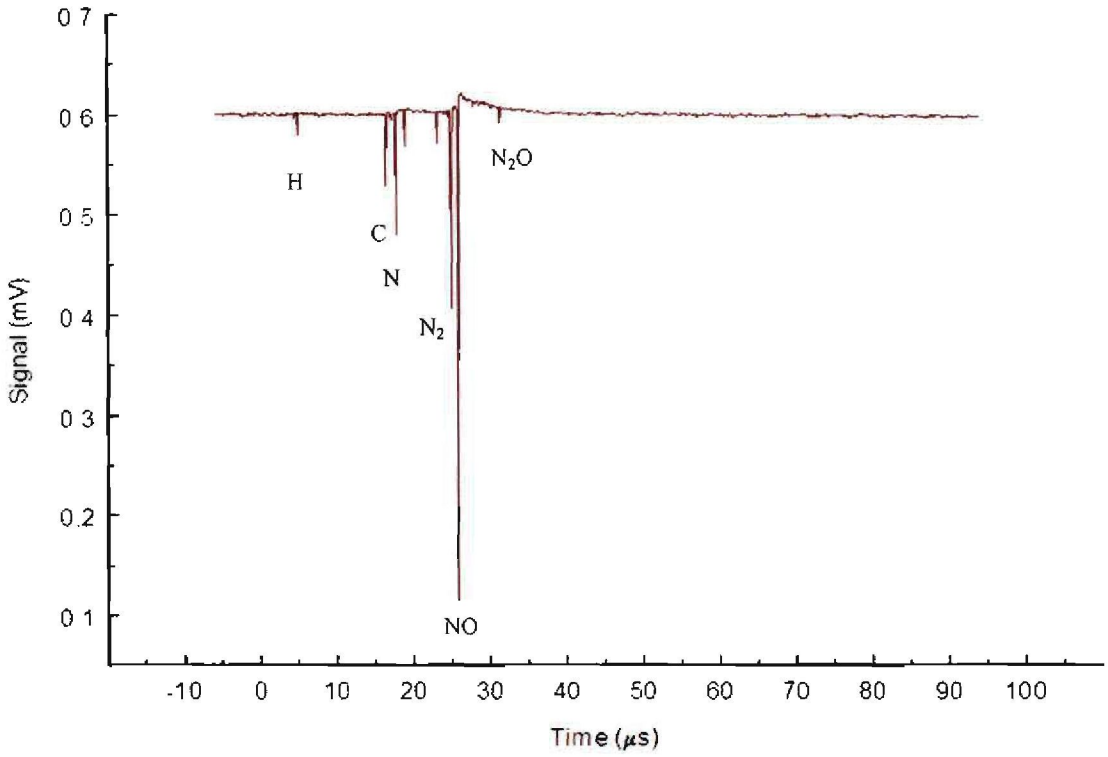

Figure 6.1 TOF mass spectrum for N_2O gas, using the Nd:YAG laser (266 nm) at 2.9 mJ and a pulse length of 6 ns.

6.2 Results of the ionization of the methyltrichlorosilane molecule using the Nd:YAG laser

The spectrum obtained using the 266 nm wavelength of the Nd:YAG laser to ionize the methyltrichlorosilane is shown in figure 6.2 as an example of a typical result. The mass peaks are identified as follows. The peak at 4.75 μs corresponds to the hydrogen ion (mass 1). At 16.3 μs the peak corresponds to carbon ion (mass 12), at 17 μs, 17.6 μs, 18.8 μs are CH^+, CH_2^+ and CH_3^+ hydrocarbons fragments respectively. The silicon ion (mass of 28) peak has a strong signal at 24.8 μs. The spectrum shows two isotopes of chlorine ions at 27.8 μs (mass 35) and 28.6 μs (mass 37) as well as the $SiCl^+$ at 37.2 μs ($Si^{35}Cl$) and $SiCl^+$ at 37.5 μs ($Si^{37}Cl$). Due to high energy and resultant high degree of ionization the mother molecule (methyltrichlorosilane) is dissociated and cannot be observed in the spectrum, also big fragments such as the $SiCl_3^+$ fragment peak were not observed.

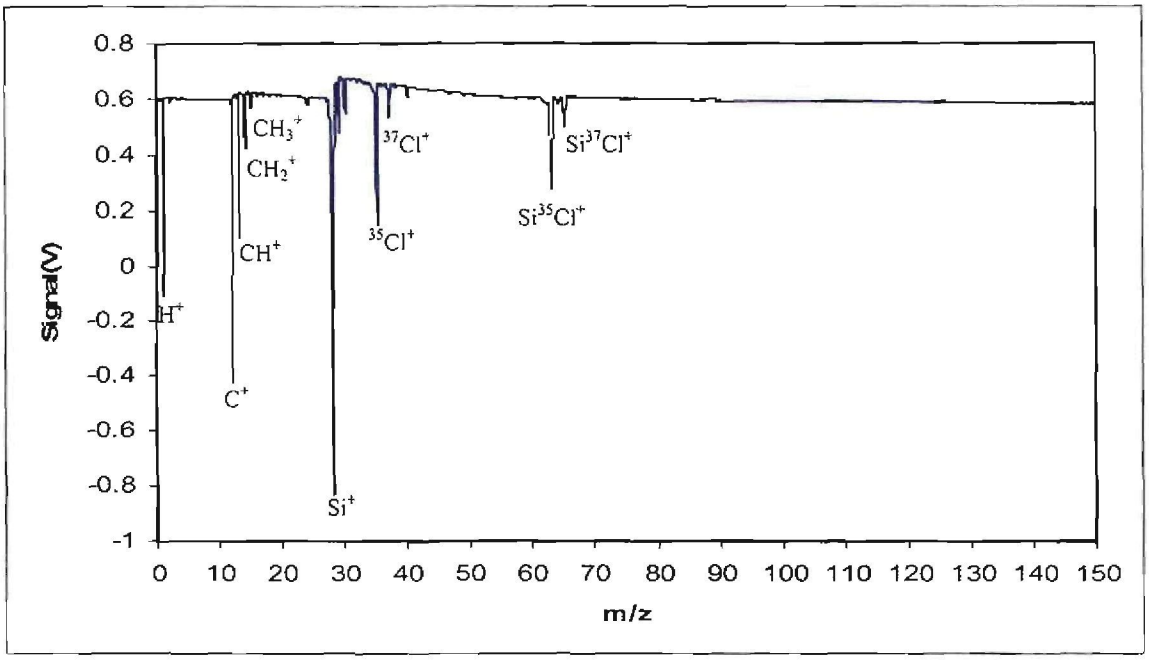

Figure 6.2 TOF mass spectrum for methyltrichlorosilane using the Nd:YAG laser (266 nm) at 2.9 mJ and a pulse length of 6 ns.

Table 6.1 Assignment of peaks from the TOF mass spectrum after excitation with Nd:YAG laser at 266 nm.

Time (μs)	Ions/fragments	m/z
4.75	H^+	1
16.3	C^+	12
17.0	CH^+	13
17.6	CH_2^+	14
18.8	CH_3^+	15
24.8	Si^+	28
27.8	$^{35}Cl^+$	35
28.6	$^{37}Cl^+$	37
37.2	$Si^{35}Cl^+$	63
37.5	$Si^{37}Cl^+$	65

6.3 Effect of different experimental parameters on ionization

6.3.1 Introduction

There are a number of factors that contribute to the ionization efficiency from the laser and the TOF system. A weak or low energy laser beam produces molecular ions with little or no fragmentation while a high energy laser beam generates an increase in fragmentation formation and ionization [Lubman, 1987]. The experimental parameters were studied in order to optimise the system. The nanosecond laser pulse energy was varied from 0.2 to 1.76 mJ to observe how its effects on ionization and to characterise the system. Lens focusing and defocusing in the ionization region was also varied (10 mm around the focus) while observing the effect it has on the mass spectrum. The delay time between the opening of the pulsed valve and the laser pulse trigger was varied from 140 μs to 1000 μs to find the optimal overlap of laser pulse with most ions in the gas pulse in the nanosecond experiment. The femtosecond laser pulse energy was varied from 0.966 mJ to 0.015 mJ. The delay time was varied from 0.3 ms to 70 ms in the femtosecond experiment for optimization.

6.3.1.1 The effect of varying laser energy and measuring peak signal using the Nd:YAG laser at 266 nm

The effects of laser energy on peak signals were studied using the Nd:YAG laser at 266 nm by varying the laser energy over a range of 0.109 mJ to 1.6 mJ. The experiment showed an increase of ion signal intensity with laser energy for the measured peaks Si^+ ion, $Si^{35}Cl^+$ and $^{35}Cl^+$. The laser energy of the beam was measured using a power meter with a conversion factor of 9.5 mV/mJ. Figure 6.3 shows an increase in peak intensity of the ion fragments Si^+ ion, $Si^{35}Cl^+$ and $^{35}Cl^+$ up to a laser energy value of approximately 1 mJ , then slightly declining up to a laser energy of 1.59 mJ and increasing again up to a laser energy of 1.6 mJ. It was concluded from this measurements to use the optimum laser energy of 1.6 mJ for all measurements with the Nd:YAG laser.

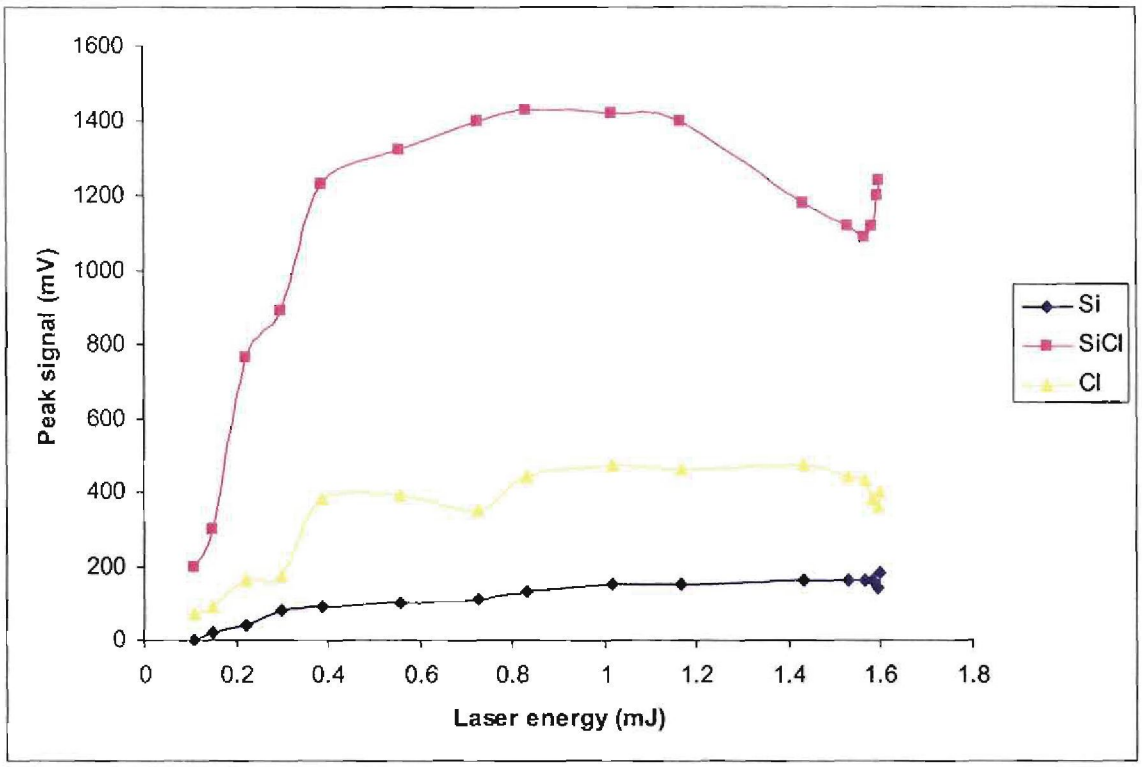

Figure 6.3 Plot of peak intensity versus laser energy using the Nd:YAG laser (266 nm), laser energy over a range of 0.109 mJ to 1.6 mJ and a pulse length of 6 ns.

6.3.1.2 The effect of laser focusing on peak signals

Setting the focus of the laser relative to the sample or the ion in the ion source is achieved by moving the lens. The focal point can be adjusted in such a way that the laser is focused in front of the sample ions or behind the sample ions in order to observe how this affects the peak signals of the measured peaks of the Si^+, $Si^{35}Cl^+$ and $^{35}Cl^+$ ions. The lens was adjusted in steps of 1 mm to observe the results. When the laser is in the optimal focused position more ions are detected due to better overlap of gas molecules and laser focus, and improved alignment of the focus with the ion extraction path. When the laser is defocused from the sample ions this leads to a reduction in measured signal intensities. Figure 6.4 shows the relationship between laser focus position and peak signal. It was observed that the peak signals increase from -1 mm and it is optimum between 0 and 1 mm and declining sharply from 2 mm. The conclusion from the measured peaks shows that the best focusing position that gives optimum peak intensities is between 0 and 1 mm.

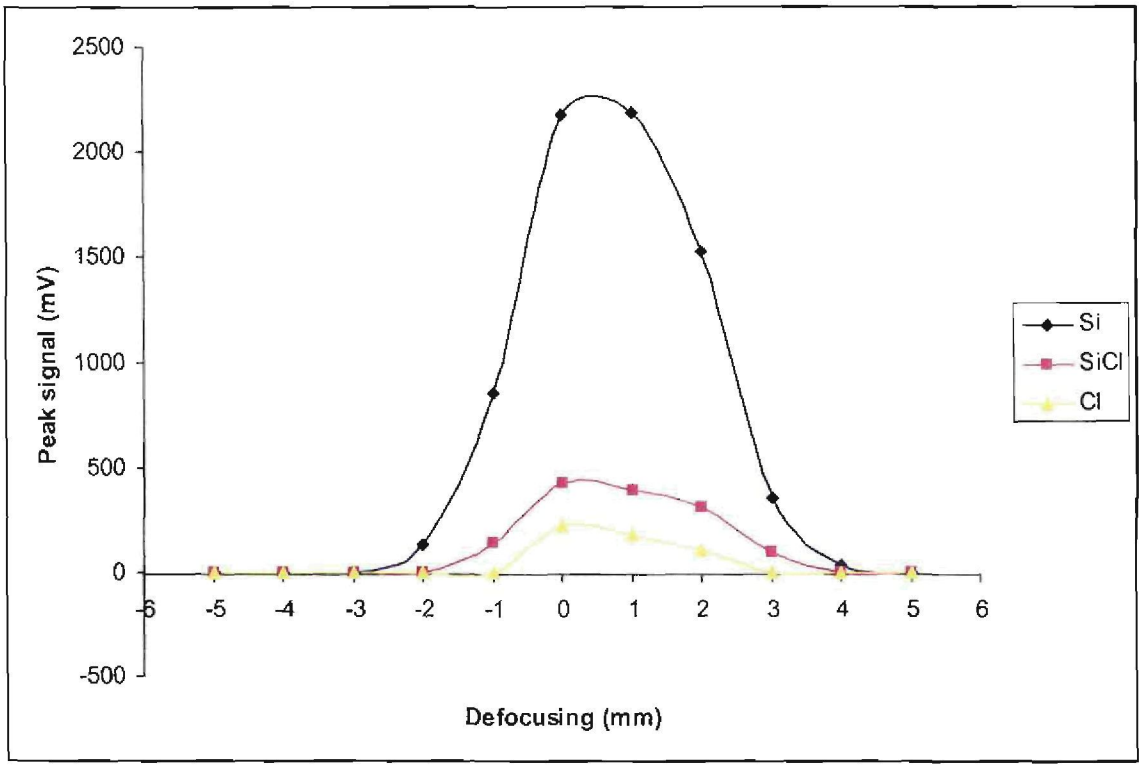

Figure 6.4 The effect of laser focus position on the Si^+, $Si^{35}Cl^+$ and $^{35}Cl^+$ ions peak signals using the Nd:YAG laser (266 nm), laser energy 1.6 mJ and a pulse length of 6 ns.

6.3.1.3 The effect of varying delay time on peak signals

By changing the relative delay time between gas pulse opening time and laser pulse trigger, the overlap between the laser pulse and the gas pulse can be changed from almost no overlap through to a situation with optimal overlap with most ions and finally with overlap of the laser pulse with only the trailing gas at the end of the pulse. Figure 6.5 shows the effect of delay time on peak signal. The plots follow the same trend whereby the peak signals are at optimum at a delay time of between 200 and 220 μs. There is an increase in ion signal again from 400 μs to about 500 μs, the ion signal stays constant with increase in delay time until about 950 μs and decrease again. The decrease from 950 μs means that as the time delay increases the gas pulse overlap with laser pulse deteriorates and eventually the trail of the gas pulse gives less and less signal. From the measurements it seems that the optimum condition for the delay time is between 400 and 900 μs.

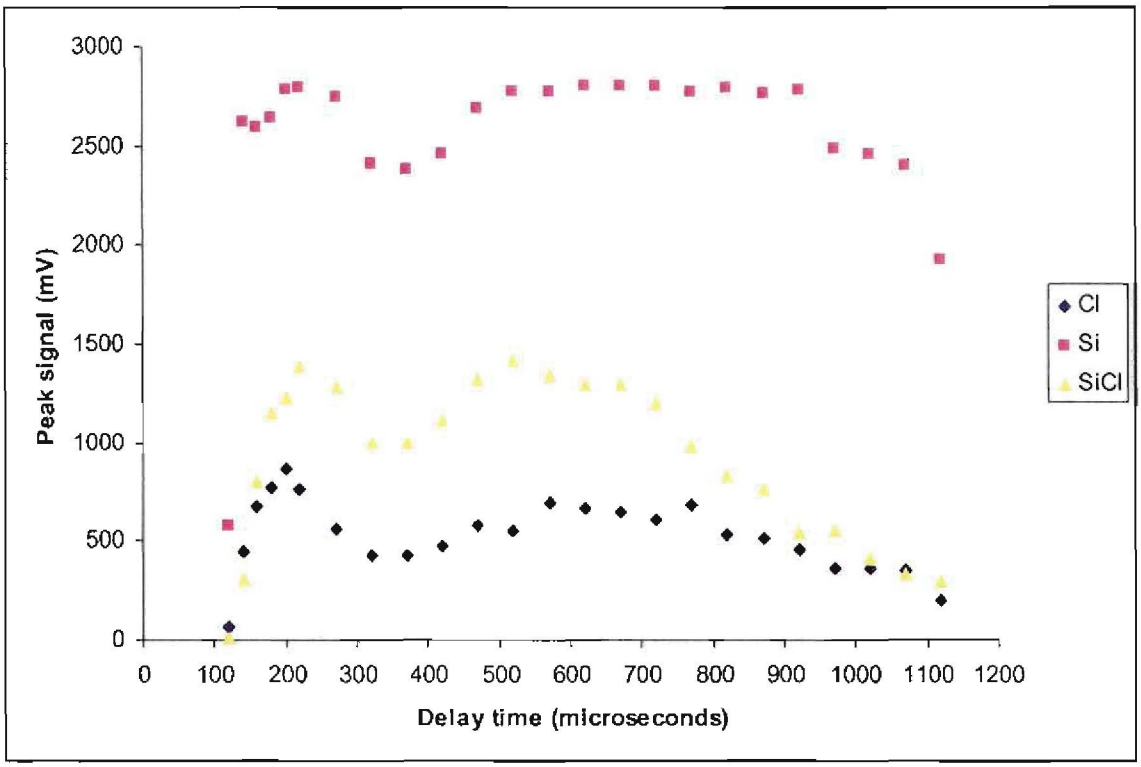

Figure 6.5 The effect of delay time on the Si^+, $Si^{35}Cl^+$ and $^{35}Cl^+$ ions peak signals using the Nd:YAG laser (266 nm), laser energy 1.6 mJ and a pulse length of 6 ns.

6.4 Results of the ionization and dissociation of the methyltrichlorosilane molecule using the dye laser

The dye laser operating with Stilbene dye gave a pulse energy of 4.4 mJ at 425nm, pulse length of 20 ns. Doubling this pulse in the BBO crystal gave an energy of 0.15 mJ at 212.5 nm at a repetition rate of 5 Hz and a pulse duration of 10 ns. The TOF results are shown in figure 6.6 and table 6.2. The silicon ion had a strong signal at 24.8 μs. The $^{37}Cl^+$ ion is observed at 28.2 μs, the $^{35}Cl^+$ isotope peak is not observed in this spectrum. The $Si^{35}Cl^+$ and $Si^{37}Cl^+$ fragments that were present when methyltrichlorosilane molecule was ionized using Nd:YAG laser (figure 6.2) are not observed at 37.2 μs and 37.5 μs. At 1064 nm, 532 nm and 425 nm no ionization was observed for both the Nd:YAG and dye lasers. Ionization of MTS is achieved only at 266 nm and 212.5 nm. What is not clearly understood is the weak signal observed in the TOF spectrum using the dye laser at 212.5 nm (figure 6.6) because from the

UV/Vis results obtained in chapter 3 the MTS molecule absorbs strongly in the region 201 nm to 232 nm. The observed results may be due to the considerably lower energy from the dye laser resulting in soft ionization (ionization producing little or no fragmentation).

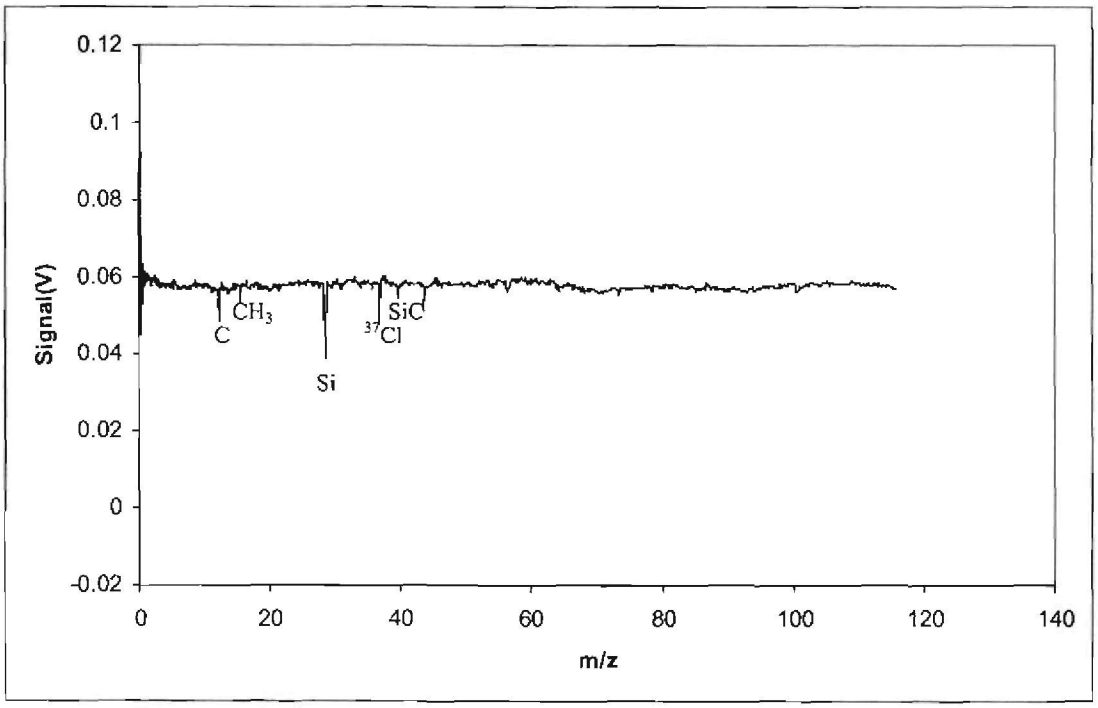

Figure 6.6 TOF mass spectrum for methyltrichlorosilane using the dye laser (212.5 nm) at 0.15 mJ and a pulse length of 10 ns.

Table 6.2 Assignment of peaks on the TOF mass spectrum in figure 6.6

Time (μs)	Ions/fragments	m/z
4.75	H^+	1
16.3	C^+	12
18.9	CH_3^+	15
24.8	Si^+	28
28.2	$^{37}Cl^+$	37
29.3	Ar^+	40
30.05	SiC^+	40

6.5 Results of the ionization of the methyltrichlorosilane molecule using the femtosecond laser at 795 nm

A time of flight mass spectrum of methyltrichlorosilane after ionization with a femtosecond laser at 795 nm and having a pulse energy of 0.966 mJ is shown in figure 6.7(a). In this experiment, the sample gas was introduced with pulse delay of 0.6 ms, laser pulse duration of 120 fs and with backing pressure of 1 atm of the carrier gas argon. This mass spectrum is an average measurement over 32 pulses. The assignments of the peaks are made as follows. The peaks at 4.71 μs, 16.3 μs, 17.6 μs, 20.9 μs, 24.8 μs, 27.8 μs and 28.6 μs are assigned to H^+, C^+, CH_2^+, Ar^+, Si^+, $^{35}Cl^+$ and $^{37}Cl^+$ respectively. The peaks at 37 μs, 46 μs, 50 μs, 54 μs and 56.4 μs are assigned to $Si^{35}Cl^+$, $SiCl_2^+$, $CH_3SiCl_2^+$, $SiCl_3^+$ and $CH_3Si^{35}Cl_3^+$ respectively. There is a strong overshoot observed in the mass spectrum, which is due to electronic mismatch of impedances in the amplifier. Also the large signal of the Ar^+ peak that is seen contributes to the observed overshoot.

The broadening of the higher mass peaks could be reduced by lowering the laser energy, in which case the peaks are resolved more clearly as shown in figure 6.7 (b). Although the absolute peak sizes are smaller, the isotopic species can be distinguished. The main result in both figures 6.7 (a) and figure 6.7 (b) is the presence of the parent molecular ion as well as large fragments, especially $SiCl_3^+$.

Other larger fragments observed are the $Si^{35}Cl_2^+$ ion, $CH_3Si^{35}Cl_2^+$ ion and $Si^{35}Cl_3^+$ ion which were not detected using nanosecond lasers (figure 6.2 and 6.6). This corresponds to what has been observed by others doing similar work, that femtosecond ionization can cause parent molecule ionization without fragmentation. [Clara et al., 2000].

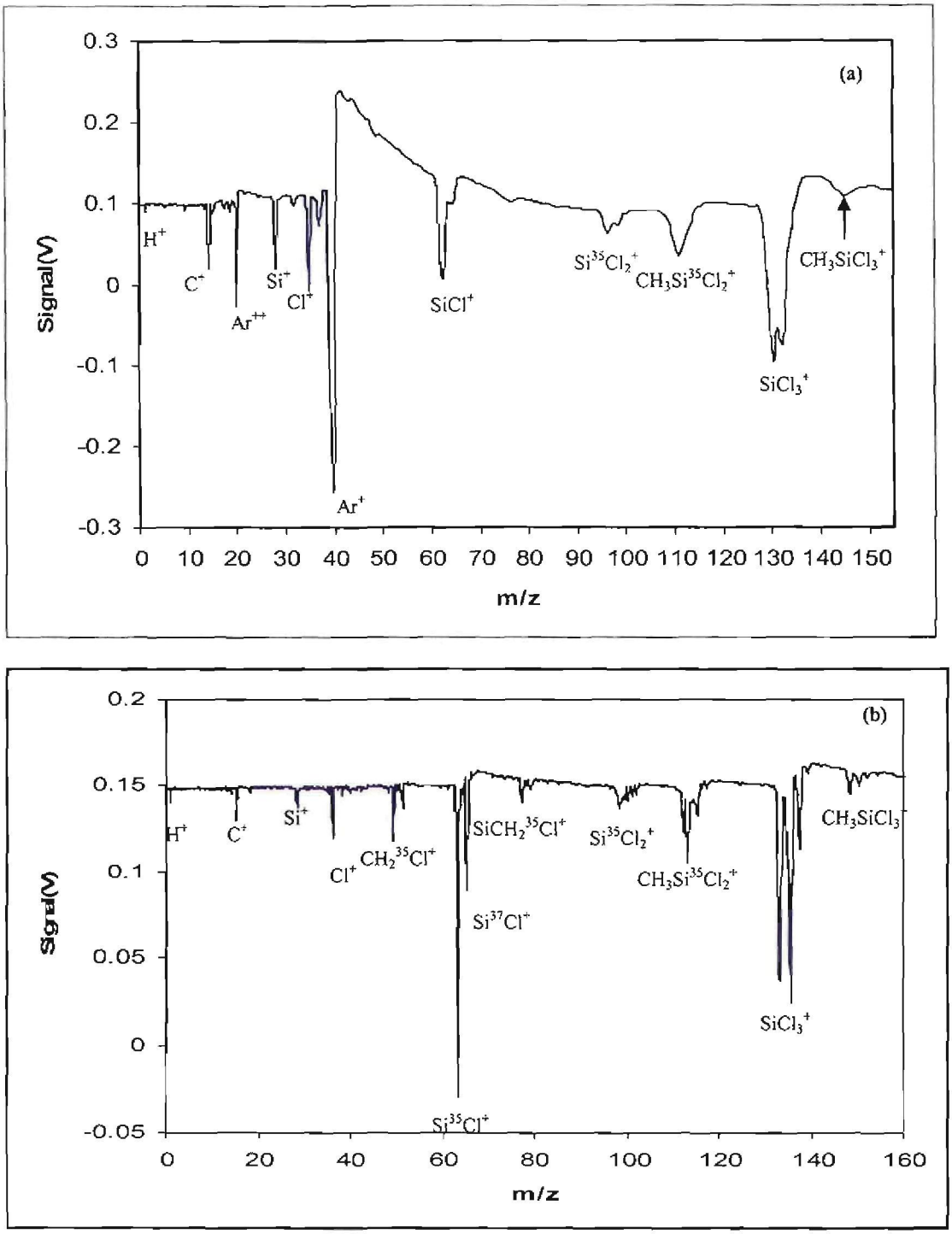

Figure 6.7 TOF mass spectra for methyltrichlorosilane using a femtosecond laser (795 nm) (a) at laser intensity of 0.966 mJ per pulse and a pulse length of 120 fs and 0.6 ms delay time and (b) 0.0813 mJ. Large fragments are observed, including the parent molecule. Peak broadening is visible in (a), most likely due to collisional ionization.

Table 6.3 Assignment of peaks from the TOF mass spectrum after excitation with a femtosecond laser at 795 nm.

Time (μs)	Ions/fragments	m/z
4.71	H^+	1
16.3	C^+	12
20.9	Ar^{++}	20
24.8	Si^+	28
27.8	$^{35}Cl^+$	35
28.6	$^{37}Cl^+$	37
29.3	Ar^+	40
37.2	$Si^{35}Cl^+$	63
46.1	$Si^{35}Cl_2^+$	98
49.6	$CH_3Si^{35}Cl_2^+$	113
54.1	$Si^{35}Cl_3^+$	133
56.4	$CH_3Si^{35}Cl_3^+$	148

6.5.1 Effect of varying laser intensity on peak signals

The femtosecond laser pulse energy was varied from 0.966 mJ to 0.015 mJ and the mass spectra obtained are shown in figure 6.8 with shifted baselines for simplicity. The spectra clearly show a decrease in peak signal with laser energy. Another interesting observation is that when the laser energy is increased peak width also increases. Following the above-mentioned observation the $SiCl_3^+$ peak was looked at to observe the effect of laser energy on the peak height as well as peak width.

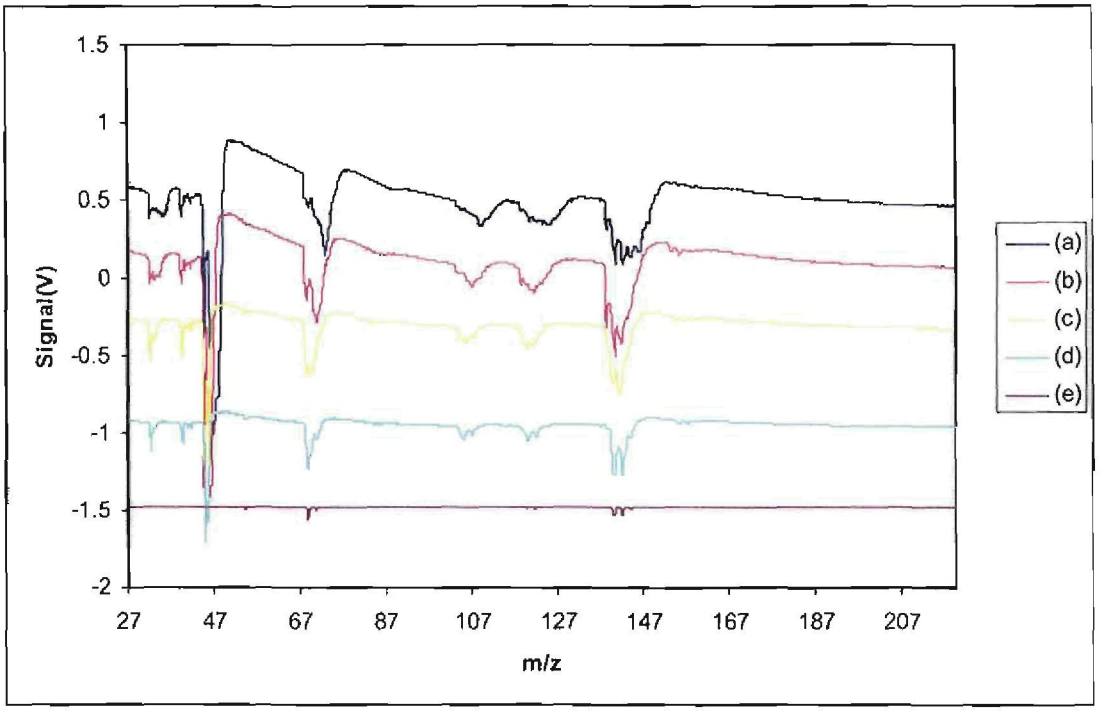

Figure 6.8 TOF mass spectra for methyltrichlorosilane using a femtosecond laser (795 nm) with laser energy (a) 0.966 mJ (b) 0.507 mJ (c) 0.2732 mJ (d) 0.0813 mJ (e) 0.015 mJ, 120 fs pulse length and 0.6 ms delay time

The laser energy was varied from 0.035 to 0.563 mJ and effect of this on the $SiCl_3^+$ peak was observed. The results are shown in figure 6.9. At higher laser energies the mass peak is broad and the broadening disappears at laser energy of 0.138 mJ where the broad peak becomes separated into two peaks of different isotopes of chlorine.

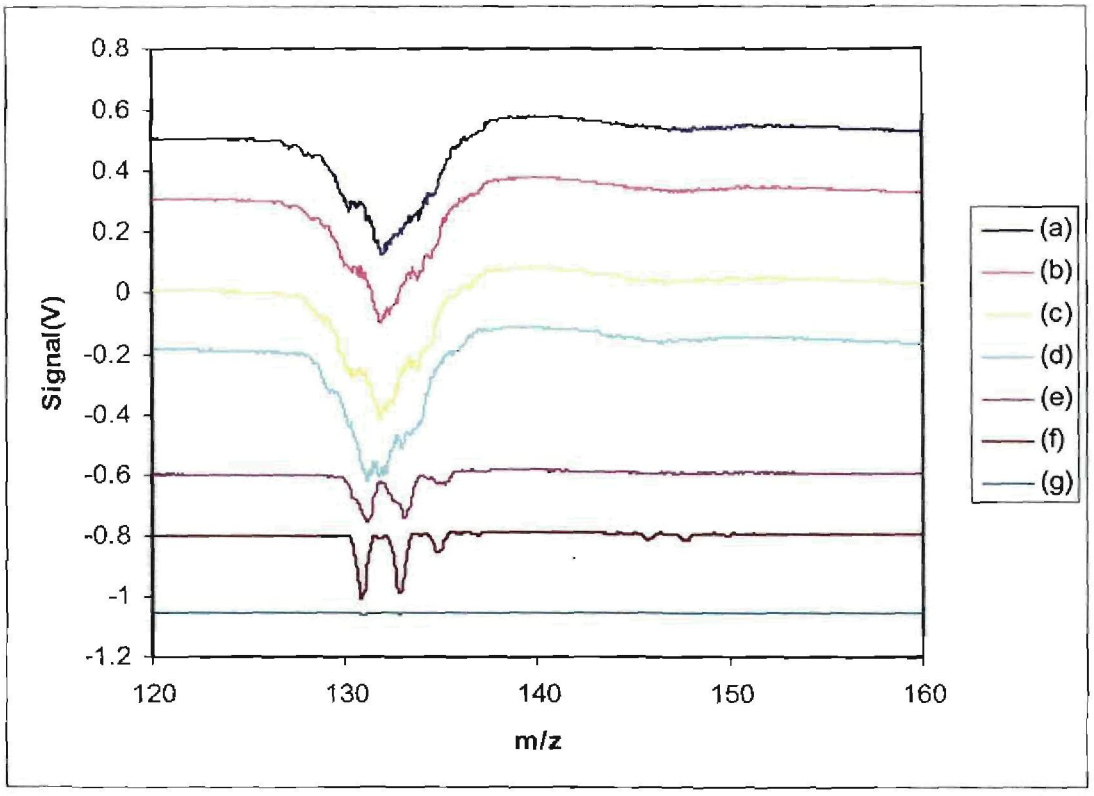

Figure 6.9 TOF mass spectra for methyltrichlorosilane observing the $SiCl_3^+$ peak (133 amu) using a femtosecond laser (795 nm), a pulse length of 120 fs with a delay time of 0.6 ms and laser energy of (a) 0.563 mJ (b) 0.461 mJ (c) 0.364 mJ (d) 0. 204 mJ(e) 0.138 mJ (f) 0.0665mJ (g) 0.035 mJ.

The broadening might be due to the large number of ions being produced, which can result in a large cloud of ions having different kinetic energies, rather than a small localized ionization region. This will result in ions starting their travel time at different velocities and arriving at the detector at different times, therefore a broader feature is observed. The repulsive force between many positive ions known as coulomb repulsion may contribute to this phenomenon.

The graph of peak signal versus laser energy was plotted in figure 6.10 for the $SiCl_3^+$ peak from 0.035 mJ to 0.563 mJ (a to g on figure 6.9) at a delay time of 0.6 ms. The results clearly show that peak signal increases with laser energy.

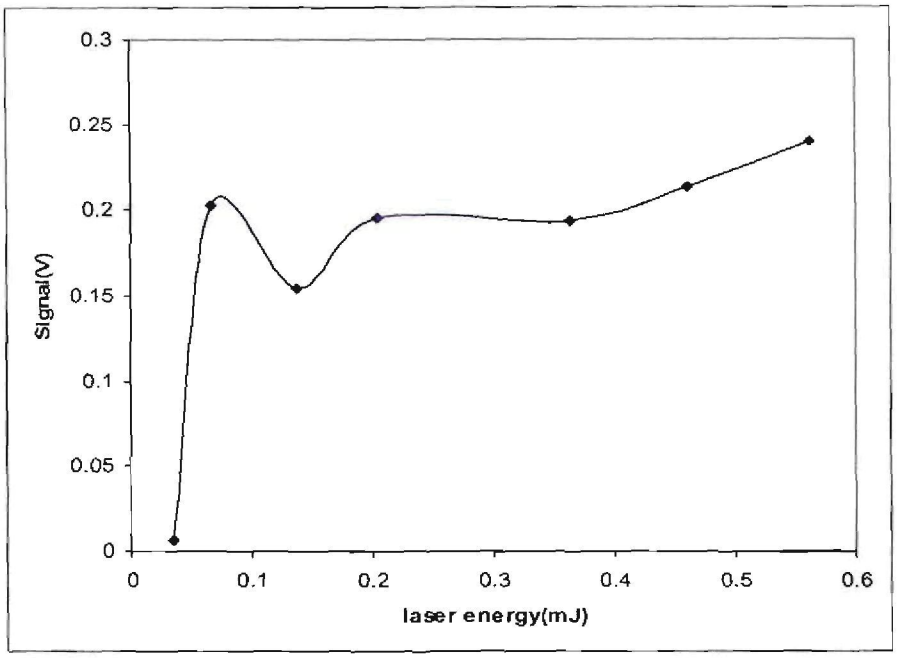

Figure 6.10 The effect of laser energy on peak signal for $SiCl_3^+$ peak using a femtosecond laser (795 nm), a pulse length of 120 fs for energies 0.035 to 0.563 mJ with delay time of 0.6 ms

The graph of peak width versus laser energy is shown in figure 6.11 for laser energy 0.035 to 0.563 mJ (a to g on figure 6.9). The results show that peak width increases with laser energy up to 0.563 mJ. A sudden peak broadening is observed from 0.204 mJ.

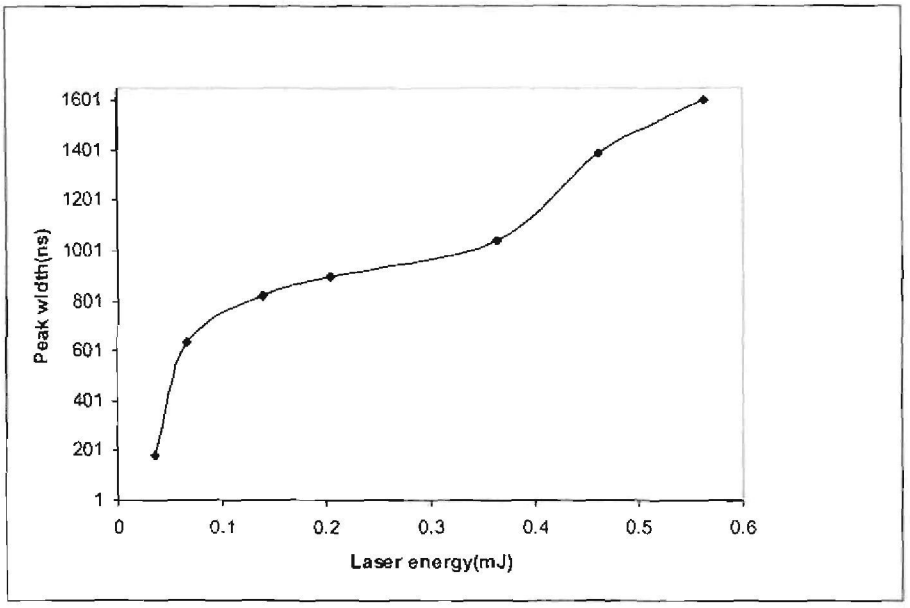

Figure 6.11 The effect of laser energy on peak width for $SiCl_3^+$ peak using a femtosecond laser (795 nm), a pulse length of 120 fs for laser energies 0.035 to 0.563 mJ with delay time of 0.6 ms

6.5.2 The effect of delay time on peak signal

By changing the relative delay time between gas pulse opening time and laser pulse trigger, the overlap between the laser pulse and the gas pulse can be changed from almost no overlap through to a situation of optimal overlap of laser pulse with most ions. The delay time was varied from 0.3 ms to 70 ms and spectra were recorded to show the effect of delay time. From figure 6.12 it is observed that from 2 ms the peaks are separated into two peaks of different isotopes of chlorine. The peak starts broadening at 0.35 ms and it is at maximum signal at 0.6 ms to 1.2 ms, which is where the laser pulse optimally overlaps with the gas pulse.

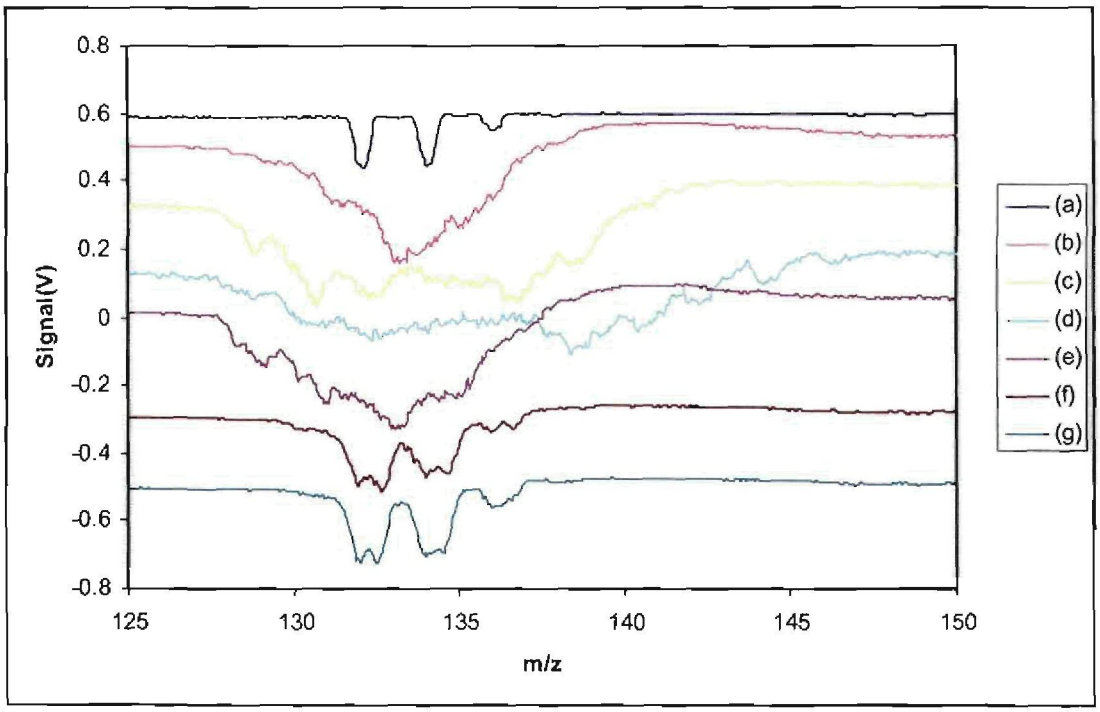

Figure 6.12 TOF mass spectra for methyltrichlorosilane observing the $SiCl_3^+$ peak (133 amu) using a femtosecond laser (795 nm), laser energy 0.966 mJ and delay times (a) 0.3 ms (b) 0.6 ms (c) 0.7 ms (d) 0.8 ms (e) 1.2 ms (f) 4 ms (g) 11ms

The effect of delay time was plotted as a function of peak signal and it is shown in figure 6.13. From figure 6.13 at 0.3 ms and below refers to the laser pulse being there before the gas pulse (no sample to ionize). There is a sharp increase in ion signal from 0.3 ms to about 2 ms, showing a point of optimum gas molecules overlapping with the laser pulse. The sudden drop off from 2.1 ms or above refers to the laser pulse overlapping with the trailing edge of the gas pulse. Then as the time delay increases the gas pulse overlap with the laser pulse deteriorates and eventually the trail of the gas pulse gives less and less signal.

From the measurements it can be concluded that the TOF-MS with the femtosecond laser works best with the delay time between 0.6 ms and 2 ms, since an optimal overlap between the laser pulse and the gas pulse was observed, but care should be taken to avoid too large numbers of sample molecules that may result in peak broadening.

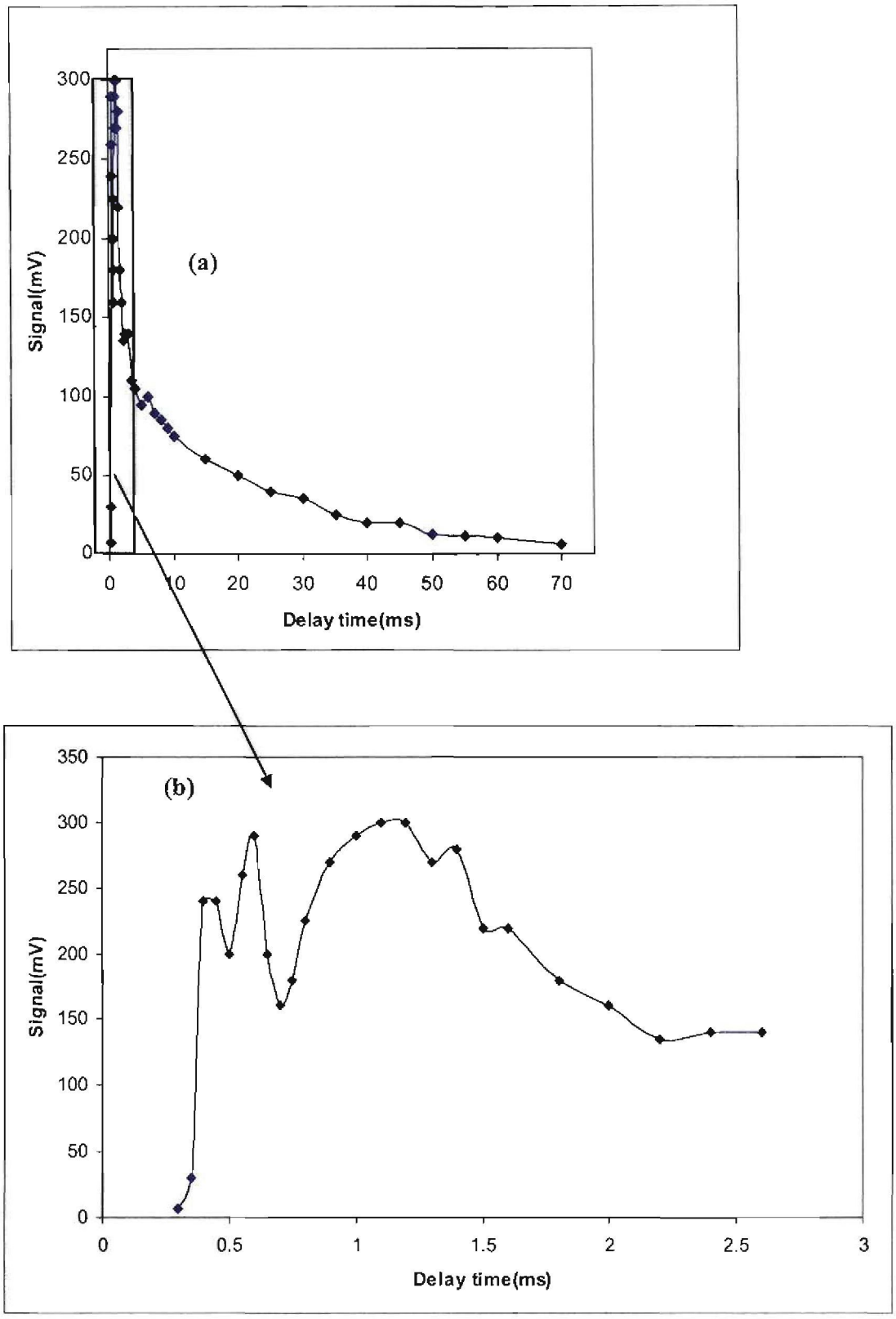

Figure 6.13 (a) The effect of delay time on peak signal using a femtosecond laser (795 nm), 120 fs pulse length, from 0.3 ms to 2.6 ms. (b) expansion of (a)

6.5.3 Results of the ionization of the methyltrichlorosilane molecule using the femtosecond laser at 795 nm and 397.5 nm.

Time of flight mass spectra of methyltrichlorosilane after ionization with a femtosecond laser at 795 nm and 397.5 nm with a pulse energy of 0.1563 mJ is shown in figure 6.14. In this experiment, the experimental parameters used are laser pulse duration of 120 fs, gas pulse delay of 0.55 ms and with backing pressure of 1 atm of the carrier gas, argon. The mass spectra are an average measurement over 32 pulses. The results indicate a similar trend observed in the two mass spectra, with same number of peaks in both cases. The difference observed is that in the 795 nm spectrum the peaks are slightly higher in signal compared to the spectrum measured at 397.5 nm. It seems that ionization in the femtosecond laser seems not to be wavelength dependent, since the shorter wavelength photons are expected classically to produce more ionization, due to their higher photon energies.

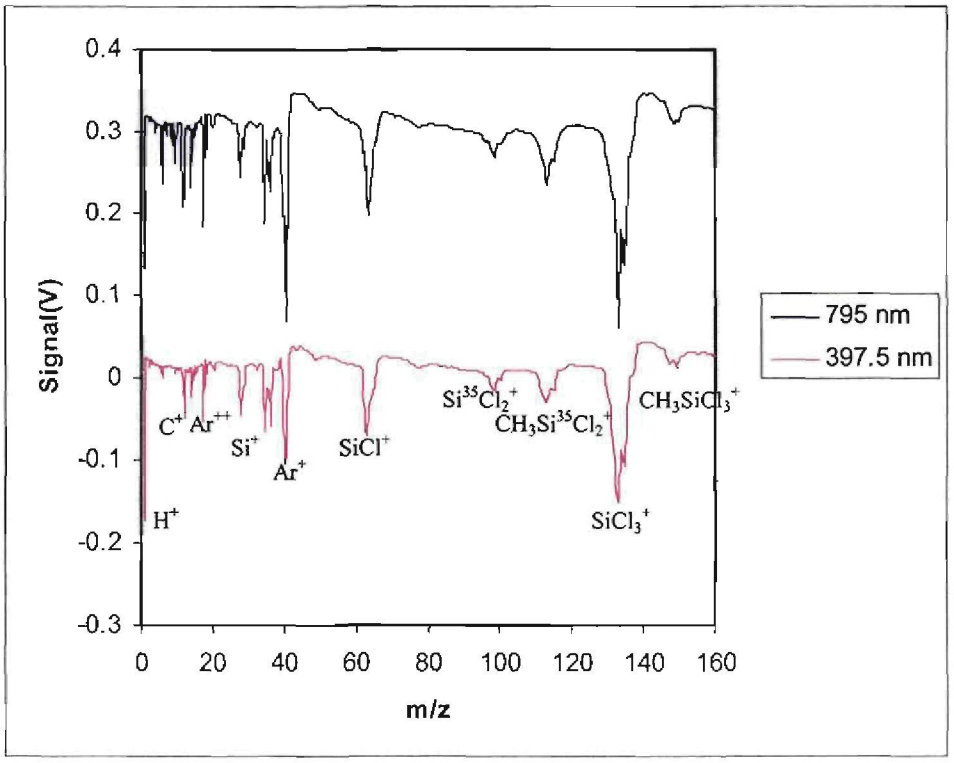

Figure 6.14 TOF mass spectra for methyltrichlorosilane using a femtosecond laser (795 nm and 397.5 nm) and same laser energy in both cases of 0.156 mJ per pulse and a pulse length of 120 fs.

6.5.4 Discussion

Mass spectroscopic techniques using nanosecond non resonant multiphoton ionization has been used to analyse methyltrichlorosilane (MTS), but the detection of the parent molecule and other large fragments ions was not observed. One reason for this could be that when a resonant intermediate state is excited in the multiphoton process the parent molecule undergoes fragmentation into neutral fragments before ionization occurs. This corresponds to what has been reported in literature for nanosecond laser ionization. For longer laser pulse lengths (nanoseconds), there is enough time for one or more intermediate states to be reached in the excitation ladder to dissociate and produce neutral fragments. These fragments then absorb further photons and either reaches the ionization limit or fragment further [Andrews and Demidov, 2002].

This mechanism is for the nanosecond experiment and is called ladder switching. From previous studies [Allendorf and Melius, 1993] reaction (2), shown below, is considered to be a favourable dissociation path in all the reactions of methyltrichlorosilane that were studied. The reason was that it involves the breaking of weak CH_3-$SiCl_3$ bonds. The reaction involves the formation the methyl radical and trichlorosilyl radical.

$$CH_3SiCl_3 \rightarrow CH_3\bullet + \bullet SiCl_3 \qquad (2)$$

Absorption of the second photon by CH_3 and $SiCl_3$ molecules results in the ionization which gives products Si^+, $SiCl^+$,CH_3^+ C^+, and H^+ which are observed in the nanosecond mass spectrum.

The result is different for the multiphoton femtosecond mass spectrum (figure 6.7 and 6.14). The strongest peaks produced by the MTS ion are the $SiCl^+$ ion, $SiCl_3^+$ ion and $SiCl_2CH_3^+$ fragment ion. The parent MTS ion peak is also observed whereas in the nanosecond laser time of flight spectrum it was not detected. A strong peak of Ar^+, which is the carrier gas used in the experiments, is also observed. Theoretically, a minimum of seven photons are required in the femtosecond multiphoton ionization of methyltrichlorosilane, since the wavelength of the femtosecond laser is 795 nm. In this case the photons are absorbed before dissociation can take place in the

intermediate state, so ionization of the parent MTS into the MTS ion occurs after absorption of seven or more photons followed by possible further fragmentation of the MTS ion into various fragment ions. This can be explained in the suggested equations showing possible pathways for the ionization and dissociation of MTS [Osterhold et al., 1994]:

$$CH_3SiCl_3 \rightarrow CH_3SiCl_3^+ \quad (3)$$

$$CH_3SiCl_3^+ \rightarrow CH_3 + SiCl_3^+ \quad (4)$$

$$CH_3SiCl_3^+ \rightarrow CH_3SiCl_2^+ + Cl \quad (5)$$

$$CH_3SiCl_3^+ \rightarrow CH_3SiCl_2 + Cl^+ \quad (6)$$

$$CH_3SiCl_3^+ \rightarrow CH_3Cl + SiCl_2^+ \quad (7)$$

The products $CH_3SiCl_3^+$, $SiCl_3^+$, $CH_3SiCl_2^+$, Cl^+ and $SiCl_2^+$ are indeed observed in the mass spectrum. Other products observed in the mass spectrum that are not shown in the equations may be from many fragmentation channels as a result of further absorption of photons of the formed fragments ($CH_3SiCl_3^+$, $SiCl_3^+$, $CH_3SiCl_2^+$, Cl^+ and $SiCl_2^+$) to produce more ions.

More work is required before the mechanism of ionization of the methyltrichlorosilane molecule using the nanosecond and femtosecond lasers can be fully understood. The results from this work confirm that the ultra fast ionization is the appropriate method over nanosecond ionization for ionization and characterization of the methyltrichlorosilane molecule.

Chapter 7

Conclusions

Molecular modelling using the Spartan program was employed to obtain an understanding of the molecular properties of methyltrichlorosilane. Calculations of the FT-IR spectra, bond lengths and bond angles as well as the dipole moment were carried out. The calculations of bond lengths and bond angles were reproduced and correspond to what was revealed in literature. FT-IR calculations correspond with literature values and the molecule was characterized.

UV/Vis, FT-IR and Raman measurements were carried out to characterize the molecule. UV/Vis measurements revealed that the molecule has strong absorption bands at 201 and 232 nm.

The study revealed the successful ionization and characterization of the methyltrichlorosilane molecule using both the nanosecond and femtosecond laser systems. It was discovered that the measurements depend on experimental parameters in the time of flight mass spectrometer, namely laser energy, laser beam focusing and the delay time between the gas pulse and the laser pulse. Laser energy had an effect whereby the ion signal increased with laser energy for the overall spectrum. This was confirmed by laser energy and peak signal plots for few selected peaks (Si^+ $SiCl^+$ and Cl^+). The laser energy used for all measurements of the Nd:YAG laser was 2.9 mJ. Also the delay time between the laser pulse and the gas pulse had to be set at the appropriate time to give an optimum signal which was found to be between 400 and 900 μs for the nanosecond laser and 0.6 to 2 ms for the femtosecond laser. The results showed that the best focusing position of the laser beam (using a lens to adjust the focus) giving optimum peak intensities was between 0 and 1 mm for both the nanosecond and the femtosecond lasers. All measurements were done under the above mentioned conditions.

The dye laser provided poor results in terms of ionization whereby few peaks were detected with very weak peak signals from the mass spectrum of methyltrichlorosilane. The laser energy (0.15 mJ) from the dye laser may have been too low. The differences observed in the femtosecond mass spectra obtained at 795 nm and 397.5 nm is that in the 795 nm spectrum the peaks are slightly higher in signal compared to the spectrum measured at 397.5 nm. The interesting observation with the femtosecond laser mass spectra was the detection of the parent ion ($CH_3SiCl_3^+$) and other larger fragments ($Si^{35}Cl_2^+$ ion, $CH_3Si^{35}Cl_2^+$ ion and $Si^{35}Cl_3^+$ ion) that were not observed in the nanosecond mass spectra. The results obtained in this study show that multiphoton ionization using the femtosecond laser is the appropriate and effective method over nanosecond ionization for ionization and characterization of the methyltrichlorosilane molecule.

There is still a wide scope of work that can be done in the research of the photochemistry of MTS. Lasers can be used to selectively excite specific energy levels within a molecule using the pump probe technique with a femtosecond laser system. The pump probe technique can also be used for excitation of the excited states and fragments produced in ionization. Any level of individual quantum states (rotational, vibrational and electronic) within a molecule may be excited selectively by the pump probe coherent control method [Wayne, 2005]. Future work involves the attempt to control fragmentation by selectively ionizing specific fragments of a molecule or controlling the ionization process in order to obtain certain products.
These applications of lasers may provide a better understanding of the multiphoton ionization process of MTS. The challenge to improve designs for the chemical vapour deposition process in the PBMR is an ongoing project that will be extensively explored.

APPENDIX

References

Allendorf, M. D. and Melius,, C.F., Theoretical study of the thermochemistry of molecules in the Si-C-Cl-H system, *J. Phys. Chem.,* 1993, **97**, 720-728.

Andrews, D L., Demidov, A. A., An Introduction to Laser Spectroscopy, 2nd Edition., eds., Kluwer Academic Publishers,. New York, 2002, 375.

Armour,M. A., Hazardous laboratory chemicals disposal guide, 3rd edition, CRC Press, 2003, 319.

Bessmann, T. M., Sheldon, B. W., Moss, T. S., III, Kaster, M. D., Depletion effects of silicon carbide deposition from methyltrichlorosilane, *J. Am. Ceram. Soc.,* 1992, **75**, 2899.

Burnelle, L. and Duchesne, J., The infrared spectrum of methyltrichlorosilane, *J .Chem. Phys.,* 1952, **20**, 1324.

Clara, M., Braun, J. E., Heller, Th., and Neusser, H. J., Femtosecond laser mass spectroscopy of ferrocenes: Photochemical stabilization by bridged cyclopentadienyl rings?, *Int. J. Mass. Spectrom.,* 2000, **203**, 71-81.

Copley, J. R .D., and Udovic, J. T., Neutron time of flight spectroscopy, *J. Res. Natl. Inst. Stand. Technol.,* 1993, **98**, 71.

Ge, Y.,Gordon, M. S., Battaglia, F., and Fox, R. O., Theoretical study of the pyrolysis of methyltrichlorosilane in the gas phase. 2. Reaction paths and transition states, *J. Phys. Chem.,* 2007, **111,** 1475-1486.

Geusic, J.E., Marcos, H.M., and Van Uitert, L.G., Laser oscillations in Nd-doped yttrium aluminum, yttrium gallium and gadolinium garnets, *Applied Physics Letters,* 1964, **4**, 182-184.

Ghosh, S. K., Berkowitz, M., and Parr, R.G., Transcription of ground state density functional theory into a local thermodynamics, *Proc. Natl. Acad. Sci.,* 1984, **81,** 8028-8031.

Hankin, S. M., Tasker, A. D., Robson, L., Ledingham, K. W. D., Fang, X., Mckenna, P., McCanny, T., Singhal, R. P., Kosmidis, C., Tzallas, P., Jaroszynski, D. A., Jones D. R., Issac, R. C., and Jamison, S., Femtosecond laser time of flight mass spectrometry of labile molecular analytes: laser desorbed nitro aromatic molecules, *Rapid Commun. Mass. Spectrom.*, 2002, **16,** 111-116.

Henry, W. J., Shusterman, A. J., and Nelson, J. E., the molecular modelling workbook for organic chemistry, wavefunction, Inc, Irvine, CA (USA), 1998, 10-60.

Höltje, H.-D., Sippl, W., Rognan, D., and Folkers, G., Molecular modelling-basic principles and applications, Second edition, 2003, 2-30.

Iijima T., Shimoda T., and Hattori H., Molecular structure of chlorotrimethylsilane and methyltrichlorosilane as investigated by gas-phase electron diffraction, *J. Mol. Struct.,* 1995, **350,** 57-61.

Josiek, A., Langlais, F., Residence-time dependent kinetics of CVD growth of SiC in the MTS/H_2 system, *J. Cryst. Growth.,* 1996, **160,** 253.

Lubman, D. M., Optically selective molecular mass spectroscopy, *Anal .Chem.,* 1987, **59,** 31A-40A.

Mcnab, L. R., and Shiell, R. C., Laser spectroscopy, *Phys. Educ.,* 1994, **29,** 164-169.

Mousavipour, S. H., Saheb, V., Ramezane, S., Kinetics and mechanism of pyrolysis of methyltrichlorosilane, *J. Phys. Chem.,* 2004, **108,** 1946-1952.

Opsal, R. B., Owens, K. G., Reilly, J. P., Resolution in the linear time of flight mass spectrometer, *Anal. Chem.,* 1985, **57,** 1884.

Osterhold, T. H., Allendorf, M. D., and Melius, C. F., Unimolecular decomposition of methyltrichlorosilane:RRKM calculations, *J. Phys. Chem.*, 1994, **98**, 6995-7003.

Papasouliotis, G. D., and Sotirchos, S. V., On the homogeneous chemistry of the thermal decomposition of methyltrichlorosilane thermodymic analysis and kinetic modeling, *J. Electrochem. Soc.*, 1994, **141**, 1599-1611.

Prystupa, D. A., Anderson A., Lefebvre J. H., and Torrie B. H., Raman and infrared study of crystalline methyltrichlorosilane, *J. Raman. Spectrosc.*, 1990, **21**, 429-433.

Qtaitat, M. A. and Mohamad, A. B., *Mol. Biomol. Spectrosc.*, Spectra and structure of silicon containing compounds. XVII. Vibrational and microwave spectra, molecular structure, barrier to internal rotation and *ab initio* calculations of methyltrichlorosilane 1994, **50A**, 621-637.

Skoog D. A., Holler E. J., and Nieman T. A., Principles of instrumental analysis, fifth edition, Inc. USA, 1998, 299-442.

Soliman, M. S., Khattab, M.A., and El-Kourashy A. G., Laser Raman and infrared spectra and normal coordinate analysis of methyltrichlorosilane and methyltrichlorogermane, *Mol. Biomol. Spectrosc.*, 1983, **39A**, 621-625.

Spartan '06 for Windows and Linux, Tutorial and user guide, Wavefunction, Inc, Irvine, CA (USA), 2006, 226-335.

Svyatkin, V. A., Mal'tsev, A. K., and Nefedov, O. M., Study of isotopic splitting in infrared spectrum of CH_3SiCl_3 molecule, *J. Chem. Phys.*, 1977, **5**, 1164-1167.

Tafesse, F., Structural chemistry tutorial letter 101, University of South Africa, 2007, 8-9.

Takeo, H. and Matsumura, C., The microwave spectra, molecular structures, and quadrupole coupling constants of methyltrichlorosilane and trichlorosilane, *Bull. Chem. Soc. Jpn.*, 1977, **50**, 1633-1634.

Telle, H. H., Urena, A. G., and Donoven, R. J., Laser chemistry: Spectroscopy, dynamics and applications, 2007, 51-63.

Wayne, C. E., and Wayne, R. P., Photochemistry, Inc, USA (New York), 2005, 36-87.

Xu,Y., Cheng, L., Zhang, L., Yin, H., and Yin, X., High toughness,3D textile, SiC/SiC composites by chemical vapor infiltration, *Material Science and Engineering,* 2001, **A318**,183-188.

Cameo chemicals chemical datasheet, methyltrichlorosilane. Available at: http://cameochemicals.noaa.gov/chemical/3974 [Accessed 29 October 2008].

PBMR power generation. Available at: http://www.pbmr.co.za/ [Accessed 24 October 2008].

Molecular modelling. Available at: http://en.wikipedia.org/wiki/Molecular_modelling [Accessed 26 October 2007].

Computational chemistry. Available at: http://www2.lv.psu.edu/jbe10/research/spartan/index.html [Accessed 26 October 2007].

Dipole moment. Available at: http://hyperphysics.phy astr.gsu.edu/hbase/electric/dipole.html#c1 [Accessed 5 May 2008].

The basis sets lab activity. Available at: http://www.shodor.org/chemviz/basis/index.html [Accessed 15 May 2008].

Materials and process simulation center. Available at: http://www.wag.caltech.edu/home/jang/genchem/infrared.html [Accessed 12 June 2008].

Infrared spectroscopy. Available at: http://en.wikipedia.org/wiki/Infrared_spectroscopy [Accessed 26 June 2008].

Thermo scientific. Available at: http://www.thermo.com/nicolet/ [Accessed 18 August 2008].

Raman spectroscopy. Available at: http://carbon.cudenver.edu/public/chemistry/classes/chem4538/raman.htm#Introduction [Accessed 28 June 2008].

Kaiser optical systems inc. Available at: http://www.kosi.com/raman/index.html [Accessed 9 May 2008].

Ultraviolet/Visible Spectroscopy . Available at: http://www.chemistry.ccsu.edu/glagovich/teaching/316/uvvis/uvvis.html [Accessed 17 June 2008].

Ultraviolet and Visible Absorption Spectroscopy (UV-Vis). Available at: http://www.chem.vt.edu/chem-ed/spec/uv-vis/uv-vis.html [Accessed 12 September 2008].

Bruker optics. Available at: http://www.brukeroptics.com/ [Accessed 12 September 2008].

Ti-Sapphire laser. Available at: http://en.wikipedia.org/wiki/Ti-sapphire_laser [Accessed 22 September 2008].

A state of the art Titanium Sapphire lasers. Available at: http://www-atom.fysik.lth.se/Kurser/FLaserfysik/KHz%20Lab.doc [Accessed 30 September 2008].

Mode locked lasers. Available at: http://www.rp-photonics.com/mode_locked_lasers.html [Accessed 17 October 2008].

Chirped pulse amplification. Available at: http://www.rp-photonics.com/chirped_pulse_amplification.html [Accessed 17 October 2008].

Nd:YAG laser. Available at: http://en.wikipedia.org/wiki/Nd:YAG [Accessed 11 June 2008].

Lasalle University. Available at: http://www.lasalle.edu/academ/chem/laserweb/dyelaser.html [Accessed 11 June 2008].

Excimer. Available at: http://en.wikipedia.org/wiki/Excimer [Accessed 22 August 2008].